Check for updates

Advanced Functional Materials

ADVANCED FUNCTIONAL MATERIALS
www.afm-journal.de

REVIEW OPEN ACCESS

Cyclic Olefin Copolymers as Versatile Materials for Advanced Engineering Applications

Giulia Fredi[1,2] | Norma Mallegni[2,3] | Andrea Dorigato[1,2] | Mario Milazzo[2,4]

[1]Department of Industrial Engineering, University of Trento, Trento, Italy | [2]National Interuniversity Consortium For Materials Science and Technology (INSTM), Florence, Italy | [3]National Research Council, Institute For the Chemistry of Organometallic Compounds, Pisa, Italy | [4]Department of Civil and Industrial Engineering, University of Pisa, Pisa, Italy

Correspondence: Andrea Dorigato (andrea.dorigato@unitn.it) | Mario Milazzo (mario.milazzo@unipi.it)

Received: 2 February 2026 | **Revised:** 7 April 2026 | **Accepted:** 17 April 2026

Keywords: biocompatible materials | COC | optics | organ-on-a-chip | self-healing polymers | synthetic polymers

ABSTRACT

Cyclic Olefin Copolymers (COCs) constitute a class of thermoplastics that has garnered substantial interest in the scientific community since its debut in the 1950s and subsequent commercialization in the 1980s through the Ziegler-Natta catalysis process. The success of this polymeric class is attributed to its remarkable physico-chemical and mechanical properties, such as glass-like transparency, low density, and high tensile modulus and elongation at break. These qualities render COCs suitable for several different applications, spanning from the structural domain, where they may also exhibit self-healing properties, to the fields of bioengineering and electronics, for making advanced sensing systems or as constitutive materials for microfluidic devices. This review paper seeks to provide a comprehensive overview of COCs, from their chemical synthesis and engineering technology, and progressing toward their latest engineering applications. The goal is to underscore the versatility of COCs in comparison to other polymeric materials, while also addressing current limitations. in conclusion, future trends in the utilization of COCs in engineering will be shown, together with an analysis of their impact and sustainability within the global context of the circular economy.

1 | Introduction and General Chemistry of COCs

1.1 | Definition and Structure of COCs

Polyolefins – poly(ethylene), poly(propylene), poly(styrene), poly(butadiene), and their copolymers – account for more than 50% of global polymer production. Their success stems from outstanding properties combined with low production costs. Nonetheless, they have notable limitations: the glass-transition temperature (T_g) and melting point (T_m) are constrained by the non-polar nature of polyolefins, and any significant increase in T_g or T_m typically requires the synthesis of well-defined copolymers [1]. Consequently, modifying general-purpose polyolefins to elevate performance toward engineering-plastic levels is a current focus of both industrial and academic research.

Cyclic olefin copolymers (COCs) are an innovative, newer class of polymers derived from cyclic olefin monomers and ethylene. Several commercial COC families exist, differing in monomer structures and polymerization methods [2]. References to COCs date back to the 1950s: vinylic polymerization of norbornene using Pd (II) catalysts was patented in 1967, followed by extensive studies with diverse metal catalysts. The first commercial COCs, produced via Ziegler–Natta catalysis, appeared in the late 1980s

Giulia Fredi and Norma Mallegni contributed equally to this work.

This is an open access article under the terms of the Creative Commons Attribution License, which permits use, distribution and reproduction in any medium, provided the original work is properly cited.
© 2026 The Author(s). *Advanced Functional Materials* published by Wiley-VCH GmbH

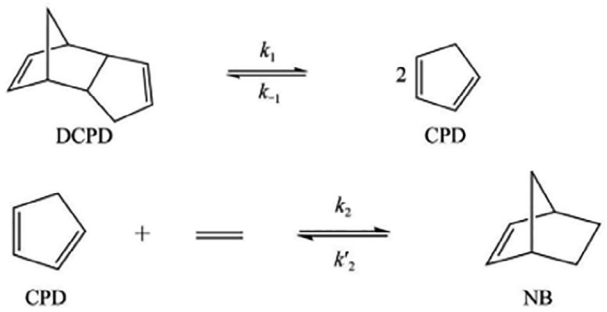


FIGURE 1 | Scheme of the synthesis of NB starting from DCPD.

[3]. Metallocene-based COCs emerged once suitable metallocene catalysts became available in the mid-1980s. These catalysts, which facilitate the incorporation of cyclic and linear olefins, enabled large-scale copolymerization of ethylene and norbornene (NB) [4]. In 1989, Kaminsky developed a metallocene-catalyzed process, particularly with zirconocene and half-sandwich titanium catalysts activated by methylaluminoxane (MAO), that yielded a perfectly transparent and highly rigid material [3, 5].

In general, COCs are produced by chain copolymerization of cyclic monomers such as 8,9,10-trinorborn-2-ene (norbornene) or 1,2,3,4,4a,5,8,8a-octahydro-1,4:5,8-dimethanonaphthalene (tetracyclododecane) with ethylene. For example, Ticona manufactures TOPAS COCs from NB (cyclic olefin) and ethylene, whereas Mitsui Chemicals uses tetracyclododecane to produce APEL COC [6–8].

Norbornene monomer synthesis is complex and poses engineering safety challenges, leading to long-term monopolies and high prices. Most accounts appear in patents spanning decades and lack systematic evaluation. A comprehensive review of the cracking of dicyclopentadiene (DCPD) to cyclopentadiene (CPD) and subsequent NB production (Figure 1) is provided by Li et al. [9].

Cyclic olefin polymers (COPs) are closely related to COCs and share many advantages, but differ in synthesis. COPs are prepared by ring-opening metathesis polymerization (ROMP) of cyclic monomers, followed by hydrogenation (e.g., Japan Synthetic Rubber's ARTON; Zeon Chemicals' ZEONEX and ZEONOR). Representative polymerization schemes for COCs and COPs are shown in Figure 2. Beyond synthesis, COPs typically exhibit higher moisture uptake, a more limited T_g range, higher cost due to more complex processing, and lower flowability than COCs, which restricts injection molding [8]. As with typical thermoplastics, COPs can lose strength and stability upon heating and show inferior resistance to organic solvents. To mitigate these issues, cross-linkable norbornenyl copolymers prepared via ring-opening metathesis polymerization (ROMP) have recently been developed to yield cyclic-olefin vitrimers with tunable cross-link density and thermo-mechanical properties [10]. However, a detailed analysis of COPs' synthesis and properties is beyond the scope of this review.

Different ethylene–norbornene copolymerizations processes have been reported using ordinary metallocenes, bridged zirconocenes, linked half-titanocenes (constrained-geometry

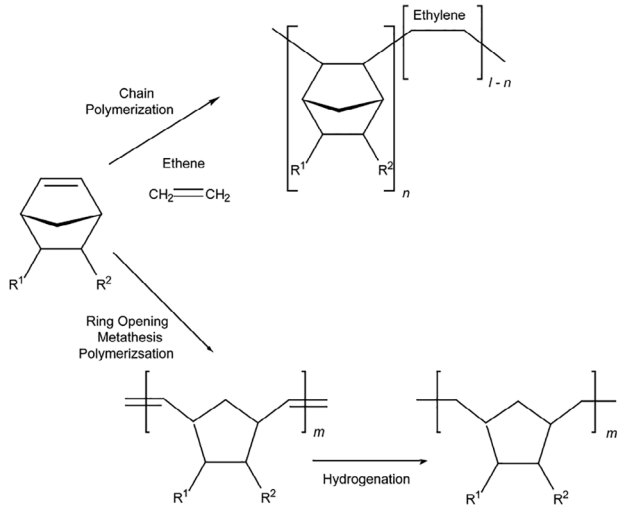


FIGURE 2 | Typical polymerization schemes for COCs and COPs (adapted with permission from [2]).

type), non-bridged half-titanocenes, and others [6]. Commercial COCs (e.g., TOPAS) produced with metallocene catalysts are ultrapure (suitable for advanced pharma packaging and food-contact films), crystal-clear (glass-like, amorphous), and high-barrier (resistant to moisture, alcohols, and acids).

The world's first commercial metallocene-based COC plant began operation in September 2000 in Oberhausen, Germany, with a capacity of 66 million lb/yr. Ethylene and cyclopentadiene were first reacted to form 2-norbornene (a bicyclic olefin), which was then copolymerized with ethylene to yield the final polymer. The resulting COC had a carbon main chain without double bonds [11]. Norbornene, being bulkier than ethylene and possessing a rigid bridged-ring structure, suppresses crystallization. Random incorporation into the main chain renders the COC fully amorphous. Norbornene also stiffens and strengthens the polymer and raises both T_g and heat-distortion temperature (HDT) in proportion to its incorporation [12]. As with thermal properties, mechanical performance depends on grade and comonomer ratio: higher NB content generally increases elastic modulus. Flowability (processability) can be tuned via molecular weight. Because bulky cyclic units are randomly or alternately attached to the backbone, the copolymer is amorphous and exhibits high T_g, optical clarity, low shrinkage, low moisture absorption, and low birefringence. Arndt et al. reported that COCs from alternating copolymerization with 14–37 mol% norbornene are completely amorphous, but some crystallinity appears at lower and higher incorporation, suggesting stereoregularity at those NB levels [13].

Extensive studies have correlated composition, structure, and thermal properties in ethylene–norbornene copolymers. In such systems, the statistics and stereoselectivity of norbornene insertion can be controlled through catalyst choice [14–16]. Efficient syntheses employ early transition-metal catalysts, including scandium, titanium, zirconium, and vanadium complexes [17–19]. The copolymer structure depends strongly on catalyst identity and geometry. Depending on a metallocene's ability to form blocks of cyclic units and to control stereoregularity within norbornene segments, copolymers with distinct properties are obtained [20]. Ethylene (E)/norbornene (N) copolymers can

16163028, 2026, 47, Downloaded from https://advanced.onlinelibrary.wiley.com/doi/10.1002/adfm.75610 by Cochrane France, Wiley Online Library on [16/10/2026]. See the Terms and Conditions (https://onlinelibrary.wiley.com/terms-and-conditions) on Wiley Online Library for rules of use; OA articles are governed by the applicable Creative Commons License

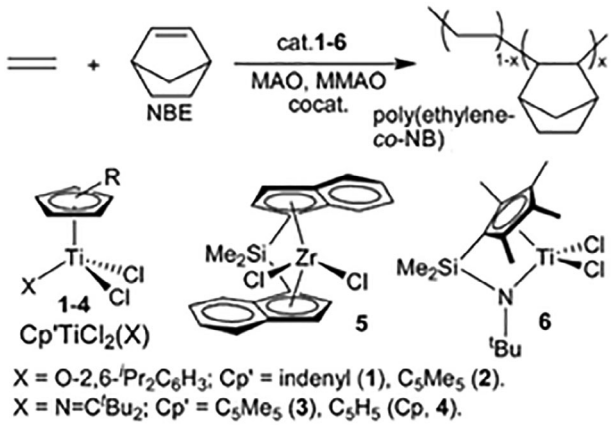


FIGURE 3 | Examples of synthesis of COCs by using non-bridged half titanocenes and other metallocenes and methylaluminoxane (MAO) cocatalyst. Reprinted with permission from [23].

display various sequence types: alternating (NENEN) or random sequences in blocks (isolated: EENEE; mesodyads: ENNE; longer blocks: ENNNE). Alternating copolymers are partially crystalline with melting points up to 320°C and the lowest T_g. Crystallinity decreases and disappears as norbornene content rises, and the copolymer becomes amorphous above ~14 mol% NB [5]. Nuclear magnetic resonance (NMR) studies show that COCs can be grouped into two chain-structure classes depending on composition: below 50 mol% NB, chains are mainly alternating while, above 50 mol%, chains contain repeating NB blocks of varying length with relatively low stereoregularity. All materials exhibit a single T_g that varies linearly with composition. Young's modulus, yield stress, and microhardness increase with NB content from 38 to 62 mol% [21, 22]. Although the copolymers studied by Scrivani et al. were thermorheologically simple, structural heterogeneity induced by varying NB content is expected to affect chain and segmental dynamics.

1.2 | Synthesis of High-T_g COCs

Despite progress, efficient syntheses of random, high-molecular-weight copolymers with high NB contents (>50 mol%) and high T_g (>150°C) remain limited [23]. This is because catalytic activity and molecular weight typically decline as NB content increases, and because achieving repeated NB insertion is challenging, leading to structures containing few NB repeats and significant alternating E–NB sequences. Nomura et al. reported an efficient route to high-molecular-weight random copolymers with high NB content using the non-bridged half-titanocene $CpTiCl_2(N = CtBu_2)$, as summarized in Figure 3.

Alternatively, late transition-metal catalysts (nickel [24–27] and palladium [28]) show great promise for ethylene–norbornene copolymerization (Figure 4). Since Goodall et al. first reported copolymerization of ethylene with polar norbornenes using classic nickel catalysts (I) [29], numerous Ni and Pd catalysts have been explored, including salicylaldimine (II), phenylimino-propanamido Ni (III), α-diimine Pd (IV), phosphine-sulfonate (V), β-diketiminato Ni (VI), anilino-anthraquinone Ni (VII), and anilino-naphthoquinone Pd (VIII). Recently, Liu et al. used a phosphine-sulfonate Pd catalyst (IX) for the copolymerization of ethylene with norbornene or polar norbornenes [30]. These catalysts perform exceptionally well, yielding copolymers with T_g values from 35°C to 127°C. They also copolymerize ethylene with polar norbornenes at high activity (up to 1.0×10^6 g·mol^{-1}·h^{-1}), high molecular weight (up to 200 kg·mol^{-1}), and high NB incorporation (up to 36.7 mol%).

To develop low-cost, high-performance catalysts for COCs, Zhang et al. synthesized bidentate pyridyl-amido hafnium complexes and applied them to ethylene–norbornene copolymerization [31]. These catalysts exhibited high activity (up to 16.3×10^6 g·mol^{-1}·h^{-1}) and produced copolymers with up to 50.3 mol% NB incorporation, T_g up to 184.3°C, and molecular weight up to 1.876×10^6 g·mol^{-1}. Bihun-Kisiel et al. reviewed vanadium complexes bearing diverse ligands for ethylene–norbornene copolymerization, analyzing how complex structure and reaction conditions affect activity and polymer properties [32].

1.3 | Synthesis of COCs With Higher Fracture Toughness

Although vinyl-addition copolymerization of cyclic olefins with ethylene is economically attractive, various synthetic strategies target alternative macromolecular architectures to overcome the brittleness of commercially available ethylene-based COCs [33]. For example, Wang et al. prepared heat-resistant, transparent COCs with bimodal molecular-weight distributions via one-pot reactive blending using two selective catalysts. The resulting ethylene/NB copolymers retained high T_g, balanced tensile properties, and high transparency [34].

Property enhancement strategies also include introducing comonomers such as α-olefins or substituted cyclic olefins to increase backbone repulsion [35, 36]. While this generally improves chain mobility and promotes substantial plastic deformation, it can also reduce tensile strength.

Very recently, Huang et al. presented the synthesis of COCs with ultra-high-molecular weight (UHMW), up to 2046 kDa, and relatively narrow molecular weight distribution (M_w/M_n <1.66), prepared through an efficient quasi-living catalytic system under mild polymerization conditions. Compared with traditional COCs with lower molecular weight but similar norbornene (NBE) incorporation, the prepared UHMW-COC showed a higher T_g, improved tensile strength (up to 73.5 MPa), elongation at break (6.8%), and impact strength (4.0 kJ·m^{-2}), lower wear rate and friction coefficient, and enhanced barrier properties [37]. In 2025, the same authors proposed the synthesis through quasi-living copolymerization of block-type COCs, composed of well-defined hard-soft and hard-soft-hard segments, with relatively high molecular weight (M_n > 200 kDa) and narrow molecular weight distribution (M_w/M_n < 1.42). Compared to random copolymers, di-block COCs showed superior tensile strength (56.2 MPa) and elongation at break (254%), while tri-block COCs, prepared with the same hard-soft segments and an additional hard segment, highlighted even better mechanical properties (tensile strength of 67.3 MPa, elongation at break of 287%, optical transmittance > 90%) [38]. Although NB/α-olefin copolymerization is attractive, α-olefin insertion after NB incorporation is difficult

16163028, 2026, 47, Downloaded from https://advanced.onlinelibrary.wiley.com/doi/10.1002/adfm.75610 by Cochrane France, Wiley Online Library on [16/10/2026]. See the Terms and Conditions (https://onlinelibrary.wiley.com/terms-and-conditions) on Wiley Online Library for rules of use; OA articles are governed by the applicable Creative Commons License

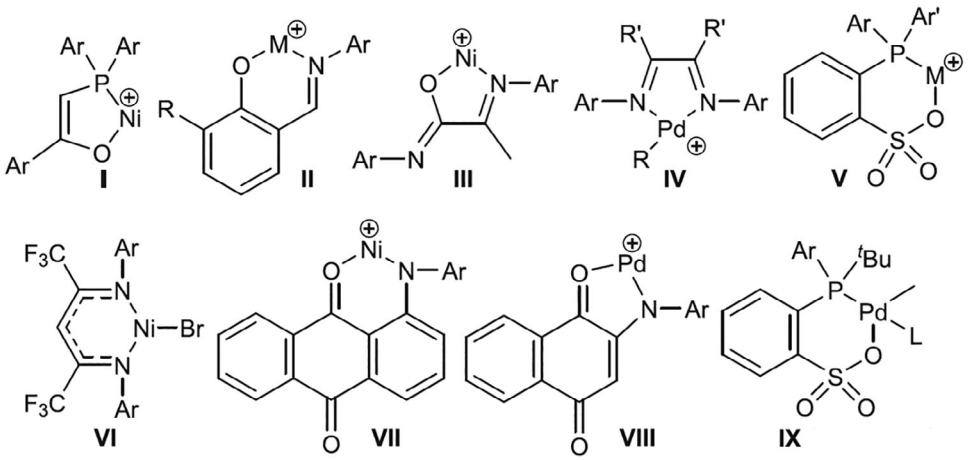


FIGURE 4 | Selected palladium and nickel catalysts for ethylene/norbornene copolymerization (M = Pd, Ni), (adapted with permission from [30]).

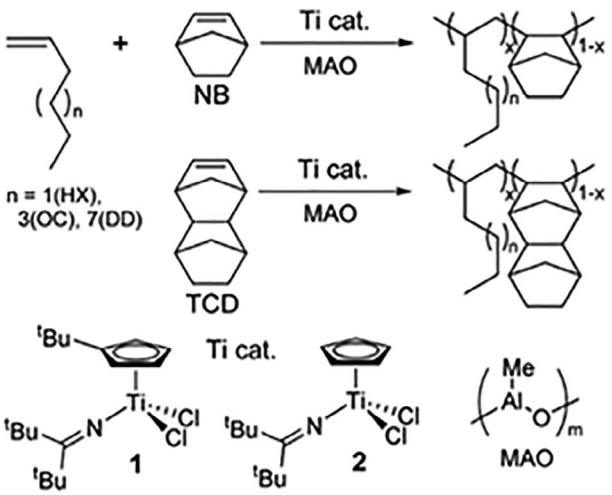


FIGURE 5 | Copolymerization of Norbornene (NB) and Tetracyclododecene (TCD) with α-Olefin (1-Hexene, 1Octene, 1-Dodecene) using two different kinds of half-titanocenes and MAO co-catalyst (reprinted with permission from [6]).

with linked-metallocene catalysts, as highlighted by Tritto and Boggioni [39, 40] and by Shiono et al. [41]. Indeed, catalytic activity and number-average molecular weight (M_n) decrease as α-olefin content increases in NB/1-octene copolymerization using $[H_2C(Me_2C_5H_2)_2]ZrCl_2$ (e.g., activity 200 kg polymer/mol-Zr·h, M_w = 8500, NB 65.6 mol%, T_g = 85°C) [42]. An exception is provided by fluorenyl-based linked half-titanocenes such as $[Me_2Si(fluorenyl)(NtBu)]TiMe_2$ (Flu-CGC), reported by Shiono et al., which produce copolymers of NBE with propylene and with α-olefins (1-hexene, 1-octene, 1-decene). Polymers from Flu-CGC exhibit narrow molecular weight distributions due to living characteristics in both NB and propylene polymerizations. However, activities are low, and α-olefin incorporation depends on ligand substituents and cocatalyst [43]. More recently, Zhao and Nomura studied NB and Tetracyclododecene (TCD) copolymerization with α-olefins (1-hexene, 1-octene, 1-dodecene) using half-titanocenes with MAO or MMAO [6, 44], chosen because of their effectiveness in ethylene copolymerizations [45]. The reaction scheme is shown in Figure 5. Apisuk et al. also synthesized high-T_g COCs via copolymerization of ethylene with TCD using $(tert\text{-}BuC_5H_4)TiCl_2$(N = $CtBu_2$)-MAO, achieving remarkable activities and efficient comonomer incorporation [46].

In a recent paper, Zhang et al. prepared ethylene/tetracyclododecene (E/TCD) copolymers with different TCD incorporations and molecular weight, synthesized by using two selective metallocene catalysts at different relative ratios. Upon the optimization of the catalyst concentration, the obtained COC exhibited optimal tensile strength (54.6 MPa) and elongation at break (5.0%). To further improve heat resistance and toughness, norbornene bearing soft alkyl tails was introduced as the third monomer to give E/TCD/nC-NB terpolymers. The introduction of flexible alkyl side chains improved the toughness of the polymer, with a 48% increase in elongation at break compared with the E/TCD copolymer, maintaining also excellent optical properties [47].

For NB/1-octene copolymerization in the presence of half-titanocenes and MAO, the resulting copolymers possess high molecular weights, unimodal molecular-weight distributions, and uniform compositions (i.e., no cross-linking), as confirmed by DSC thermograms.

Incorporating hydroxylated cyclic units into COCs enhances thermal properties, especially T_g, via hydrogen bonding among hydroxyl groups. Naga et al. investigated copolymerization of ethylene or propylene with various cyclodiolefins using zirconocene/MAO catalysts, followed by hydroboration to introduce hydroxyl groups into unsaturated cyclic units [48]. The T_g increased markedly by ~2.4–2.5 K per 1 mol% of hydroxylated cyclic units, irrespective of copolymer structure, and shape-memory behavior improved.

More recently, Tanaka et al. reported NB/1,5-hexadiene copolymerization using a fluorenylamido-ligated titanium catalyst [49]. The resulting copolymers bear pendant vinyl groups and remain soluble in various solvents even at >85% conversion, indicating negligible cross-linking. The T_g could be tuned from 79°C to >300°C by composition. Post-functionalization of pendant vinyl groups via Ru-catalyzed metathesis yielded

16163028, 2026, 47, Downloaded from https://advanced.onlinelibrary.wiley.com/doi/10.1002/adfm.75610 by Cochrane France, Wiley Online Library on [16/10/2026]. See the Terms and Conditions (https://onlinelibrary.wiley.com/terms-and-conditions) on Wiley Online Library for rules of use; OA articles are governed by the applicable Creative Commons License

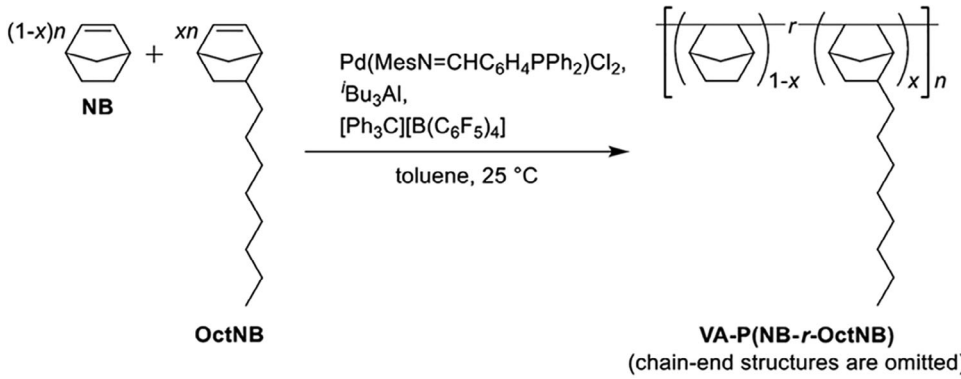


FIGURE 6 | Palladium (II)-catalyzed vinyl-addition copolymerization of norbornene (NB) and 5octyl-2-norbornene (OctNB) (adapted with permission from [33]).

fluoroalkyl-functionalized COCs with increased hydrophobicity (higher contact angle). Song et al. synthesized hydroxy-functionalized COCs with high activity and controlled hydroxyl content (≈17.1 mol%) using an ansa-dimethylsilylene(fluorenyl)(amido)titanium complex [50].

Very recently, Chae et al. produced NB-based COCs with high M_n (>10^3 kDa) via Pd(II)-catalyzed vinyl-addition copolymerization of NB and 5-octyl-2-norbornene (OctNB), aiming to improve fracture resistance through entanglement-network formation (Figure 6) [33]. Tensile tests showed increased toughness and elongation at break up to M_n = 680 kDa, effectively decoupling stiffness from brittleness.

An additional approach by Dong et al. examined ethylene–dicyclopentadiene–styryl terpolymerization catalyzed by fluorene-methylene-pyridine scandium complexes. The terpolymers exhibited higher elongation at break and breakdown voltage than ethylene/DCPD copolymers while retaining similar optical properties and tensile strength [51]. Aiming at increasing the fracture toughness through the insertion of large amounts of cyclic comonomers in COCs, Gao et al. investigated the synthesis of COCs containing both linear polyethylene and poly(ethylene-co-norbornene) segments, prepared from chain shuttling copolymerization of ethylene and norbornene by using two different kinds of *ansa*-metallocene catalysts.

The prepared multiblock copolymers presented much improved transparency, mechanical properties, and processability [52, 53].

1.4 | Synthesis of COCs With Higher Thermal Stability

Exploration of new polycyclic fused norbornenes for COCs and COPs with enhanced thermal stability has been limited, largely because bulky *endo*-substituents at NB 5,6-positions hinder polymerizability [54–56]. Hong et al. reported COCs with high T_g, good mechanical performance, high transparency, and excellent film-forming ability via effective copolymerization of ethylene with a bulky cyclic olefin prepared in good yield by Diels–Alder reaction [57]. More recently, Funahashi et al. synthesized NB-based monomers bearing *exo*-fused polycyclic rings and a bridgehead tertiary carbon linked to another cyclic moiety, enabling addition homopolymerization and copolymerization with 1-octene using (tBuNSiMe$_2$Flu)TiMe$_2$ [58] (Figure 7).

Nomura's recent review on non-bridged half-titanocene catalysts describes amorphous COCs produced by ethylene or propylene copolymerization not only with NB and TCD, but also with low-strain cyclic olefins – cyclopentene (CPE), cyclohexene (CHE), cycloheptene (CHP), and cyclooctene (COE) [59] (Figure 8a). As with NB and TCD systems, the T_g varies linearly with the content of low-strain cyclic olefins. The T_g also depends on ring size: introducing an additional ring into cyclohexene (e.g., tricycloundecene, TCUE) increases the T_g (Figure 8b). The same trends hold for amorphous propylene copolymers with low-strain cyclic olefins, though T_g values are higher than those of the corresponding ethylene copolymers at low cyclic-olefin contents (≤25 mol%) [60].

Zhang et al. reported the design of low-cost and high-performance COCs, constituted by ethylene copolymers with dicyclopentadiene (DCPD), synthesized using four different kinds of metallocene complexes activated with [Ph$_3$C][B(C$_6$F$_5$)$_4$] and ^{i}Bu$_3$Al. ^{1}H-and ^{13}C-NMR spectra showed that ethylene/DCPD copolymerization occurred via enhancement of the norbornene ring, leading to random sequence distributions. Compared with ethylene/norbornene and ethylene/tetracyclicdodecene copolymers, these novel ethylene/DCPD copolymers highlighted excellent optical transparency, mechanical properties, and dimensional stability [61].

2 | COC-Based Blends

2.1 | COC/Polyolefin Blends

Preparation of polymer blends is one of the most cost-effective strategies for upgrading existing polymers. Because of its olefinic character, COC is expected to be compatible with polypropylene (PP) and other polyolefins. Since the potential applications of polymeric materials are largely determined by their mechanical performance, understanding the relationship between morphology (phase structure) and physical properties of the intended blends is essential. Polypropylene (PP) in particular exhibits relatively low modulus, yield strength, and creep resistance. Therefore, the search for "reinforcing" polymeric components

16163028, 2026, 47, Downloaded from https://advanced.onlinelibrary.wiley.com/doi/10.1002/adfm.75610 by Cochrane France, Wiley Online Library on [16/10/2026]. See the Terms and Conditions (https://onlinelibrary.wiley.com/terms-and-conditions) on Wiley Online Library for rules of use; OA articles are governed by the applicable Creative Commons License

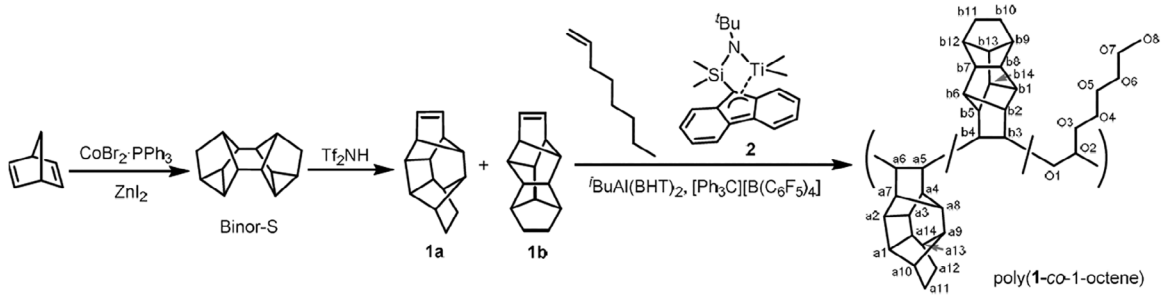


FIGURE 7 | Synthesis of NB-based monomers with *exo*-fused polycyclic rings (1a,1b) and addition homopolymerization and copolymerization with 1-octene catalyzed by (^{t}BuNSiMe$_2$Flu)TiMe$_2$ (2) (reprinted with permission from [58]).

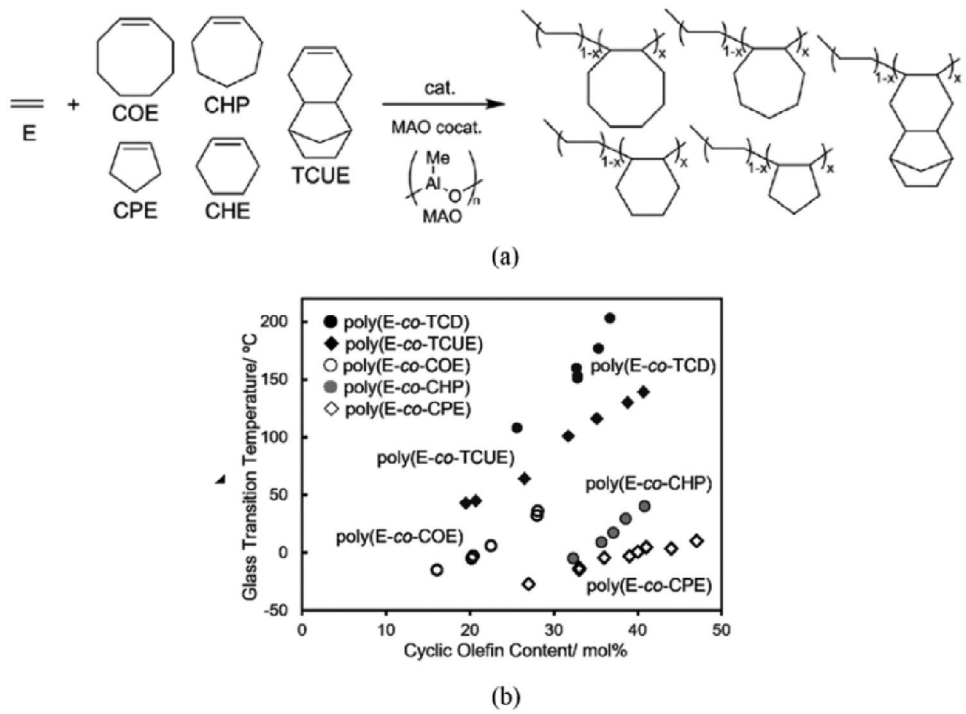


FIGURE 8 | (a) Ethylene copolymerization with low strained cyclic olefins, (b) relationship between T_g values and cyclic olefin content in the ethylene-cyclic olefin copolymers (reprinted with permission from [59]).

that can be readily blended with PP is of great interest. However, producing such blends without compatibilizers is often challenging, as PP generally shows limited compatibility with other polymers. For this reason, PP/COC blends have been extensively studied in the literature [62–71].

Šlouf et al. characterized the phase morphology of PP/COC polymer blends prepared by injection molding using scanning electron microscopy (SEM) and scanning transmission electron microscopy (STEM), to improve PP properties by forming a COC co-continuous phase that could impart higher stiffness, yield stress, and barrier properties to the PP matrix [65]. Interestingly, all studied blends exhibited a fibrillar morphology within a COC concentration range of 10–75 wt.%. Up to 30 wt.% COC, the PP matrix contained COC fibers whose average diameter increased with increasing COC content. In the 60/40 blend, the COC component formed both fibers and elongated domains with embedded PP fibers. The 50/50 blend displayed co-continuous COC and PP phases, each containing fibers of the other polymer. In the 25/75 blend, PP fibers were embedded within the COC matrix. In all compositions, the fibers exhibited aspect ratios above 20, were oriented along the injection direction, and acted as reinforcing components (see Figure 9). The tensile, dynamic, and creep behavior of these blends was subsequently investigated and modeled in detail [62, 63, 67].

Vackova et al. applied a similar experimental approach and demonstrated that the fibrous COC morphology in injection-molded PP/COC blends led to a statistically significant improvement in yield strength compared with compression-molded specimens exhibiting a particulate morphology [69].

Pimbert et al. investigated the crystallization behavior and morphology of isotactic PP blended with amorphous COC, revealing a phenomenon of fractionated crystallization when PP was finely dispersed within the COC matrix. The thermal properties and

16163028, 2026, 47, Downloaded from https://advanced.onlinelibrary.wiley.com/doi/10.1002/adfm.75610 by Cochrane France, Wiley Online Library on [16/10/2026]. See the Terms and Conditions (https://onlinelibrary.wiley.com/terms-and-conditions) on Wiley Online Library for rules of use; OA articles are governed by the applicable Creative Commons License

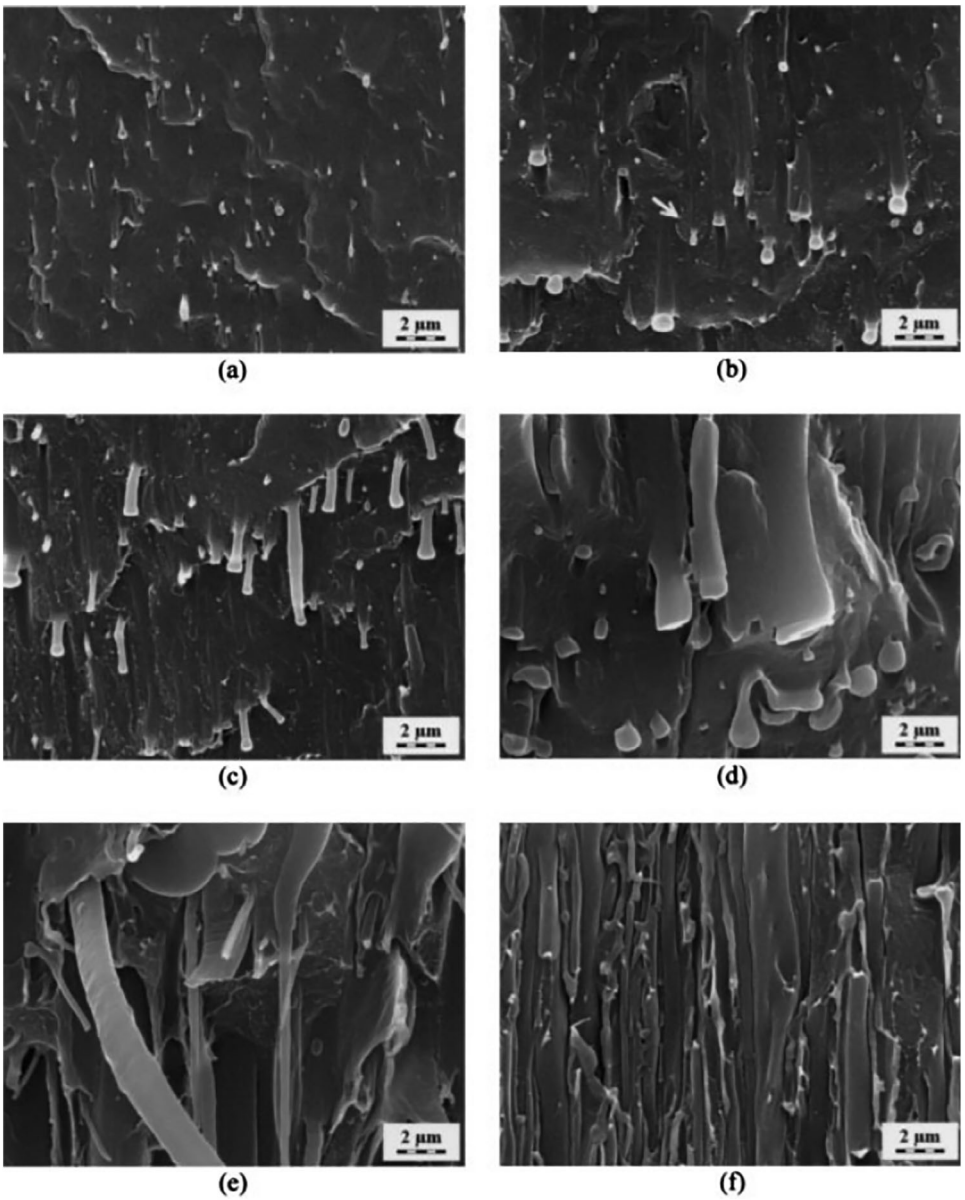


FIGURE 9 | SEM micrographs of the fracture surfaces (parallel to the injection direction) of PP/COC blends at different relative compositions. (a) 90/10, (b) 80/20, (c) 70/30, (d) 60/40, (e) 50/50, and (f) 25/75 (reprinted with permission from [65]).

morphologies of these blends aligned well with classical models of immiscible systems, including homogeneous nucleation within droplets to explain delayed PP crystallization [64, 66]. Using the Wide angle X-ray spectroscopy (WAXS), Gopanna et al. further showed that the incorporation of COC into PP modified its crystal structure without inducing new chemical reactions. The mechanical, dynamic mechanical, rheological, and morphological properties of PP/COC blends were also extensively characterized. Increasing the fraction of stiff COC enhanced tensile and flexural strength and modulus, while decreasing elongation at break and impact energy [70, 71].

Kolarik et al. prepared high-density polyethylene (HDPE)/COC blends at various compositions to obtain polyolefin materials with increased stiffness, yield, and tensile strength, correlating phase structure with dynamic, tensile, creep, and impact behavior [72, 73]. They observed sharp reductions in strain at break, tensile energy to break, and impact strength between 15% and 25 wt.% COC, where COC formed a brittle co-continuous phase. A further increase in the COC fraction reduced the ultimate properties to those typical of brittle polymers. However, tensile impact strength exhibited a local maximum at HDPE/COC = 25/75, likely corresponding to COC toughened with HDPE particles.

Lamnawar et al. examined the rheological and morphological properties of melt-blended linear lowdensity polyethylene (LLDPE)/COC systems containing 5–15 vol% COC, revealing partial phase miscibility and compatibility [74]. Dorigato et al. extended this work up to 80 vol% COC [75]. SEM revealed qualitative interfacial adhesion between LLDPE and COC, as supported by increased crystallinity and an elevated COC glass-transition temperature with increasing LLDPE fraction. As the COC content increased, the blends showed higher impact load capacity but reduced ductility. A marked reduction in

16163028, 2026, 47, Downloaded from https://advanced.onlinelibrary.wiley.com/doi/10.1002/adfm.75610 by Cochrane France, Wiley Online Library on [16/10/2026]. See the Terms and Conditions (https://onlinelibrary.wiley.com/terms-and-conditions) on Wiley Online Library for rules of use; OA articles are governed by the applicable Creative Commons License

creep compliance was also observed for COC contents above 20 wt.%.

Vackova et al. also produced HDPE/COC blends using an optimized process that yielded a fibrous COC morphology [76]. A pronounced improvement in both macro- and micromechanical properties of the HDPE matrix was achieved due to the reinforcing effect of oriented COC fibers. Combined SEM, tensile, and microhardness data, together with Equivalent Box Model (EBM) calculations, indicated unusually high interfacial adhesion and partial miscibility. The strong HDPE/COC interface, along with fibrous morphology, resulted in significant increases in elastic modulus and specific energy to break.

More recently, Zhang et al. demonstrated that combining COC with LLDPE via melt blending produced insulation materials with low dielectric constants, low coefficients of thermal expansion (CTE), and low density, i.e., suitable for communication, control, and signal cable applications [77]. Specifically, at 20 wt.% COC, the dielectric constant and CTE reached minima of 2.23 (at 1000 Hz) and 1.2×10^{-4} K^{-1}, respectively. The blend density increased by only 1.6% compared with LLDPE, while the tensile modulus rose by 56%, indicating enhanced mechanical strength with minimal weight penalty.

The incorporation of ethylene-vinyl acetate copolymer (EVA) in polyolefin blends and composites has been also technologically important. Because of its low-temperature flexibility, rubber-like behavior, low permeability, easy processing, and good impact strength, EVA is attractive as a toughening agent for polyolefins and has thus been explored in COC blends. Jafari et al. investigated the morphology and rheology of COC/EVA systems and found that the blends were biphasic but exhibited partial compatibility and miscibility at low EVA contents [78]. These blends showed a positive deviation from the rule of mixtures, suggesting strong interfacial interaction between COC and EVA. Durmus et al. prepared COC/EVA films using twin-screw extrusion and found that EVA additions (5–30 wt.%) increased the melt strength of COC, improving film-processing stability without significantly reducing transparency [79].

2.2 | COC/Elastomer Blends

Enhancing the toughness of optical plastics such as COC is technically challenging due to conflicting performance requirements. To improve toughness, several studies explored COC blends with elastomers. Rubber particles, when homogeneously dispersed, can act as cavitation centers during deformation, enhancing fracture resistance while maintaining transparency. Khanarian et al. produced transparent, rubber-toughened COC blends by incorporating styrene-butylene-styrene (SBS) elastomeric particles compatibilized with a refractive-index-matched styrene-ethylene-butylene-styrene (SEBS) copolymer [80]. The Izod impact strength increased to 50 $J \cdot m^{-1}$ while keeping haze below 5% at 5 wt.% elastomer loading. Opaque blends with toughness exceeding 500 $J \cdot m^{-1}$ were achieved at 20 wt.%. Chai et al. more recently tuned COC toughness via simultaneous addition of SBS and SEBS at various ratios, showing that these elastomers mitigated COC brittleness without compromising stiffness or moisture resistance [81].

Similarly, Doshev et al. modified COC with an ethylene-1-octene copolymer (EOC), a thermoplastic elastomer of the polyolefin family. Since both COC and EOC contain ethylene sequences, favorable interactions were expected [82]. By exploiting the EOC's ability to crosslink under peroxide treatment, selective crosslinking during blending produced reactive blends with improved compatibility. These systems displayed complete phase separation with a matrix-droplet morphology, shifting to a co-continuous structure between 25–70 wt.% COC. Peroxide addition enhanced interfacial adhesion, refined morphology, and improved mechanical performance for reactive blends with 30–60 wt.% EOC. A similar system was later examined by Pei et al. [83]. Khonadar et al. also studied COC/polyolefin elastomer (COC/POE) blends over the full composition range, characterizing viscoelastic behavior in both melt and solid states through combined experimental and theoretical approaches [84]. These blends were again found to be immiscible. More recently, the viscoelastic and morphological behavior of COC blends with polyhexene-1 (PH-1), an amorphous elastomeric polyolefin, was investigated (see Figure 10a) [85]. Rheological Cole–Cole plots and viscosity–composition data confirmed immiscibility (see Figure 10b). At low PH-1 concentrations, the blends displayed droplet–matrix morphology, transitioning to co-continuous structure at intermediate compositions. The same group further examined COC blends with a polyolefin elastomer containing 33 mol% 1-butene comonomer, reporting comparable results [86].

2.3 | COC-Based Blends for Specific Technological Purposes

Several additional studies have explored COC blends with other polymer matrices for specific technological purposes. Cheng et al. developed polyimide (PI)/COC blends for flexible printed circuit boards by grafting COC with maleic anhydride (MA) to improve dispersion within the PI matrix [87]. Reaction between amine groups of poly(amic acid) and anhydride groups of MA-grafted COC produced a network structure, enhancing thermal properties (T_g and decomposition temperature) compared to neat PI. Nazir et al. blended poly(L-lactic acid) (PLLA) with 5–30 wt.% COC by solvent casting to overcome PLLA's brittleness and low melt strength for bone-tissue engineering [88]. SEM images showed miscible blends up to 20 wt.% COC. These blends exhibited improved compressive modulus and tensile strength over neat PLLA and showed excellent cytocompatibility with preosteoblasts and bone-marrow stem cells.

In recent years, various efforts have also focused on blending COC with polymers such as epoxy resin and polyamide 6 to develop multifunctional, self-healing matrices for structural composites offering longer service life and enhanced environmental sustainability (see Section 7.5) [89–96].

3 | COC-Based Nanocomposites

Polymer matrix nanocomposites have attracted increasing attention in recent years as novel materials, since the incorporation of inorganic nanoparticles into a polymer matrix can markedly enhance its physical properties, such as stiffness,

16163028, 2026, 47, Downloaded from https://advanced.onlinelibrary.wiley.com/doi/10.1002/adfm.75610 by Cochrane France, Wiley Online Library on [16/10/2026]. See the Terms and Conditions (https://onlinelibrary.wiley.com/terms-and-conditions) on Wiley Online Library for rules of use; OA articles are governed by the applicable Creative Commons License

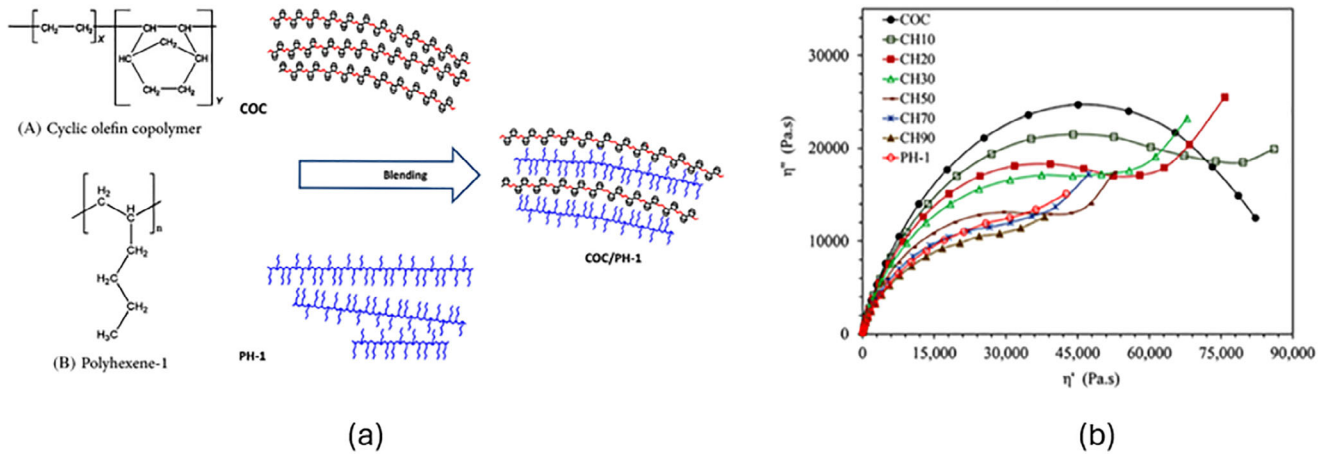


FIGURE 10 | Molecular structure of cyclic olefin copolymer (COC), polyhexene-1 (PH-1) and the relative blends. Cole–Cole plots from rheological tests on COC/PH-1 blends at 230°C (reprinted with permission from [85]).

tensile strength, dimensional stability, thermal degradation resistance, and chemical durability, while reducing gas and solvent permeability. Remarkably, these property improvements can be achieved at very low filler contents (typically 5–10 wt.%), thereby avoiding the common drawbacks associated with conventional inorganic fillers, such as embrittlement, opacity, and increased density [97]. Considering that thermoplastic polymers synthesized via metallocene-based catalysts have recently gained considerable interest among researchers and manufacturers, several studies over the past two decades have focused on the preparation and characterization of COC-based nanocomposites.

3.1 | COC-Based Nanocomposites Filled With Nanoparticles

Numerous papers have reported the development of COC composites filled with various types of nanoparticles. In particular, attention has been given to COC-based nanocomposites reinforced with silica nanofillers. Ou et al. prepared COC/SiO_2 nanocomposites by solution blending with surface-treated nanoparticles at concentrations ranging from 0.5 to 10 wt.% [98, 99]. The glass transition temperature and degradation resistance of these composites increased with silica content, while water and oxygen permeabilities of samples containing 10 wt.% organomodified SiO_2 were 32% and 36% lower than those of neat COC, respectively. Roy et al. fabricated fumed nanosilica/COC composites by melt blending and observed a significant increase in tensile strength and T_g at a nanofiller content of 3 vol% [99]. The addition of nanosilica also enhanced stiffness and hardness, improving scratch resistance and reducing the friction coefficient. Interestingly, UV–visible spectroscopy revealed that the nanocomposites retained optical transparency comparable to that of neat COC films.

Dorigato et al. prepared COC/fumed silica nanocomposites via melt compounding to study the influence of filler surface area on the thermo-mechanical and optical behavior of the resulting materials [100]. Thermogravimetric analysis showed that silica nanoparticles improved thermal degradation resistance, as the decomposition temperature increased by about 40°C compared to the unfilled matrix. Dynamic mechanical thermal analysis and tensile tests revealed a slight stiffening effect proportional to nanofiller surface area, without any loss in fracture toughness. Notably, the original transparency of neat COC was maintained at 2 vol% silica. The same authors also produced COC/SiO_2 nanocomposite foams using supercritical carbon dioxide, varying the silica content (1–5 vol%) and foaming pressure (90–150 bar) [101]. Foam density decreased with increasing pressure, while silica addition led to slightly denser structures. SEM and TEM analyses showed that silica aggregates became elongated along cell walls during foaming (see Figure 11). Mechanical testing demonstrated that nanosilica improved stiffness, strength, and creep stability of the matrix at all foaming pressures.

In another study, the same authors investigated COC/polyhedral oligomeric silsesquioxane (POSS) nanocomposites prepared by melt compounding [102]. The resulting materials retained optical transparency up to 5 wt.% nanofiller, whereas higher loadings led to the formation of a crystalline phase, as confirmed by X-ray diffraction (XRD), due to nanoparticle agglomeration. Differential scanning calorimetry (DSC) and thermogravimetric analysis (TGA) analyses revealed a decrease in T_g and stiffness, attributed to the formation of a soft interphase at the polymer–particle boundary caused by the isobutylic groups of the POSS nanoparticles.

More recently, Petrella et al. dispersed organically capped CdSe and (CdSe)ZnS core–shell colloidal nanocrystals (NCs) into COC, and deposited the resulting nanocomposites as thin films by spin coating [103]. Optical analysis indicated that incorporating luminescent (CdSe)ZnS NCs into COC could enable the fabrication of novel optical components via nanoimprint lithography. Wang et al. subsequently synthesized Sr_2CeO_4@SiO_2 core–shell nanoparticles by a sol–gel method and incorporated them into a COC matrix to produce high-frequency thermoplastic substrates with low dielectric loss [104]. With 20 vol% filler, the nanocomposites exhibited a dielectric constant of 3.5, thermal conductivity of 0.9 $W \cdot m^{-1} \cdot K^{-1}$, and a low thermal expansion coefficient (37.7 ppm $°C^{-1}$), while maintaining good moisture

16163028, 2026, 47, Downloaded from https://advanced.onlinelibrary.wiley.com/doi/10.1002/adfm.75610 by Cochrane France, Wiley Online Library on [16/10/2026]. See the Terms and Conditions (https://onlinelibrary.wiley.com/terms-and-conditions) on Wiley Online Library for rules of use; OA articles are governed by the applicable Creative Commons License

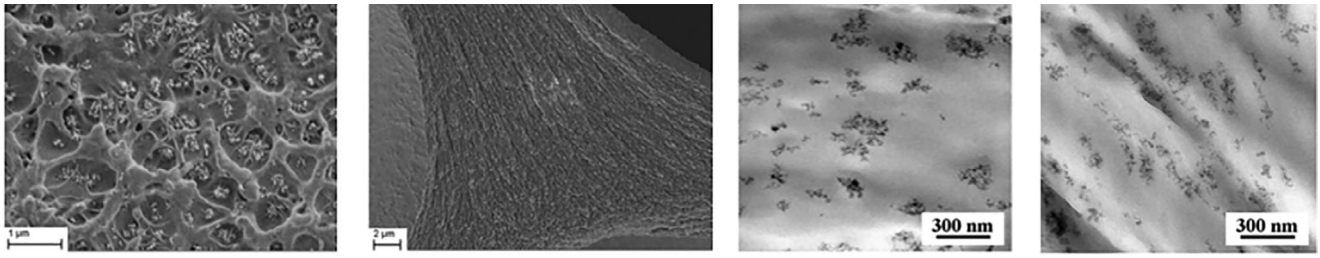


FIGURE 11 | Morphology of COC/SiO_2 nanocomposite (silica content = 3 vol%). (a) FESEM and (b) TEM images of the bulk sample, (c) FESEM and (d) TEM images of the foam prepared with a pressure of 150 bar (adapted with permission from [101]).

resistance and dimensional stability. Similarly, Ionete et al. explored the dielectric, electrical, and mechanical properties of COC/alumina composites across a wide temperature range, including cryogenic conditions down to 125 K [105]. Composites containing 10–50 wt.% Al_2O_3 displayed enhanced electrical conductivity while retaining processable viscosity levels, demonstrating their potential for high-frequency applications even at cryogenic temperatures.

Other studies have reported COC nanocomposites incorporating TiO_2 [106] and hydroxyapatite (HA) nanoparticles [107, 108]. For example, HA nanoparticles with diameters equal to 60 ± 20 nm were synthesized and dispersed (concentration equal to 1–30 wt.%) into COC using sodium dodecyl sulfate (SDS) as a coupling agent to improve dispersion and interfacial adhesion, producing hybrid composites suitable for bone-tissue engineering. The compressive modulus and strength increased by approximately 140% and 185%, respectively, while cell adhesion and proliferation were enhanced ninefold and threefold after one day of culture with preosteoblasts, confirming excellent cytocompatibility.

3.2 | COC-Based Nanocomposites Filled With Nanotubes

Comparatively, less attention has been given to COC-based nanocomposites containing nanotubes. In 2012, Chen et al. prepared COC nanocomposites with two types of multiwalled carbon nanotubes (MWCNTs) of different aspect ratios and found that CNT addition markedly improved thermo-oxidative stability and DC conductivity (by more than 10^9 times at 2 wt.% CNTs) [109]. More recently, a blend of COC and polyolefin elastomer (POE) filled with MWCNTs exhibited a co-continuous morphology for 40–60 wt.% COC, with nanotubes localized within the POE phase and at interfacial regions [110]. Electrical and rheological percolation thresholds occurred at 1 wt.% and 0.5 wt.% CNT, respectively, and maximum conductivity (10^{-5} $S{\cdot}cm^{-1}$) was achieved at 3 wt.%. Pal et al. investigated the thermo-mechanical properties of COC nanocomposites containing organically modified halloysite nanotubes (mHNTs) compatibilized with maleic-anhydride-grafted polyethylene (MA-g-PE) [111]. The modification of HNTs enhanced dispersion and interfacial bonding, improving composite performance, while MA-g-PE acted as a bridging compatibilizer between the polar nanofiller and the nonpolar COC (see Figure 12).

3.3 | COC-Based Nanocomposites Filled With Lamellar Nanofillers

The greatest research attention, however, has focused on COC-based nanocomposites with lamellar nanofillers. Wu et al. prepared COC/layered silicate nanocomposites by intercalating COC chains into organically modified layered silicates via solution mixing [112]. XRD and TEM analyses indicated that most silicate layers were disorderedly intercalated within the COC matrix. These nanocomposites showed improved storage modulus and reduced water permeability relative to neat COC. Plasma treatment further modified surface properties, rendering the films hydrophilic as evidenced by a decrease in water contact angle.

Several studies have also reported COC nanocomposites filled with conductive lamellar carbonaceous nanofillers, such as exfoliated graphite nanoplatelets and graphene. In 2012, Kaşgöz et al. investigated the morphology and rheology of COC nanocomposites prepared by twin-screw extrusion with graphite (G) and expanded graphite (EG) fillers at various loadings [113, 114]. SEM revealed that pristine graphite retained its stacked structure, while EG was well-dispersed within COC, forming three-dimensional "house-of-cards" networks without compatibilizers. Rheological percolation thresholds were approximately 21.5 phr for G and 3.8 phr for EG. In a subsequent study, the same authors showed that the simultaneous addition of carbon fibers (CF) and EG increased electrical conductivity relative to single-filler systems, due to the formation of additional conduction pathways between CF rods and EG sheets [115]. They later compared COC nanocomposites with different carbon fillers, highlighting the crucial influence of filler aspect ratio on processability and conductivity of the resulting materials [113, 114].

Lai et al. fabricated transparent COC/thermally reduced graphene oxide (TRGO) composite films exhibiting excellent water-vapor barrier properties [116]. With only 0.06 wt.% (0.028 vol%) TRGO, water vapor permeability was reduced by 21%, while high transparency and flexibility were preserved. Following thermal annealing and surface modification, permeability decreased by 65%. More recently, Dorigato et al. produced electrically conductive COC/exfoliated graphite nanoplatelet (xGnP) foams via supercritical CO_2 processing, starting from unfoamed nanocomposites [117, 118]. For both bulk and foamed materials, xGnP incorporation enhanced thermal stability, storage modulus, and T_g across all foaming pressures. While nanofiller addition significantly reduced electrical resistivity

16163028, 2026, 47, Downloaded from https://advanced.onlinelibrary.wiley.com/doi/10.1002/adfm.75610 by Cochrane France, Wiley Online Library on [16/10/2026]. See the Terms and Conditions (https://onlinelibrary.wiley.com/terms-and-conditions) on Wiley Online Library for rules of use; OA articles are governed by the applicable Creative Commons License

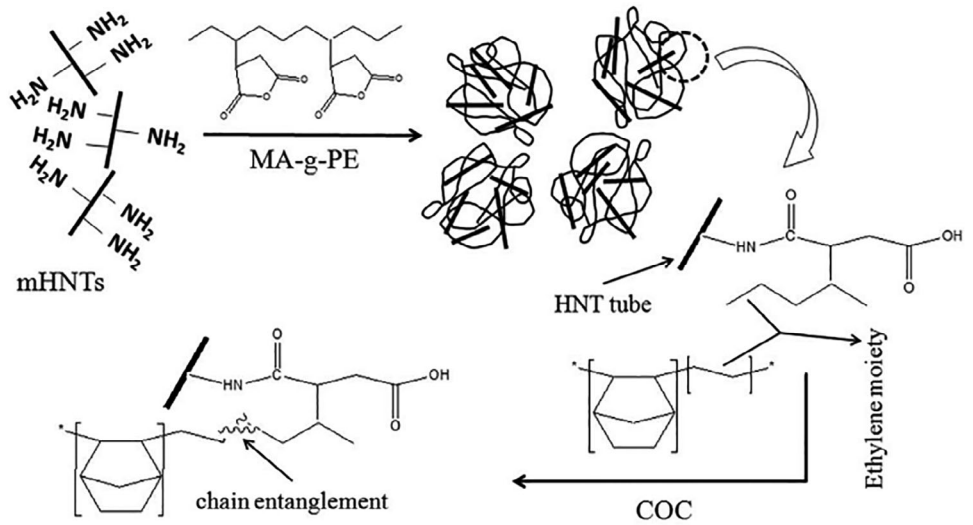


FIGURE 12 | Formation mechanism of COC/mHNTs nanocomposites compatibilized with MA-g-PE (reprinted with permission from [111]).

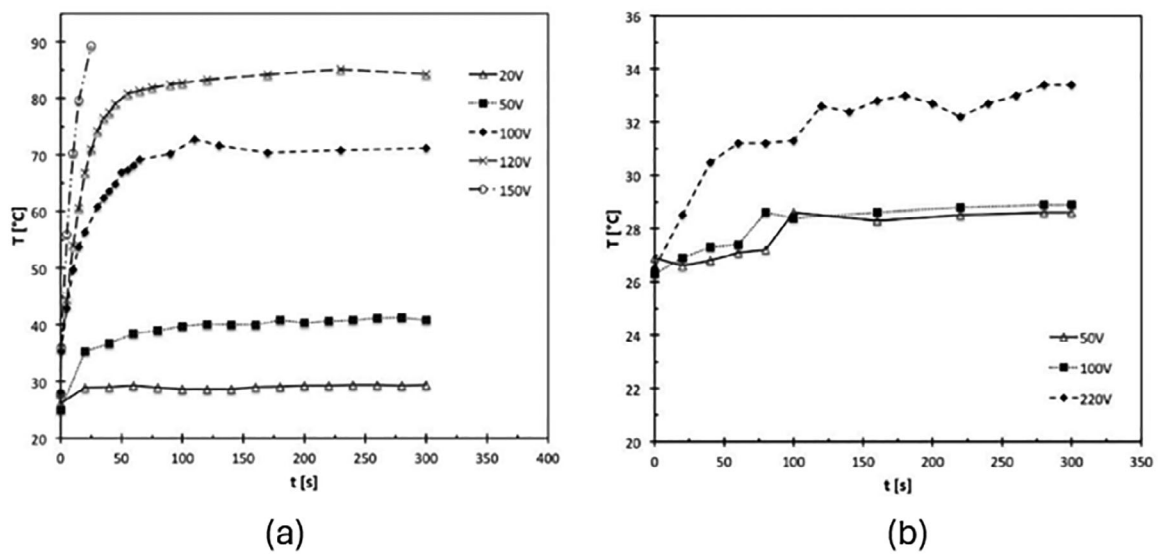


FIGURE 13 | Evolution of the surface temperature with time of COC/xGnP nanocomposite at different applied voltages (xGnP content = 20 wt.%). (a) Bulk sample, (b) sample foamed at a pressure of 150 bar (reprinted with permission from [118]).

in bulk samples, foaming disrupted conductive pathways, increasing resistivity. Surface heating tests under voltage application showed that bulk materials exhibited substantial temperature rises at low voltages, whereas foamed samples displayed more moderate heating (see Figure 13).

4 | Functionalized Cyclic Olefin Copolymers

Controlled functionalization strategies have become central to expanding the utility of COCs toward advanced functional materials to overcome some intrinsic limitations, such as brittleness due to their structural rigidity, low surface polarity, and limited interfacial compatibility.

Two overarching approaches have dominated the functionalization of COCs: (i) incorporation of precursor comonomers during coordination polymerization that enable post-polymerization conversion to polar groups, and (ii) direct copolymerization with functionalized cyclic olefins or reactive dienes that introduce latent or active functional handles. A critical design challenge is maintaining high molecular weight ($M_n \geq 10^4$–10^5 g·mol^{-1}) and narrow molecular weight distributions (explicit dispersity (Đ) $\lesssim$ 2), as these parameters directly determine mechanical integrity, processability, and optical homogeneity.

A notable precursor strategy employs organoaluminum-functional α-olefins as masked polar comonomers. In this methodology, norbornene was copolymerized with 7-octenyldiisobutylaluminum (ODIBA) using ansa-dimethylsilylene(fluorenyl)(t-butylamido)dimethyltitanium activated by $Ph_3C[B(C_6F_5)_4]$, followed by CO_2 insertion and protic workup to generate carbonyl functionalities [119]. Under optimized conditions involving excess borate and

16163028, 2026, 47, Downloaded from https://advanced.onlinelibrary.wiley.com/doi/10.1002/adfm.75610 by Cochrane France, Wiley Online Library on [16/10/2026]. See the Terms and Conditions (https://onlinelibrary.wiley.com/terms-and-conditions) on Wiley Online Library for rules of use; OA articles are governed by the applicable Creative Commons License

triisobutylaluminum scavenger, polymer yields reached 0.89 g with M_n up to 3.41×10^5 g·mol^{-1} and M_w/M_n as low as 1.46. Importantly, functional group incorporation was controlled within 0–1.8 mol% without catastrophic chain transfer or broadening of dispersity. Even this modest functionalization substantially altered surface properties: water contact angles decreased from 104° for unmodified COC to 89° at 1.8 mol% carboxyl content [119]. Such fine-tuned polarity modulation is highly relevant for adhesion layers, coatings, and biointerfaces where transparency and thermal stability must be preserved.

Reactive diene terpolymerization offers an alternative route to functional COCs with tunable backbone unsaturation. Vanadium-catalyzed terpolymerization of ethylene, α,ω-dienes (1,5-hexadiene or 1,7-octadiene), and cyclic olefins such as norbornene produced high-molecular-weight reactive polyolefins (M_w up to 2.0×10^5 g·mol^{-1}) with unimodal molecular weight distributions and subambient T_g values between −30 and −3°C [120]. Detailed NMR analysis revealed controlled insertion pathways generating methylene-1,3-cyclopentane (MCP) and vinyl-tetramethylene (VTM) units, with unsaturation preserved in pendant side chains. Subsequent thiol–ene addition enabled introduction of polar groups, including thioglycolic acid derivatives and N-acetyl-L-cysteine. This strategy effectively decouples polymer backbone formation from functional group installation, allowing precise post-polymerization control of polarity and cross-link density.

Building upon this concept, dynamically cross-linked polyolefin elastomers were synthesized by grafting <2.0 mol% thiol-derived functional groups onto reactive COC-type backbones [121]. Hydrogen bonding between amide and hydroxyl functionalities generated reversible supramolecular cross-links that dramatically enhanced mechanical performance. The resulting materials exhibited fracture strengths up to 10.2 MPa and toughness values up to 22.6 MJ·m^{-3}, while maintaining low stiffness (Young's modulus ≈2.5 MPa), elongation at break exceeding 600%, and elastic recovery of 90% at 680% strain. Notably, these dynamic cross-links allowed reprocessing and recycling without significant loss of mechanical performance. The study demonstrates that minimal functionalization (<2 mol%) can induce large changes in macroscopic properties, highlighting the efficiency of supramolecular interactions within COC-based systems.

Block copolymer architectures further expand the property landscape of functionalized COCs. Fluorenylamido titanium catalysts enable living/controlled copolymerization of norbornene with α-olefins to produce A–B–A triblock structures comprising glassy PNB segments (T_g ≈400°C) and rubbery poly(ethylene-co-propylene) or atactic polypropylene soft blocks [122]. These materials achieve stress-at-break values between 16 and 20 MPa with elongations above 1000%. By incorporating hydroxyl-functionalized norbornene derivatives (via 10-undecen-1-ol), tensile strength increased to 20.2 MPa at $\varepsilon \approx 1164\%$, while elastic recovery remained above 85%. Simultaneously, surface wettability was modulated: water contact angles decreased from 109° (non-functional block copolymer) to values as low as 90° depending on hydroxyl content [122]. The enhanced performance was attributed to hydrogen bonding within the glassy domains, reinforcing physical cross-links.

Statistical copolymerization strategies also enable tuning of thermal and optical properties. Anilinonaphthoquinone-ligated nickel complexes activated by MMAO or $B(C_6F_5)_3$ catalyzed the copolymerization of norbornene and styrene to yield poly(NB-co-styrene) with styrene incorporation up to 59 mol% and M_n up to 7.8×10^4 g mol^{-1} [123]. Increasing styrene content systematically reduced T_g from 329°C at 4 mol% styrene to 128°C–172°C at 32–59 mol%, enabling wide thermal tunability. Importantly, single T_g values in DSC traces confirmed uniform statistical structures. Because polynorbornene and polystyrene exhibit opposite birefringence signs, such copolymers provide a route to low- or zero-birefringence optical substrates.

Another approach to functionalized COCs involves the use of cyclopropane-containing norbornadiene dimers as monomers. Titanium-catalyzed addition polymerization of these strained monomers proceeds with high chemoselectivity and controlled molecular weight growth (Đ < 1.3), yielding M_n up to 6.2×10^4 g·mol^{-1} in copolymerizations with 1-octene [124]. The cyclopropane moiety remains intact during polymerization but undergoes selective protic acid-mediated ring opening during post-polymerization modification. Aromatic, acyloxy, and alkoxy groups were introduced at high incorporation levels without cross-linking or backbone degradation. This latent-strain activation strategy provides an orthogonal handle for installing diverse functional groups while preserving backbone integrity.

Across these systems, several unifying principles emerge. First, functional group incorporation levels as low as 1–2 mol% can significantly modify surface energy, hydrogen-bonding capability, and mechanical performance. Second, maintaining high molecular weight (10^4–10^5 g·mol^{-1}) and controlled dispersity is essential to prevent embrittlement and preserve optical homogeneity. Third, coordination–insertion catalysis provides unmatched structural control compared to radical or cationic methods, enabling predictable property–composition relationships. Finally, post-polymerization modification strategies offer modularity, allowing functional diversification from a common reactive COC scaffold.

The convergence of precise catalytic copolymerization and selective post-functionalization has thus transformed cyclic olefin copolymers from inert optical plastics into adaptable platforms for advanced functional materials. Through controlled incorporation of carbonyl, hydroxyl, amide, aromatic, and supramolecular cross-linking motifs, COCs can now be engineered to balance high T_g and transparency with toughness, elasticity, surface polarity, and processability. These advances position functionalized cyclic olefin copolymers as promising candidates for next-generation flexible electronics, optical substrates, high-barrier packaging, biomedical devices, and recyclable elastomeric materials.

5 | Key Properties of COCs

Table 1 reports a summary of the key properties of COCs, later discussed individually, which contribute to the popularity of COCs in a wide range of advanced engineering applications.

16163028, 2026, 47, Downloaded from https://advanced.onlinelibrary.wiley.com/doi/10.1002/adfm.75610 by Cochrane France, Wiley Online Library on [16/10/2026]. See the Terms and Conditions (https://onlinelibrary.wiley.com/terms-and-conditions) on Wiley Online Library for rules of use; OA articles are governed by the applicable Creative Commons License

TABLE 1 | Main properties of COCs compared to those of other commonly used polymers (adapted from [7, 8, 125]).

Property	COC	PC	PMMA	PS	PDMS
Physical					
Density [g·cm^{-3}]	1.02–1.04	1.04–1.22	1.17–1.20	1.04–1.06	1.07
Water absorption	<0.01	0.12–0.4	0.1–0.3	0.03–0.1	0.05
Contact angle of water [°]	90–91	81–84	69.1–74.7	85.3–88.5	107–110
Electrical					
Dielectric constant (frequency = 1 MHz)	2–2.2	3.2	2.2–2.6	2.4–2.7	2.8
Volume resistivity [Ω·m]	$> 10^{14}$	10^{12}–10^{15}	10^{10}	10^{18}–10^{20}	4×10^{13}
Dissipation factor	0.0001– 0.0002 (1 MHz), 0.0007 (1 THz)				
Optical					
Haze [%]	0.5–4	0.8–3	1	1–1.2	0.28
Transmittance [%] (visible)	90–91	82–91	92	90	94.5
Transmittance (near-UV)	Excellent	Poor	Good	—	Excellent
Abbe number	56–58	34	61	—	—
Refractive index	1.53–1.54	1.586–1.587	1.5	1.59–1.60	1.375–1.404
Birefringence	Low	Variable	Low	—	—
Thermal					
Thermal expansion coefficient, 23°C–80°C [°C^{-1}]	$0.6–0.7 \times 10^{-4}$	$6–7.5 \times 10^{-5}$	$0.7\text{-}6 \times 10^{-4}$	$6–8 \times 10^{-5}$	$9–9.6 \times 10^{-4}$
T_g (°C)	70–170	145-148	100-122	100	−125
Mechanical					
Young's modulus [MPa]	2500–3200	2390–2600	1300	3000–3500	0.69–3.45
Tensile strength [MPa]	35–63	55–88	63–78	40–66	0.5–9.7

5.1 | Physical Properties

COCs are inherently hydrophobic, so various approaches have been explored to increase the surface energy and improve hydrophilicity and wettability by water-based solutions, with the final aim of improving fluid handling.

COC surface wettability can be effectively modified by several chemical and physical methods, including UV/ozone oxidation, grafting, and plasma treatment [126, 127]. Plasma treatment is the most used approach. Plasma modification offers several advantages: uniform treatment, minimal penetration depth (preserving bulk properties), and environmental friendliness (no harmful gases). Plasma exposure induces ablation/etching, surface degradation, and crosslinking/branching, and the formation of new functional groups, thereby altering wettability and contact angle. Researchers have reported treating COCs with oxygen, argon, and nitrogen plasmas [128, 129]. Roy et al. [128], for instance, showed that prolonged exposure to air after COC surface treatment by oxygen plasma increased contact angles after 17 days of treatment. A general drawback is the need for sophisticated, expensive equipment. Another approach is coating or grafting, where a thin layer of material containing more hydrophilic moieties is physically deposited or covalently grafted onto COC surfaces. Techniques like physical vapor deposition, evaporation, and photo-grafting have been used to apply coatings of materials like silicon dioxide, organosilica, graphene oxide, titanium oxide, and acrylic acid. For instance, Ma et al. sputtered a silicon-dioxide (SiO_2) layer onto COC to enhance wettability [130], while El Fissi et al. deposited titanium oxide (TiO_2) by evaporation [131]. A polymer layer can also be formed by photografting, achieved by immersing COC in a monomer solution and irradiating with UV light. Using this method, layers of acrylic acid and 2-hydroxymethyl acrylate [132], or 2-methacryloyloxyethyl phosphorylcholine [133], have been created on COC, reducing the contact angle from ~90° to 20°–25°. Finally, Dawaymeh et al. used a combined approach: they enhanced the hydrophilicity of flexible COCs using argon/oxygen plasma and graphene-oxide (GO) coatings followed by chemical, thermal, and photoreduction. Increasing GO concentration and plasma duration significantly decreased contact angle (see Figure 14), confirming improved wettability, whereas GO reduction increased the contact angle and restored hydrophobicity of GO-coated COC surfaces [134].

A viable alternative to increasing the surface energy of the substrate is to add a coating, such as surfactants [135], polyethylene glicole (PEG) [136, 137] and polyethylene oxide (PEO) [138], but, however, they interfere with DNA assays amplification or cell

16163028, 2026, 47, Downloaded from https://advanced.onlinelibrary.wiley.com/doi/10.1002/adfm.75610 by Cochrane France, Wiley Online Library on [16/10/2026]. See the Terms and Conditions (https://onlinelibrary.wiley.com/terms-and-conditions) on Wiley Online Library for rules of use; OA articles are governed by the applicable Creative Commons License

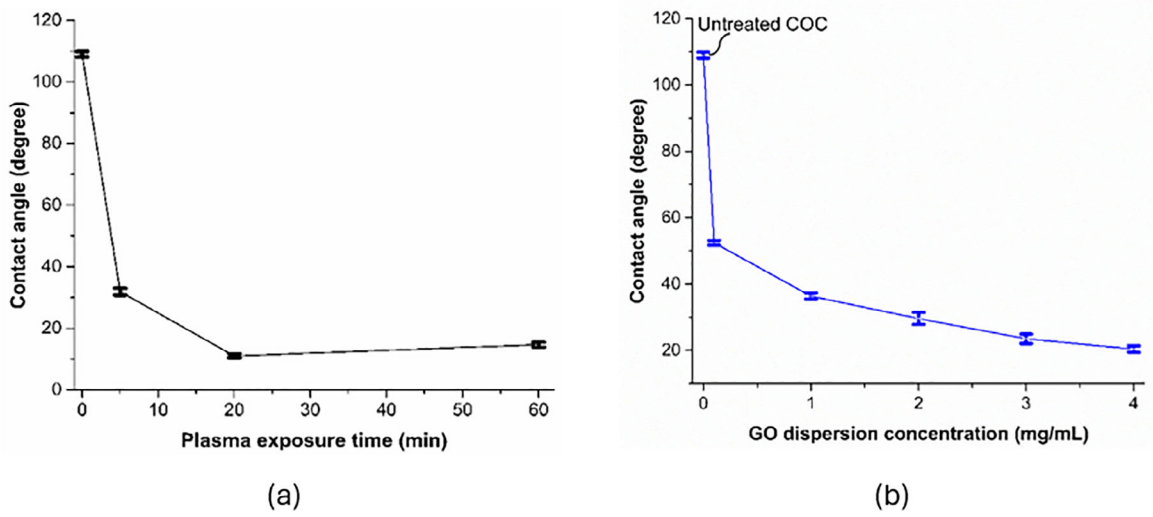


FIGURE 14 | Variation of water contact angle (a) with plasma exposure time in plasma pretreated GO-coated COC, (b) with GO dispersion concentration in GO-coated COC surface (reprinted with permission from [134]).

growth, limiting their employment. Another way to selectively alter surface wettability or attach biosensors for COC functionalization consists of the deposition of graphene oxide, since it possesses high hydrophilicity [139]. Another study reported the combination of plasma and graphene oxide deposition by reducing the contact angle to 15° [134], but the commercial feasibility is still to be assessed.

Water absorption is typically measured through immersion tests, where samples are submerged in water for extended periods, and weight gain is measured. Another method involves exposing samples to controlled humidity environments and measuring the resulting dimensional and weight changes. The low water absorption of COCs, other than ensuring geometrical stability and minimizing the risk of swelling and degradation in humid environments, also grants stability in dielectric properties, optical clarity, and refractive index. COCs typically have water absorption rates of less than 0.01%, which is significantly lower than many other polymers used in similar applications: polyamides (PAs) show water absorption rates of 1%–8%, while polyethylene terephthalate (PET) or polycarbonate (PC) typically absorb 0.2%–0.4% of water.

5.2 | Electrical Properties

Electrical insulation is a critical property in the field of electronic applications. As the electronics industry continues to evolve, with devices becoming smaller, more powerful, and operating at higher frequencies, the demand for materials with superior insulation properties has intensified, as this directly impacts the device's safety and reliability. COCs are known for their excellent electrical insulation, with bulk resistivity of around 10^{12}–10^{14} Ω·m [8, 115], which positions COCs as better insulators compared to other common polymers like polymethylmethacrylate (PMMA) and polydimethylsiloxane (PDMS). The dielectric properties of COCs are further quantified through two key parameters, i.e., the dielectric constant and the dissipation factor, both very low in COCs [140].

The dielectric constant, also known as relative permittivity, is a measure of a material's ability to store electrical energy in an electric field. It is defined as the ratio between the material's permittivity and the vacuum permittivity and can be measured as the ratio of the capacitance of a capacitor using the material as a dielectric to the capacitance of the same capacitor in vacuum. The dielectric constant is a dimensionless quantity and is always greater than or equal to 1, with 1 being the value for a vacuum. COCs are characterized by a low dielectric constant (2.2–2.4 at 1 MHz) [8], notably lower than many other common polymers used in electronics (3–3.5 for polyethylene terephthalate (PET), 3–4 for PI), and nearly one order of magnitude lower than that of traditional ceramic substrates like alumina (around 8.5) [141].

The dissipation factor, or loss tangent (tanδ), is another crucial parameter in evaluating the electrical insulation properties of COCs. It quantifies energy dissipation in dielectric materials subjected to alternating electric fields and represents the ratio of the imaginary part of the dielectric permittivity to its real part. The magnitude of tanδ inversely correlates with insulator quality: materials with low dissipation factors exhibit lower energy losses, resulting in enhanced insulation performance and improved signal integrity in electrical systems [142]. COCs exhibit remarkably low dissipation factors, typically in the range of 1×10^{-4}–2×10^{-4} at 1 MHz and 0.0007 at 1 THz [125]. This is much lower than that of epoxy resins, commonly used in printed circuit boards, which is around 0.01, and that of PI, equal to about 0.002, but also approximately half that of high-performance fluoropolymers like polytetrafluoroethylene (PTFE), which have tanδ in the range 2×10^{-4}–4×10^{-4}.

The combination of a low dielectric constant and a low dissipation factor makes COCs ideal candidates for various electronic applications [125, 143]. For example, COCs can be used as substrate materials for integrated microelectronics circuits, where their low dielectric constant helps to reduce signal delay and crosstalk between adjacent conductive lines.

16163028, 2026, 47, Downloaded from https://advanced.onlinelibrary.wiley.com/doi/10.1002/adfm.75610 by Cochrane France, Wiley Online Library on [16/10/2026]. See the Terms and Conditions (https://onlinelibrary.wiley.com/terms-and-conditions) on Wiley Online Library for rules of use; OA articles are governed by the applicable Creative Commons License

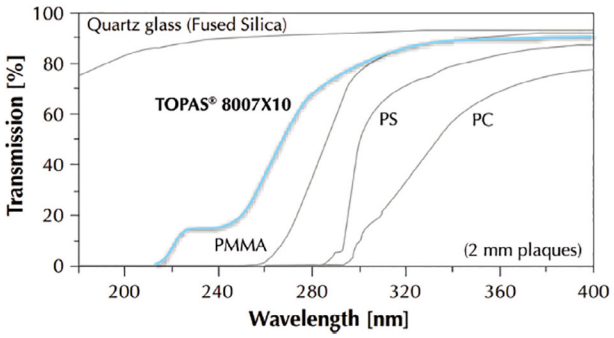


FIGURE 15 | Optical transmission in the UV range of COC (Topas8007 × 10) in comparison with other polymers (PMMA, PS, PC) and quartz glass. Duplicated with permission from [8].

In the field of high-frequency applications, such as in radar systems or satellite communications, the low dielectric loss of COCs helps to maintain signal integrity over long distances [144, 145], which is crucial for ensuring accurate data transmission and reception. Moreover, the excellent electrical insulation properties of COCs make them suitable for various sensor applications, where the stability of the dielectric properties of COCs over a wide range of environmental conditions ensures consistent and reliable sensor performance [146].

Finally, it is worth noting that the electrical insulation properties of COCs can be further tailored through the incorporation of various additives or through copolymerization with different monomers. This versatility allows for the fine-tuning of electrical properties to meet specific application requirements, further expanding the potential uses of COCs in the electronic industry [147].

5.3 | Optical Properties

In the rapidly evolving fields of optics and optoelectronics, the demand for materials that combine good optical properties with the versatility and processability of polymers is increasing, and the exceptional optical properties of COCs are among the most valuable characteristics that make them suitable for a wide range of optical and electronic applications [11, 103, 148]. These properties are quantified through several parameters, including light transmittance, birefringence, Abbe number, chromatic aberration, and autofluorescence.

Light transmittance, generally measured using spectrophotometry, measures the fraction of incident light that passes through a material and is calculated as the ratio between the intensity of the transmitted light and that of the incident light. When compared to other optical polymers, COCs stand out for their exceptional transparency in the whole visible range. For instance, COCs offer comparable or even superior light transmission to PMMA, polycarbonate (PC), and polystyrene (PS). The high transmittance of COCs in the visible range is comparable to that of high-quality optical glass, making them an excellent polymer alternative in many applications, such as optical lenses and protective covers for touchscreen displays and other electronic devices (Figure 15).

The optical clarity and transparency of COCs depend on their amorphous structure, low birefringence, high Abbe number, and low autofluorescence.

Birefringence refers to the difference in refractive indices along different axes in anisotropic materials. This property is typically measured via polarized light microscopy, which analyzes changes in light polarization as it passes through the material, or interferometry, which compares optical path lengths to determine refractive index differences. COCs exhibit remarkably low birefringence, comparable to that of optical glass, due to the low optical anisotropy and the high carbon-to-hydrogen ratios [149]. This makes them suitable for applications such as liquid crystal displays (LCDs), where it helps to minimize color separation and enhance image quality, but also in optical waveguides and fiber optics, where low birefringence helps to maintain signal integrity by reducing polarization-dependent losses.

However, the birefringence of COCs can increase when the polymer is subjected to manufacturing processes that can induce molecular orientation, such as injection molding and extrusion. Efforts to mitigate this issue have included blending COCs with other polymers that possess opposite birefringent properties, such as polyvinylidene fluoride (PVDF) and PMMA. However, blending often compromises the transparency of the resulting material due to immiscibility between the components and the resulting biphasic structure. Some authors have proposed an approach involving the terpolymerization of norbornene, ethylene, and styrene, where the negative birefringence of styrene compensates for the positive birefringence of the norbornene-ethylene copolymer [149].

More recently, Kefer et al. [150] quantified birefringence in injection-molded parts using polarimetry and prism couplers, revealing an inhomogeneous distribution within the material, with maximum birefringence observed near the injection gate (10×10^{-4}) and decreasing toward the center of the plates (1.8×10^{-4}). This anisotropic behavior can lead to polarization-dependent optical attenuation, which is crucial for the functionality of photonic structures. According to the authors, understanding and controlling birefringence not only enhances the design of low-loss waveguides but also mitigates issues such as peak splitting in Bragg gratings, thereby improving the overall efficiency and reliability of integrated photonic devices [151]. This stresses the concept that the characterization of birefringence in COC substrates is vital for optimizing their optical performance in various optical and electronics applications.

The Abbe number (ν), a measure of a material's dispersion of light, indicates the dependency of the refractive index on wavelength. A high Abbe number signifies low chromatic aberration, which is crucial for maintaining color fidelity in optical systems. The Abbe number is commonly measured using refractometry to determine refractive indices at different wavelengths, or through spectroscopic methods that analyze dispersion as a function of the wavelength. It can be calculated as reported in Equation (1),

$$\upsilon = \frac{n_D - 1}{n_F - n_C} \tag{1}$$

16163028, 2026, 47, Downloaded from https://advanced.onlinelibrary.wiley.com/doi/10.1002/adfm.75610 by Cochrane France, Wiley Online Library on [16/10/2026]. See the Terms and Conditions (https://onlinelibrary.wiley.com/terms-and-conditions) on Wiley Online Library for rules of use; OA articles are governed by the applicable Creative Commons License

where n_D, n_F, and n_C are the refractive indices at specific wavelengths (587.6, 486.1, and 656.3 nm, respectively, i.e., the Fraunhofer spectral lines D, F, and C) [152].

When compared to other optical polymers, COCs stand out for their high Abbe number, comprised between 56–58, comparable to that of optical glass and PMMA (58–61), and much higher than that of PC (34). This property makes COCs particularly suitable for high-end optical systems such as camera lenses, microscopes, medical imaging devices, and other precision instruments where color accuracy is essential. The combination of high Abbe number and polymer processability makes COCs particularly interesting for the production of complex lens shapes, offering a balance between optical performance and manufacturing flexibility that is difficult to achieve with glass [8].

Finally, autofluorescence refers to the natural fluorescence emitted by materials when exposed to light. Autofluorescence is typically measured using fluorescence microscopy, which observes emitted fluorescence under specific excitation wavelengths, or spectrofluorometry, which quantifies fluorescence intensity across wavelengths. COCs are known for their low autofluorescence, comparable to that of high-quality glasses. This is a significant advantage in applications such as microfluidic devices used in biological research or medical diagnostics, compared to other polymers commonly used in these fields, such as polyurethanes, PET, and thermoplastic elastomers [153–155]. The low autofluorescence of COCs allows for more sensitive detection of fluorescent markers or analytes, improving the overall performance of these devices while offering the manufacturing advantages of a polymer.

5.4 | Thermo-Chemical Properties

COCs have emerged as a standout material, also thanks to their exceptional chemical and thermal stability that often surpasses traditional polymers.

COCs demonstrate excellent chemical stability to a wide range of solvents, acids, and bases. This resistance is primarily due to their molecular structure consisting of rigid cyclic and linear olefin monomers without polar groups. COCs exhibit higher chemical resistance than PET and PC to organic solvents and strong acids or bases, and have comparable chemical performance to PTFE in many environments. COCs also exhibit better resistance to environmental stress cracking (ESC) than some grades of PMMA or PC, maintaining optical clarity over longer periods in challenging environments. The chemical stability of COCs is typically evaluated through exposure tests, where samples are subjected to various chemicals for extended periods. The material's integrity is then assessed through measurements of weight change (swelling, erosion), molecular weight decrease, dimensional stability, and retention of mechanical and optical properties. Spectroscopic techniques such as Fourier Transform Infrared Spectroscopy (FTIR) can also be employed to detect chemical changes such as oxidation and degradation after exposure.

The chemical stability of COCs is particularly valuable in electronic and optical applications. Electronic components are often exposed to harsh environments during manufacturing or use, such as cleaning solvents, atmospheric pollutants, or corrosive agents. For instance, in the manufacturing of printed circuit boards (PCBs), the resistance of COC to the chemicals used in the etching and plating processes ensures that COC-based substrates maintain their dimensional accuracy and electrical properties, thus improving the reliability of the final products. In optical applications, components such as lenses or protective covers may be exposed to various environmental factors or cleaning agents. The ability of COCs to withstand these exposures without degradation or loss of optical clarity ensures the long-term performance of these components.

Thermal stability is another critical property of COCs. COCs are known for their high glass transition temperatures, which can exceed 200°C for some grades. This leads to higher Vicat softening temperatures (VST) and heat distortion temperatures (HDT). In fact, certain grades of COCs can maintain their properties at temperatures exceeding 170°C, whereas PET has a T_g around 70°C and PC around 150°C. This high thermal stability makes COCs particularly valuable in applications where high-temperature performance is crucial, such as in automotive electronics or high-power Light Emitting Diode (LED) packaging, where the component is required to maintain high thermal insulation or high optical clarity also at high temperatures. Moreover, COCs show a low coefficient of thermal expansion (CTE), which is particularly interesting in applications where dimensional stability under temperature changes is critical. The CTE of COCs, as low as 0.3–1.3 × 10^{-4} K^{-1} [67, 156], helps minimize stress and potential deformation in components exposed to temperature fluctuations. Moreover, below T_g, shows a weak dependence on temperature. Hence, while glass still holds the advantage in extremely high-temperature environments, COCs offer a polymer alternative that can withstand higher temperatures than many traditional thermoplastics while providing the added benefits of lighter weight and impact resistance.

5.5 | Processing Properties

From a technological standpoint, COCs present good processability and high flowability that allow for precise molding into complex geometries without compromising optical quality. When shaping COCs, it is possible to achieve a high-dimensional stability that ensures a consistent performance of the final products over time and under varying environmental conditions, including changes in temperature, humidity, and mechanical stress.

Flowability and processability in the molten state are typically assessed through rheological tests. The high flowability and film-forming characteristics of COCs allow for the fabrication of thin, uniform components with excellent clarity. This processing advantage sets COCs apart from glass and even some other optical polymers, allowing for more complex and precise optical designs.

The dimensional stability against temperature changes is mainly attributed to their molecular structure. The rigid cyclic groups in the polymer backbone contribute to a high T_g and low CTE, while the absence of polar groups is the basis of the low moisture

16163028, 2026, 47, Downloaded from https://advanced.onlinelibrary.wiley.com/doi/10.1002/adfm.75610 by Cochrane France, Wiley Online Library on [16/10/2026]. See the Terms and Conditions (https://onlinelibrary.wiley.com/terms-and-conditions) on Wiley Online Library for rules of use; OA articles are governed by the applicable Creative Commons License

absorption tendency. These properties help COCs maintain their shape and dimensions over a wide range of temperatures and environmental conditions, especially when compared to other polymers like PET and polyamides (PAs).

The thermal stability of cyclic olefin copolymers (COCs) under processing conditions is a crucial parameter for their practical application, as melt processing operations such as extrusion and injection molding are typically carried out at temperatures significantly above the glass transition temperature (T_g). Although COCs are generally considered thermally stable materials due to their saturated hydrocarbon backbone and relatively high T_g, several studies have demonstrated that they are prone to thermal and thermo-oxidative degradation when exposed to elevated temperatures, particularly in the presence of oxygen and under prolonged residence times. In addition to oxidative degradation, repeated thermal processing cycles can exacerbate molecular weight reduction and structural changes. Recycled or reprocessed ethylene–norbornene copolymers are generally subjected to chain scission, macroradical formation, and a progressive decrease in oxidative induction time (OIT), negatively affecting their stability and performance.

A crucial aspect influencing thermal and thermo-oxidative stability of cyclic olefin copolymers (COCs) is their chemical composition, in particular the norbornene content. An increase in norbornene concentration generally leads to higher glass transition temperature and enhanced chain rigidity, which can improve the resistance to thermal degradation under inert conditions [157]. However, a different trend is frequently observed under thermo-oxidative conditions, relevant to polymer processing. The presence of bulky cyclic structures and tertiary carbon atoms in norbornene units can promote oxidative degradation pathways, making the material more susceptible to radical formation and oxygen attack at elevated temperatures [158–160].

Fundamental studies on the thermal degradation behavior of COCs were reported by Liu and co-workers, who systematically investigated the degradation kinetics of cyclic olefin copolymers with varying compositions. These authors showed that thermal degradation primarily proceeds through random chain scission mechanisms, with the onset temperature and degradation rate being strongly dependent on the norbornene content and the resulting chain rigidity [157]. More importantly, the stability of COCs under actual processing conditions has been directly investigated by the same authors, who studied the thermal oxidation and molding feasibility of COCs with high T_g (203°C) and reported that, during melt processing such as extrusion, the materials underwent noticeable discoloration, evolving from transparent to yellowish samples as a result of thermo-oxidative degradation. This behavior was attributed to the formation of unsaturated and carbonyl species generated through oxidative pathways, indicating that even relatively short exposure to high temperatures in air can induce chemical changes in the polymer structure. However, the addition of suitable antioxidants (i.e., Irganox HP2921) could effectively suppress thermal oxidation and eliminate the color stain [158].

In addition to intrinsic thermal stability, external factors, such as the presence of additives or fillers, can significantly affect the degradation behavior of COCs.

Yang et al. performed a detailed kinetic analysis of the thermo-oxidative degradation of COCs using thermogravimetric analysis (TGA) coupled with FTIR microscopy, evaluating also the effect of TiO_2 nanoparticles addition on the degradation kinetics. It was highlighted that the reactivity of the COC was enhanced by the presence of TiO_2, due to the presence of the surface hydroxyl groups on the nanoparticles, able to promote the thermal oxidation reaction. On the other hand, TiO_2 particles, bearing the high thermal conductivity as well as a greater heat capacity value, absorbed most of the heat transmitted from the surroundings and retarded the diffusion of the heat inside the macromolecules, shifting the occurrence of the primary weight-loss stage from 454°C to 473°C [106].

Gutiérrez-Villarreal and co-workers demonstrated that transition metal stearates, such as iron, cobalt, and manganese stearates, act as pro-degradant species that accelerate thermo-oxidative degradation. Their results showed a significant reduction in oxidation resistance and activation energy in the presence of these additives, highlighting the sensitivity of COCs to catalytic oxidation processes [159, 160].

In a recent paper, it has been demonstrated that the incorporation of natural additives (i.e., hesperidin, curcumin, and clove extract) into a commercial COC (Topas E-140) could significantly improve the thermal-oxidative stability, with an increase in oxidative induction time (OIT) and a delay in thermal degradation processes, also under repeated thermal reprocessing conditions [161].

These findings indicate that, despite their favorable combination of high glass transition temperature, optical clarity, and mechanical performance, COCs are not completely inert under melt processing conditions. Thermo-oxidative degradation can occur under typical processing temperatures, especially in the presence of oxygen, long residence times, or pro-degradant species. Therefore, careful optimization of processing parameter, such as temperature profiles, residence time, and atmosphere control, together with the use of appropriate stabilizing additives, is essential to preserve the material properties and ensure long-term performance.

5.6 | Biocompatibility

COCs have low surface energy, which can be detrimental to some applications, such as biomedical applications, particularly cell attachment. One way to improve the compatibility and functionalization of COCs is to modify the surface chemistry to selectively promote or inhibit cell adhesion [162], increasing biocompatibility [163]. Various methods, such as low-pressure plasma treatment using different gases, such as oxygen, argon, and nitrogen plasma [127], UV/ozone treatment [164], electron beam treatment [165], laser structuring [154, 166], chemical functionalization, including self-assembled monolayers [167], and physical modeling, can be used to modify the surface chemically [154]. Aubrecht et al., for instance, locally modified the surface of thermoplastic COC material using medium-energy carbon, oxygen, and nitrogen ions to enable selective cell growth on polymer surfaces [168].

16163028, 2026, 47, Downloaded from https://advanced.onlinelibrary.wiley.com/doi/10.1002/adfm.75610 by Cochrane France, Wiley Online Library on [16/10/2026]. See the Terms and Conditions (https://onlinelibrary.wiley.com/terms-and-conditions) on Wiley Online Library for rules of use; OA articles are governed by the applicable Creative Commons License

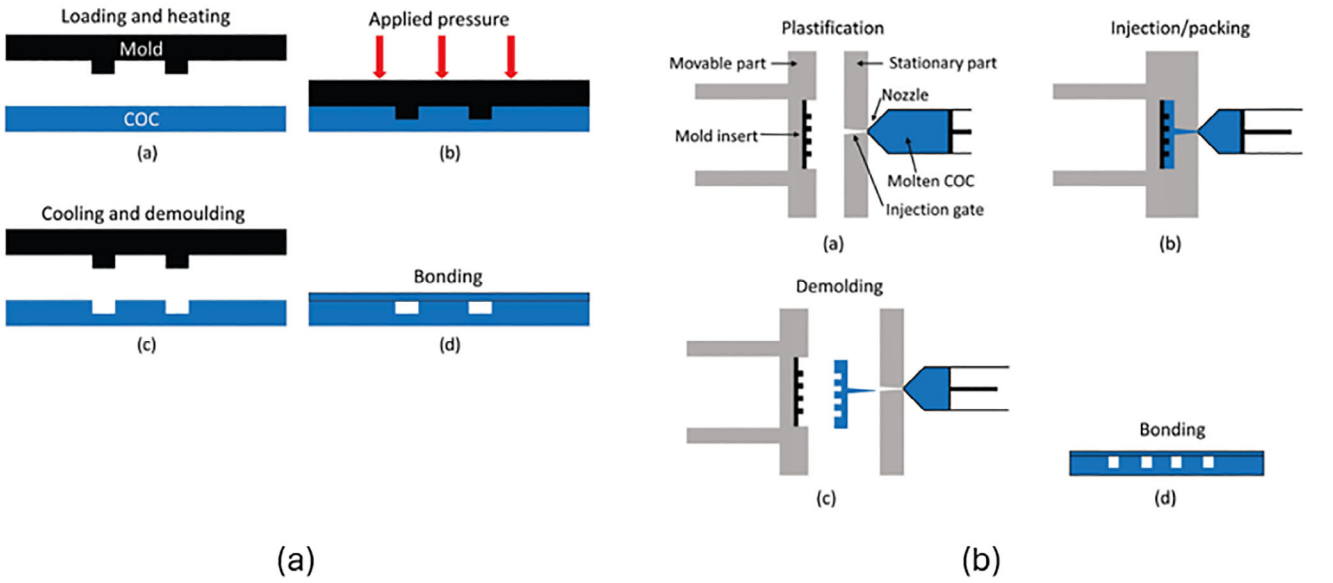


FIGURE 16 | Schematic diagram of COC (a) hot embossing and (b) injection molding processes (reprinted with permission from [8]).

6 | Processing Technologies

Different processing techniques can be adopted for different COC applications [12]. COCs are processable by all conventional methods, including injection molding, cast and blown film extrusion and coextrusion, injection blow molding, and injection-stretch blow molding. In general, COCs do not require drying or other pretreatment before processing. From an environmental perspective, it is important to note that COCs are highly recyclable, as they can be remelted at high temperatures and repurposed for different applications, with the added benefit of sterilizing the recyclates [8]. Selection of the most-suitable COC grade as the raw material depends on the fabrication approach, targeted structure, and properties such as glass-transition temperature.

6.1 | Hot Embossing

COC films/sheets are typically used for hot embossing and rapid prototyping, whereas pellets are generally used for injection molding. In hot embossing, a COC sheet is placed into a mold, then heat and pressure are applied for a specified duration. The system is subsequently cooled under pressure and demolded (see Figure 16a). This technique, employed to fabricate nanoscale COC structures, is comparatively inexpensive, offers high precision, and operates at lower temperatures, thereby reducing shrinkage and facilitating demolding. However, due to its longer cycle time, it is less suitable for high-volume production than injection molding (see Figure 16b) [169]. The use of hot embossing to fabricate COC microchannels began in the early 2000s [170, 171]; applied load, temperature, and holding time are the key parameters for optimizing fabrication.

6.2 | Injection Molding

For injection molding, COCs exhibit good flowability, can replicate submicron-scale surface features, and readily fill complex thin-walled parts. Major commercial COC grades suitable for injection molding include Zeonex (Nippon Zeon, Japan), Arton (Japan Synthetic Rubber, Japan), Apel (Mitsui, Japan), and Topas (Ticona division of Celanese AG, Summit, USA, and Frankfurt, Germany) [11]. COCs also show low and substantially isotropic shrinkage during molding, resulting in minimal warpage. Up to 10% regrind can be added by molders.

In injection molding, COC pellets are fed into the hopper, conveyed by the screws to the mold at a specified injection speed while being heated to the processing temperature. The molten COC is then injected into the mold at high pressure and maintained at the demolding temperature. When the part can be safely removed, the mold opens, and the part is ejected.

For precision optics, injection-molded COC components can be significantly less expensive than glass analogs, which may require costly grinding and polishing to achieve tight tolerances [12]. In post-molding operations, COCs can be readily metallized by vacuum deposition with aluminum, chromium, silver, or other metals. Notably, injection molding of COCs has also been used for developing microchannels for biomedical applications. In particular, Abdulrahman et al. provided a comprehensive review of thermoplastic microfluidic device production via this technique (see schematic in Figure 16b, 14b) [8].

6.3 | Subtractive Manufacturing

Subtractive manufacturing is advantageous in research settings due to its comparatively low cost and ability to quickly implement new designs, making it well-suited to early development. Techniques include computer numerical control (CNC) micromachining, laser ablation, and xurography (digital cutter/plotter) [8].

Micromachining (micromilling) is a low-cost, time-efficient option for manufacturing polymer microfluidic devices.

16163028, 2026, 47, Downloaded from https://advanced.onlinelibrary.wiley.com/doi/10.1002/adfm.75610 by Cochrane France, Wiley Online Library on [16/10/2026]. See the Terms and Conditions (https://onlinelibrary.wiley.com/terms-and-conditions) on Wiley Online Library for rules of use; OA articles are governed by the applicable Creative Commons License

Applicable to various materials, it produces complex structures without hazardous chemicals. As in conventional machining, material is removed by a tool tip to generate the desired geometry or microchannel; parameters such as depth of cut and spindle speed are critical. However, the resulting microchannels often exhibit high surface roughness that is problematic for applications such as electrophoresis [172].

Xurography is a rapid-prototyping approach and one of the newest techniques applied to COCs, with limited publications to date. It shows strong promise for future COC devices due to broad manufacturing flexibility and minimal need for specialized facilities or expensive equipment. As interest grows, machining quality is improving, with current resolutions around 250 μm [173]. In xurography, a digital cutter (blade) patterns thin polymer films, which are then laminated to create channels. Its simplicity makes it especially attractive for research groups. Compared with other methods, xurography is relatively new, as most polymer applications were published after 2010, and its use in COCs remains in early implementation [174].

In laser ablation, a high-intensity laser beam removes material from the polymer substrate, and regions at the focal point are vaporized. Laser machining enables complex structures and is cost-accessible, but drawbacks include low throughput, possible chemical modification, high surface roughness that affects optical properties, and the need to remove polymer debris. Laser ablation has been applied to polymers such as Polyimide (PI) and Polymethyl Methacrylate (PMMA), but its use with COC matrices remains limited [8]. For example, Cai et al. fabricated COC microchannels 300 μm wide and 200 μm deep via CO_2 laser ablation [175].

6.4 | Additive Manufacturing

The layer-by-layer nature of additive manufacturing minimizes waste, reduces energy consumption, and operates at atmospheric pressure, enabling one-step fabrication of 3D structures and eliminating the bonding step [176].

Kaluza et al. recently examined the impact of 3D-printing parameters on the THz optical characteristics of COC. They showed that certain printing parameters significantly affect optical behavior while suboptimal settings degraded THz properties, notably altering refractive index and increasing absorption coefficient [177].

Gunaserkaran et al. manufactured COC coversheets on polycrystalline silicon photovoltaic cells via 3D printing to reduce reflection losses; gahnite ($ZnAl_2O_4$) was added at varying loadings to enhance antireflection behavior. COC with 3 wt.% gahnite achieved optimal power conversion efficiency (PCE) in both open (18.1%) and controlled (18.9%) environments, with the lowest reflectance (4.2%) and highest transmittance (95.5%), thereby increasing absorbance [178]. Similarly, Refaai produced 3D-printed COC coversheets for polycrystalline Si (p-Si) solar cells and incorporated silicon nitride (Si_3N_4) particles to further improve antireflection properties [179]. The coversheet with 3 wt.% Si_3N_4 exhibited the highest light absorption, with 89.9% transmittance and 6.2% reflectance (see Figure 17a), yielding higher PCEs of 22.3% (regulated environment) and 20.1% (sunlight exposure) (see Figure 17b).

In a very recent study, the viability of using various 3D-printed plastics in high-vacuum (HV) and ultra-high-vacuum (UHV) environments was assessed by evaluating outgassing properties for both fused-deposition modeling and stereolithography materials [180]. COCs exhibited promising characteristics both in HV and UHV conditions. A comparison of machined and 3D-printed parts showed that challenges such as porosity and surface roughness were not of major concern for these applications.

7 | COCs for Advanced Engineering Applications

COCs have emerged as a significant class of materials for a large number of engineering applications. Figure 18 reports schematically the main fields in which COCs have been successfully employed thanks to their remarkable physico-chemical and mechanical properties.

The first two domains concern optical and electronic applications. The unique combination of electrical insulation, optical clarity, thermal and chemical resistance, and dimensional stability makes COCs particularly well-suited for a wide range of optical components and electronic devices. The applications in optics include lenses for both prosthetics and industrial applications, while electronics components and circuits have been employed in telecommunications industries and to develop neural prosthetics. In fact, COCs offer comparable electrical performance, optical clarity, and thermal and dimensional stability comparable to glass in most environments, with the added benefits of being lighter, cheaper, more impact-resistant, and easier to process into complex shapes.

Micro-fluidics and bioengineering are two fields of application in which COCs have been playing a significant role because of their transparency, moisture resistance, chemical resistance, and the ability to withstand common sterilization methods, i.e., gamma radiation, steam, and ethylene oxide. Relevant applications are not limited to prosthetics, but include devices for cell cultures and testing, portable devices for forensic analyses, equivalent models for living organs (i.e., Organ-on-a-chip – OoC), and pre-filled devices.

Final applications of COCs concern their use in composites that have the ability of self-healing, with remarkable uses in many industries, including those related to automotive and aerospace, and the possibility to fabricate films for packaging applications.

The following subsections will explore the main results achieved by the scientific community in the use of COCs for advanced engineering applications.

7.1 | COCs in Optics

Due to their high clarity and low birefringence, COCs are used in optical films for liquid crystal display (LCD) and organic light-emitting diode (OLED) displays, touch screens, and lenses in mobile devices and cameras. The excellent chemical

16163028, 2026, 47, Downloaded from https://advanced.onlinelibrary.wiley.com/doi/10.1002/adfm.75610 by Cochrane France, Wiley Online Library on [16/10/2026]. See the Terms and Conditions (https://onlinelibrary.wiley.com/terms-and-conditions) on Wiley Online Library for rules of use; OA articles are governed by the applicable Creative Commons License

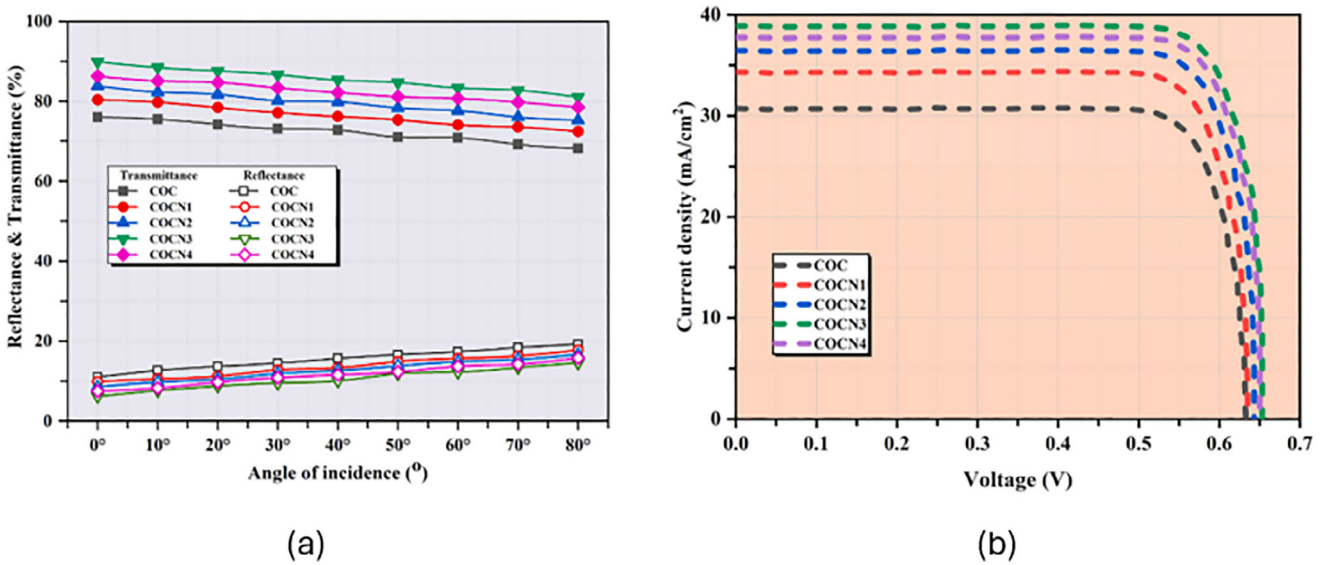


FIGURE 17 | Optical and electrical properties of neat COC and relative composite 3D printed coversheets. (a) Reflectance and transmittance at different incident angles, (b) I-V performance curves under direct solar radiation (reprinted with permission of [179]).

resistance, lightweight nature, and high specific strength and toughness further enhance their appeal in applications where performance and durability are critical. For example, Zhang et al. [181] explored the application of COCs in the assembly of camera modules (CMA), focusing on their compatibility and weldability with polycarbonate lenses and supports. This is a critical application since the mechanical clamping forces, necessary for connecting lenses in the CMA, can lead to lens distortion and ultimately to degradation in image quality. Hence, the authors highlighted the need for a more effective joining method that maintains optical performance and proposed picosecond laser welding as an alternative joining technique. The study highlighted the successful formation of joints in PC-PC, COC-COC, and PC-COC (Figure 19) combinations. The paper also discusses the difficulties encountered during laser welding, particularly when working with different types of plastics, which have hindered the broader adoption of laser welding techniques in CMA. On the one hand, non-ultrafast lasers produce a significant heat-affected zone (HAZ), which can impose limitations on the thickness of the joining components; on the other hand, ultrafast lasers, despite producing a smaller HAZ, still face challenges in achieving effective welds. Therefore, the authors emphasized the necessity of optimizing welding parameters, such as laser power and scan speed, to ensure stable and effective welds and prevent lack of fusion or overheating.

COCs can also be used in displays as a component in light management films or as barrier layers for organic optoelectronic devices like OLEDs. Since these films are designed to be a barrier to chemicals, water, and oxygen, COC is a good candidate. However, its insolubility in most organic solvents poses challenges in its deposition, as traditional polymer processing, such as the spin coating cannot be applied. Therefore, several authors have explored other deposition processes. For example, Singaravelu et al. [182] studied the resonant infrared pulsed laser deposition (RIR-PLD) of COC films. They compared the deposition of COC films using a tunable free-electron laser (FEL) tuned to the C—H stretch resonance at 3.43 μm, and a non-resonant nanosecond laser at 1.064 μm. The results showed that the FEL was able to deposit smooth, homogeneous films, while the non-resonant laser caused thermal degradation and deposition of particulates. In fact, FEL-deposited COC had an average roughness of only 10 nm, compared to 68 nm for the non-resonant laser. The authors also measured the ablation threshold of the COC target under single FEL pulses, which was found at around 5.5 $J \cdot cm^{-2}$. This data was used in combination with thermodynamic modeling to conclude that the RIR-PLD process allows for the evaporation and redeposition of intact polymer chains. This demonstration of a low-temperature, selective deposition technique for an insoluble polymer like COC is an important development for its use in optical barrier applications.

Micro-/nano-lenses have gained interest in the development of bioengineering devices used for optical applications like endoscopic imaging. Shinoj et al. investigated the potential of self-aligned polymeric microlens array (MLA) embedded in optical fibers via micro-compression molding. The authors performed a dedicated optimization of the parameters for different materials, i.e., PMMA, PC, Topas COC, aiming at achieving the best optical properties in terms of focal and spatial resolution [183]. Appasamy et al., in contrast, investigated a new injection molding technique for manufacturing high-throughput plastic microlenses using metallic master molds obtained via melting and electroforming. Such molds were later employed with two plastic materials, i.e., COC and Poly IR 2, to manufacture microlenses with focal lengths ranging from 200 μm to 1.9 mm. This technique enabled a high-volume production of devices with a cycle time of about 60 s per chip [184].

Using a different and cheaper manufacturing process, Baek et al. developed COC-based MLAs (main dimension in the order of 300 μm) using compression molding and thermal reflow (Figure 20). The approach pursued by the authors, different from previous reports [183–185], included the insertion of a light screen between the lenses to minimize optical interference,

16163028, 2026, 47, Downloaded from https://advanced.onlinelibrary.wiley.com/doi/10.1002/adfm.75610 by Cochrane France, Wiley Online Library on [16/10/2026]. See the Terms and Conditions (https://onlinelibrary.wiley.com/terms-and-conditions) on Wiley Online Library for rules of use; OA articles are governed by the applicable Creative Commons License

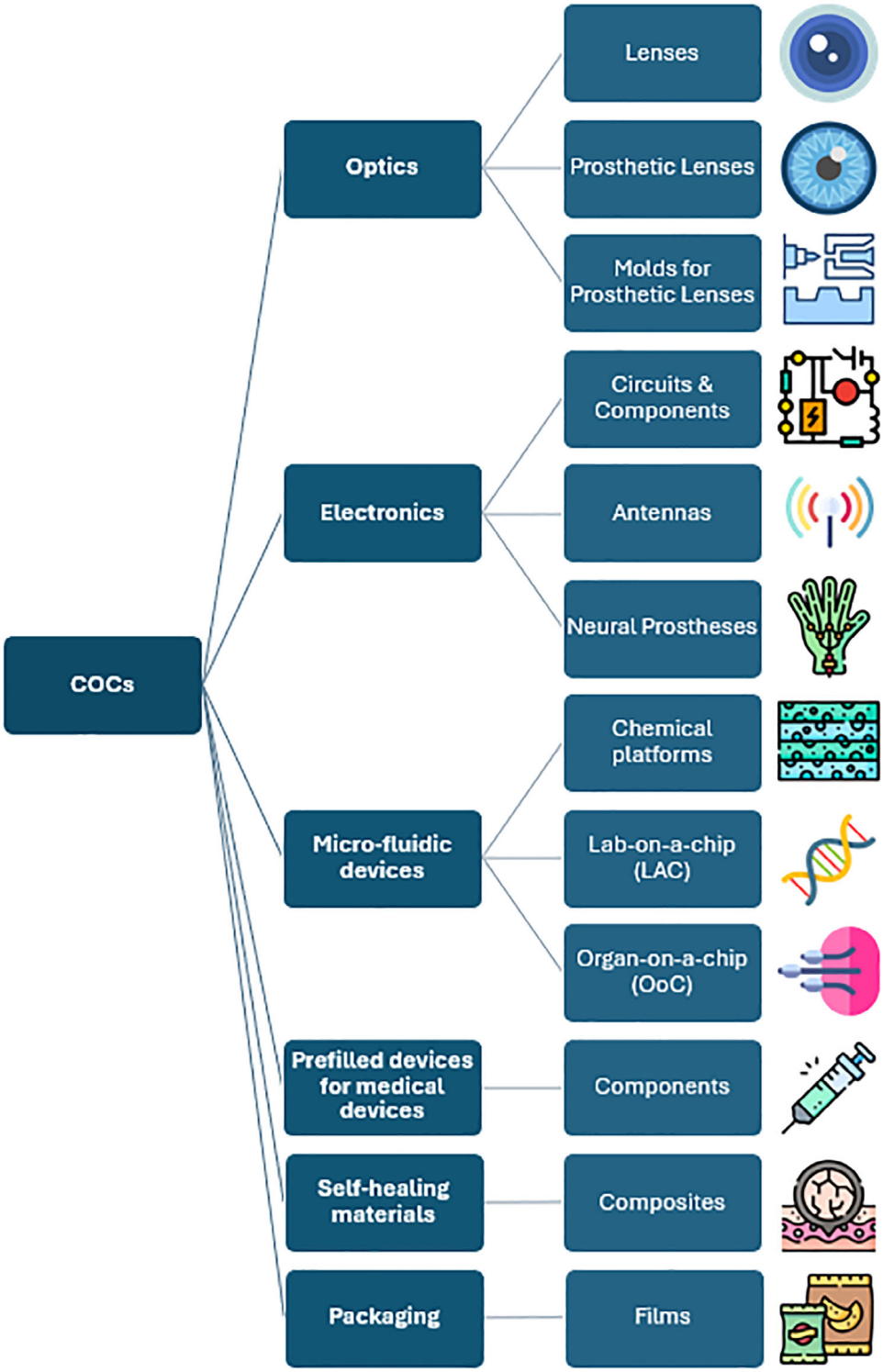


FIGURE 18 | COCs for advanced engineering applications. Icons made by Freepik, Iconjam, Futuer Flat, and Juicy_fish from www.flaticon.com.

thus achieving higher optical properties [186]. Furthermore, the developed COC-MLAs possessed a lower water absorption rate and higher stiffness than other similar devices while maintaining excellent optical transparency. Such features make these COC-MLAs remarkable candidates for both packaging and optics applications in small robotic systems [186]. In a different work, Yeo et al. aimed at a different objective related to the fabrication and wettability assessment of polymeric surfaces shaped in the form of nano-lens arrays (NLAs). The NLAs were replicated on different material surfaces, i.e., PDMS, COC, and PMMA, using replica-molding and hot-embossing techniques. Theoretical and experimental evaluations showed that the NLAs enhanced the hydrophilicity of PMMA and the hydrophobicity of PDMS surfaces in the Wenzel wetting state. In contrast, the presence of NLA on COC surfaces did not affect its wettability [185].

16163028, 2026, 47, Downloaded from https://advanced.onlinelibrary.wiley.com/doi/10.1002/adfm.75610 by Cochrane France, Wiley Online Library on [16/10/2026]. See the Terms and Conditions (https://onlinelibrary.wiley.com/terms-and-conditions) on Wiley Online Library for rules of use; OA articles are governed by the applicable Creative Commons License

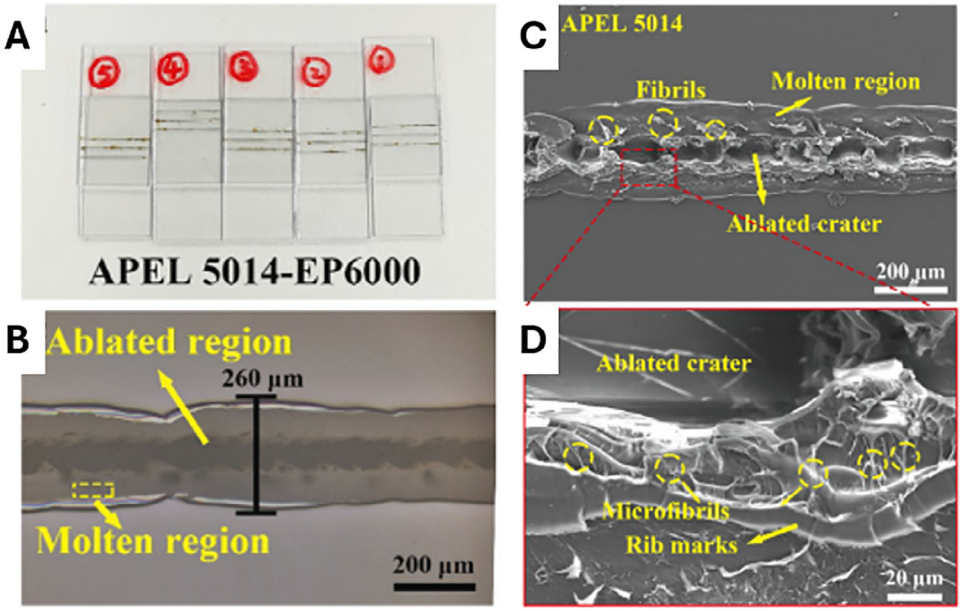


FIGURE 19 | Investigation of the picosecond laser welding of COC (APEL 5014) and PC (EP 6000), two commonly used materials for the production of optical lenses. Photographs (A), optical images of the welding seam (B), and SEM micrographs of the welding region (C,D) of APEL 5014 with EP 6000. Duplicated with permission from [181].

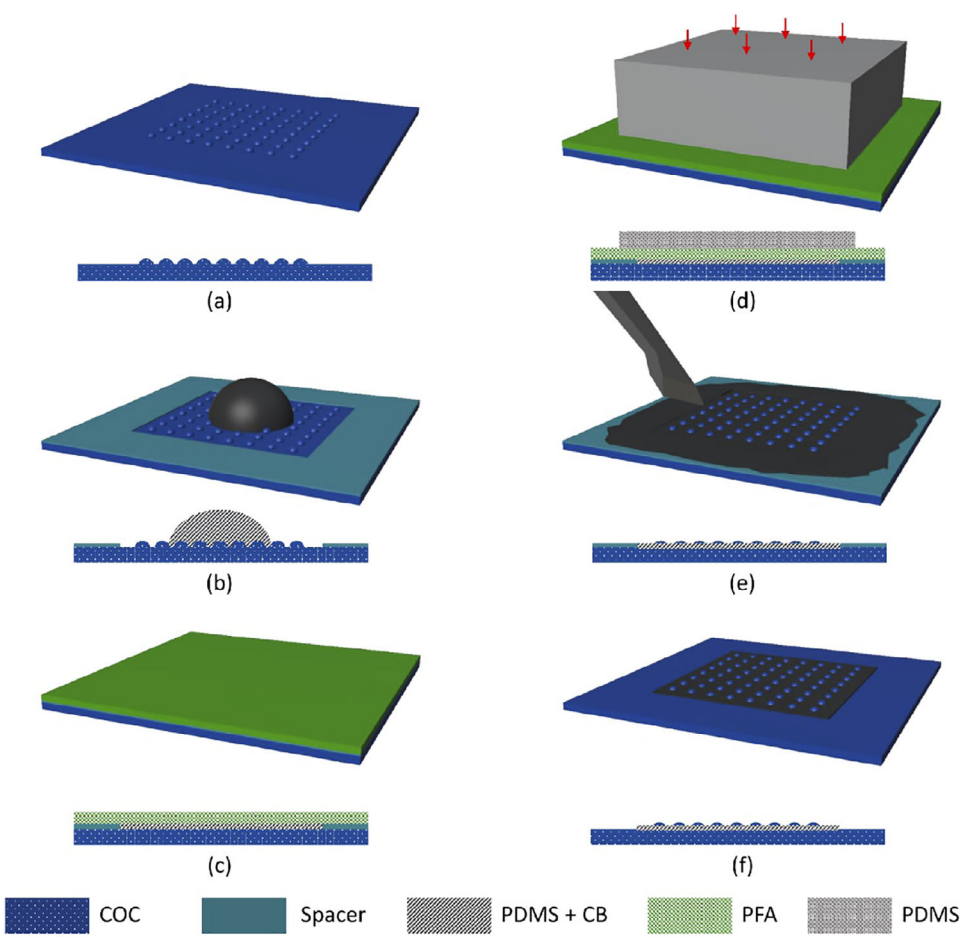


FIGURE 20 | Fabrication steps to achieve COC-MLA devices. (a) Compression molding and thermal reflow of COC. (b) Place a spacer, and PDMS-CB mixture on the MLA, (c) place a PFA film, (d) place a PDMS block, and apply pressure. Cure the mixture. (e) Remove the PDMS block and the PFA film. Isolate the light screen. (f) Remove the spacer. Reproduced with permission under the terms of Creative Commons license [186]. Copyright 2021, Optica Express.

16163028, 2026, 47, Downloaded from https://advanced.onlinelibrary.wiley.com/doi/10.1002/adfm.75610 by Cochrane France, Wiley Online Library on [16/10/2026]. See the Terms and Conditions (https://onlinelibrary.wiley.com/terms-and-conditions) on Wiley Online Library for rules of use; OA articles are governed by the applicable Creative Commons License

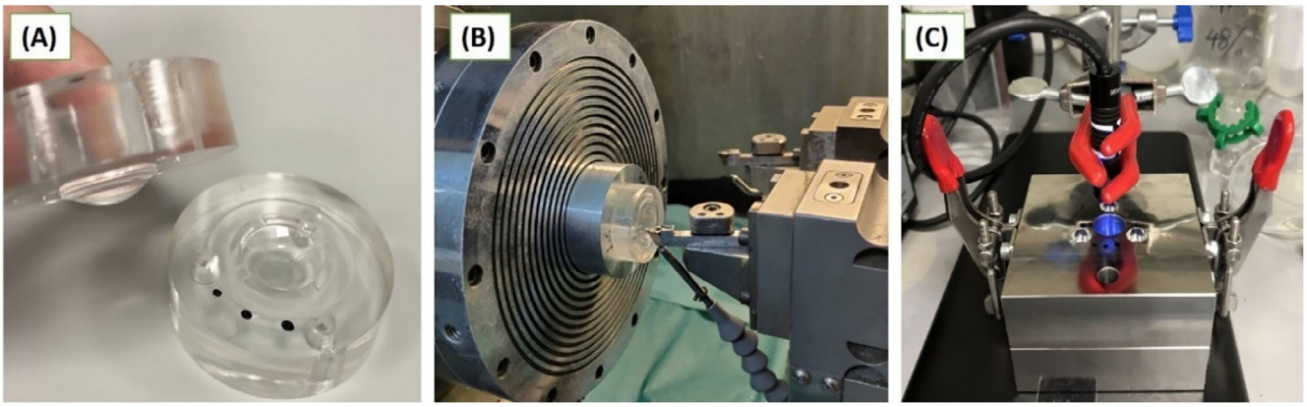


FIGURE 21 | COC-based molds for manufacturing contact lenses. (A) Final shape of the mold. (B) Milling the mold in the workshop. (C) Employment of the mold in the fabrication of contact lenses. Reproduced with permission under the terms of Creative Commons license [189]. Copyright 2022, MDPI.

Retinal prosthetics has been another targeted application explored with COCs since such devices can be an effective solution against genetic disorders like *retinitis pigmentosa*, one of the leading causes of blindness. In the common practice, contact lenses are made by a high-precision injection molding process, supported by a fast ultraviolet (UV) light-curing process, using polymers such as polyethylene (PE) or polypropylene (PP) [187], and a precise mold ensures a level of fabrication repeatability, which can be geometrically customized in terms of dimensions and curvature.

In this framework, Baek et al. developed COC-based retinal prostheses, assessing the ability of the material to enhance longevity and suitability in retinal implant packaging [188]. In their comparative study, COC outperformed materials like PDMS, PI, colorless transparent polyimide (CPI), and liquid crystal polymer (LCP) in optical transparency. Thanks to its superior encapsulation properties due to thermoplasticity and its ability to be fabricated into a micro-lens array, COC gained interest for further investigations for advanced retinal prostheses.

A different use of COCs was delivered by Musgrave et al., who experimentally studied reusable COC-based molds for producing soft contact lenses via injection molding (Figure 21) [189]. The developed COC molds demonstrated a stable surface roughness even after exposure to more than 20 kW of UV light at 365 nm. Moreover, the surface roughness of COC molds and manufactured lenses remained unchanged after repeated mechanical and fabrication tests, demonstrating the reliability and high performance of COC molds in maintaining a high optical surface quality and proving the efficacy of the approach involving COC as a constitutive material for making a fabrication tool for soft contact lens manufacturing. Table 2 summarizes the main applications for COCs in optics.

7.2 | COCs in Electronics

The low dielectric constant, low loss factor, and thermal stability of COCs allow their use in capacitors that require high-temperature resistance and in antennas and frequency selective surfaces (FSS) where signal integrity is critical [125, 144, 145].

For example, Zheng et al. [140] proposed a novel copper-clad laminate (CCL) based on COC for microwave and millimeter-wave circuit applications. CCLs are a type of Printed Circuit Board (PCB) material that consists of a dielectric substrate with copper foil laminated on one or both sides. They serve as the base material for fabricating various high-frequency circuit components and antennas. The COC-based CCL exhibited a low dielectric constant of 2.34 and a low loss tangent of 0.001, which outperformed the commonly used ceramic-filled PTFE (RT/Duroid 5880 substrate. The researchers fabricated microstrip transmission lines and found that the COC-based CCL had lower insertion loss compared to the commercial PTFE-based RT/Duroid 5880 substrate. The authors also designed and tested low-loss substrate-integrated waveguide (SIW) and half-mode SIW (HMSIW) baluns on the COC-based CCL, demonstrating their potential for use in differential systems and balanced-unbalanced signal conversion. These results indicate that COCs, thanks to their excellent dielectric properties and compatibility with standard manufacturing processes, are promising materials for high-frequency capacitors and antenna substrates.

More recently, Xiao et al. [146] studied the effect of blending COCs with different T_gs into PP films for metalized film capacitors, which are widely used in high-power electrical equipment such as converter stations, electric vehicle inverters, and pulse power supplies due to their high energy density and power handling capabilities. However, the operating temperatures of these capacitors are increasing, often exceeding 100°C, which requires dielectric films with improved thermal stability and breakdown strength. The authors found that the addition of COC enhanced intermolecular interaction forces, leading to a reduction in defects of the films. COCs with higher T_g also inhibited molecular mobility and improved the thermal stability of the films, limiting charge transport at high temperatures. Compared to neat PP, the conductivity of the PP/COC films was 91.6% lower, and the breakdown strength was 45.7% higher at 125°C when using a COC with a T_g of 134°C. This demonstrates that selecting COCs with appropriate T_g values can significantly improve the dielectric properties of PP films for high-temperature capacitor applications. Also, the ability to tailor the COC structure to optimize the blend's structure and thermal stability highlights the potential of COCs as a versatile additive for enhancing the

16163028, 2026, 47, Downloaded from https://advanced.onlinelibrary.wiley.com/doi/10.1002/adfm.75610 by Cochrane France, Wiley Online Library on [16/10/2026]. See the Terms and Conditions (https://onlinelibrary.wiley.com/terms-and-conditions) on Wiley Online Library for rules of use; OA articles are governed by the applicable Creative Commons License

TABLE 2 | Summary of the COCs for optical applications.

Application	Processing	Main Properties	Main Results	Refs.
Neural electrodes	Compression molding, metal layer deposition, laser ablation, photolithography	Low water absorption, transparency, biocompatibility, chemical resistance, thermoplasticity	Excellent in vitro biocompatibility, durability in accelerated aging tests	[190]
Retinal prostheses	Thermoforming	High optical transparency superior to PDMS, PI, CPI, and LCP in transparency. Thermoplasticity for encapsulation. Can be fabricated into micro-lens arrays	Potential for enhanced longevity and suitability for retinal implant packaging. Enables self-contained image acquisition within the device (camera-free design)	[188]
Micro-lens arrays	Compression molding and thermal reflow	High optical transparency. Low water absorption rate. High stiffness	Inserting a light screen between the lenses minimizes optical interference and obtains clearer individual images. Economical fabrication method. Potential applications in biomimetic robotics	[186]
Microlens-ended fibers	Microcompression molding	High focusing ability, spatial resolution, relevant imaging capability	potential biomedical diagnostics applications such as fluorescence-based imaging and sensing. Optimized microlens fabrication	[183]
Microlens	Injection-molding	Reliable and repeatable microlens patterns	High-volume production with short cycle times (approximately 60 s per chip	[184]
Nanolens array	Replica molding and hot embossing	Hydrophilicity and hydrophobicity were reinforced by the nanolens array.	Wettability measured experimentally closely aligned with theoretical predictions.	[185]
Molds for soft contact lenses	Compression molding, UV curing	High surface roughness stability. Transparency, Reusability. Compatibility with polymeric lenses	Optical surface quality after repeated uses. Lenses with consistent power and curvature	[189]

performance of polymer dielectrics used in advanced metalized film capacitors.

The exploitation of the low loss in the THz regime was also investigated by Sharma et al. [125], who demonstrated the use of an ultra-thin COC substrate to fabricate a flexible and freestanding frequency selective surface (FSS) operating in the THz frequency range. An FSS is a periodic array of structures designed to manipulate the transmission, reflection, or absorption of electromagnetic waves at specific frequencies. The researchers designed a metasurface composed of parallel gold strips connected by a vertical gold strip, which can exhibit either single-band or dual-band transmission characteristics depending on the symmetry of the unit cell (Figure 22). By displacing the central vertical strip, the researchers could break the symmetry of the metasurface and achieve dual-band transmission peaks at 1.04 THz and 1.67 THz, with high-quality factors of 4.52 and 16.63, respectively. Hence, the use of the COC substrate, thanks to its low loss tangent even at such high frequencies, enabled the fabrication of a flexible and lightweight FSS with improved performance compared to traditional rigid substrates.

Recent innovations have explored COC as a substrate material for flexible electronics, such as MXene-and graphene oxide-based humidity sensors [191] or transparent conductive film electrodes containing silver nanowires (Ag NWs) for touch screens and wearable devices. This last example was proposed by Dawaymeh et al. [192]. The authors developed a simple and environmentally friendly method to directly coat Ag NWs on COC substrates using ultraviolet/ozone (UVO) treatment (Figure 23).

This approach eliminated the need for complex pre- and post-treatment processes required for Ag NWs on other polymer substrates. The strong adhesion between the Ag NWs and the

16163028, 2026, 47, Downloaded from https://advanced.onlinelibrary.wiley.com/doi/10.1002/adfm.75610 by Cochrane France, Wiley Online Library on [16/10/2026]. See the Terms and Conditions (https://onlinelibrary.wiley.com/terms-and-conditions) on Wiley Online Library for rules of use; OA articles are governed by the applicable Creative Commons License

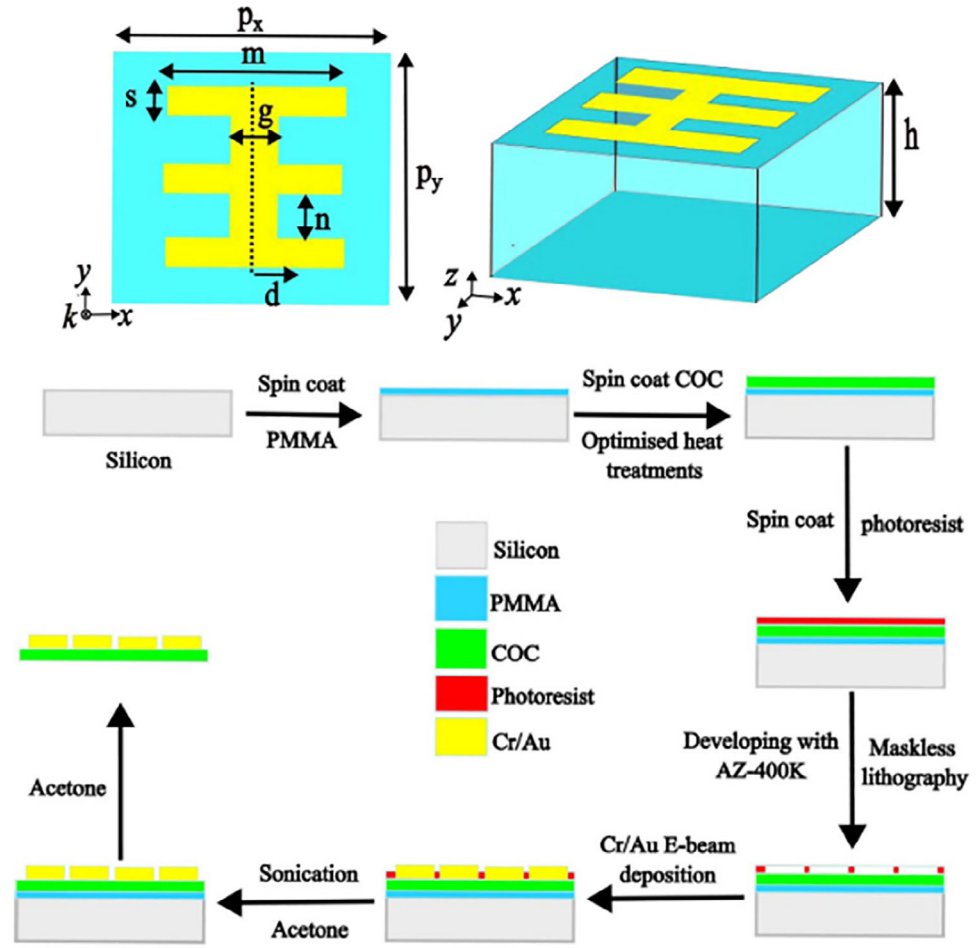


FIGURE 22 | Unit cell of the proposed metasurface with COC and metallic layer and schematic diagram for the fabrication of metasurfaces on a COC substrate [125].

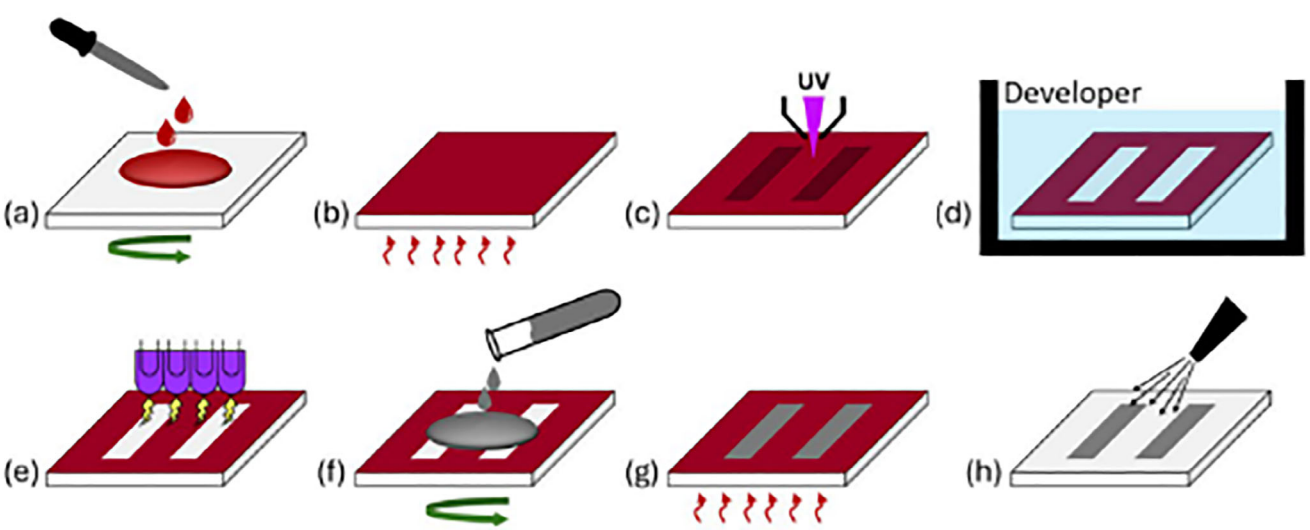


FIGURE 23 | Schematics of the production process of Ag NW-based electrodes on a COC substrate. (a) Spin coating of the photoresist layer; (b) heating at 100°C for 2 min; (c) photolithography of the photoresist; (d) development of the photoresist; (e) UVO treatment; (f) spin coating of Ag NW; heating at 110°C for 30 min; (h) removal of the photoresist and N_2 drying. Duplicated with permission from [192].

16163028, 2026, 47, Downloaded from https://advanced.onlinelibrary.wiley.com/doi/10.1002/adfm.75610 by Cochrane France, Wiley Online Library on [16/10/2026]. See the Terms and Conditions (https://onlinelibrary.wiley.com/terms-and-conditions) on Wiley Online Library for rules of use; OA articles are governed by the applicable Creative Commons License

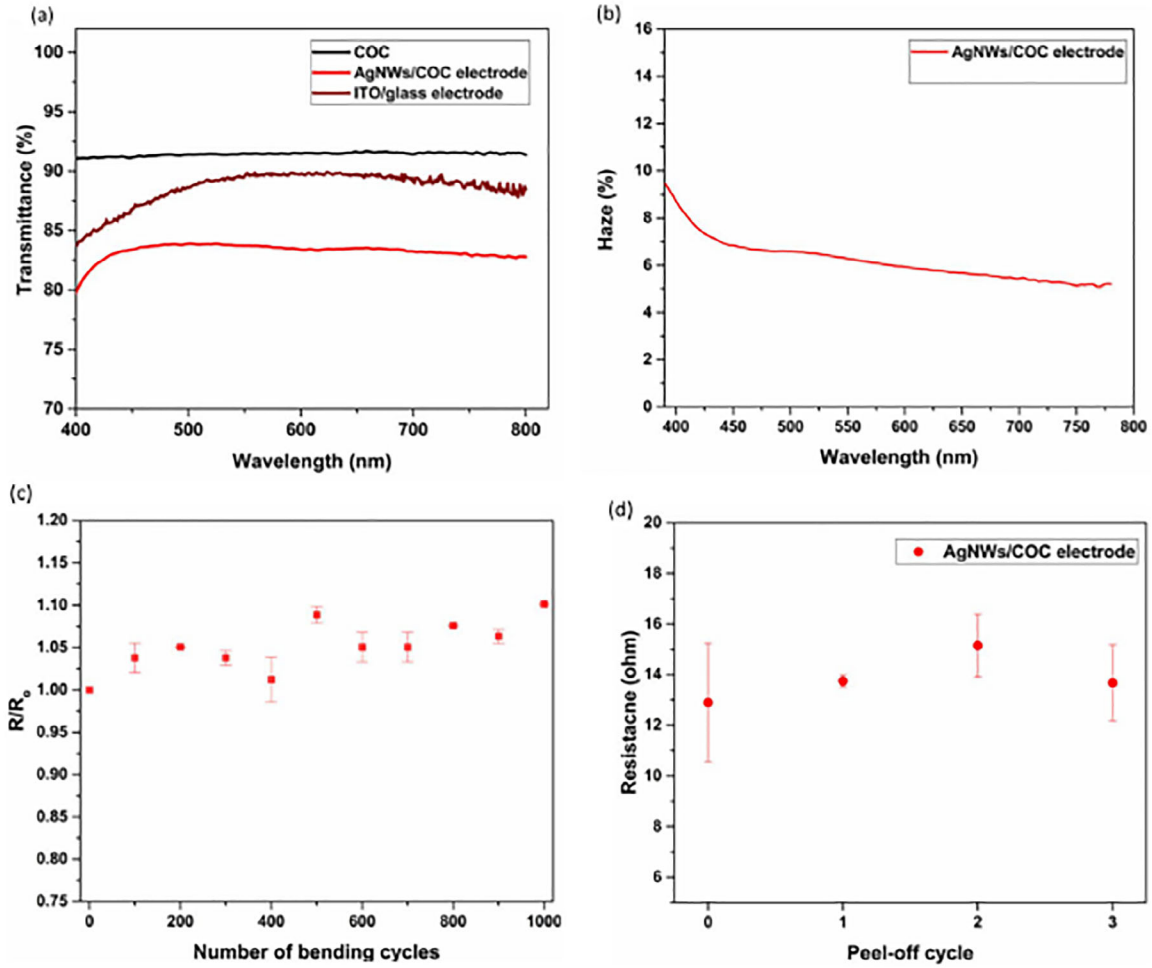


FIGURE 24 | Optical and mechanical evaluation of the COC/Ag NW electrodes. (a) Optical transmittance in comparison with ITO glass electrode; (b) haze as a function of the wavelength; (c) relative resistance over repeated bending; (c) resistance variations during tape peeling test. Duplicated with permission from [192].

COC substrate was a key advantage, highlighting COC's potential for robust coatings and films. The resulting Ag NWs/COC electrodes exhibited high optical transmittance (84%), low sheet resistance (13 $\Omega \cdot sq^{-1}$), a smooth surface, and high mechanical stability, maintaining performance even after tape-peeling and bending tests (Figure 24). The authors also fabricated an LED circuit using the Ag NW/COC electrodes as interconnections, demonstrating their suitability for flexible electronic applications. The simplicity and environmental benefits of the UVO coating approach, combined with the high performance of the Ag NWs/COC electrodes, make this work a significant advancement toward realizing the commercial potential of flexible electronics using COC substrates.

Finally, Baek et al. fabricated biocompatible neural electrodes through a combination of compression molding of COC films, metal layer deposition, and laser ablation. The eventual use of photolithography allowed the patterning of the electrodes. The resulting electrodes demonstrated excellent biocompatibility in vitro and durability in accelerated aging tests. Overall, the assessed low water absorption and transparency made COC a valuable material for long-term implants, particularly in static or quasi-static scenarios [190].

7.3 | Microfluidic Devices

7.3.1 | Chemical Engineering Applications

The ability to mold COCs into complex shapes makes them ideal for microfluidic applications in diagnostics and drug delivery systems. The biocompatibility of COCs further enhances their utility in medical electronics. A recent review of Agha et al. [8] highlighted the main features of COCs in microfluidic applications. Interestingly, authors also focused on two key challenges of COCs, i.e., the surface wettability and the bonding with other components of the microfluidic device.

Bonding is a critical stage in the fabrication of microchannels, as it creates the enclosed path. In fact, bonding a variety of inorganic and organic polymers to create multilayer structures can be challenging, since these materials often resist direct bonding and

16163028, 2026, 47, Downloaded from https://advanced.onlinelibrary.wiley.com/doi/10.1002/adfm.75610 by Cochrane France, Wiley Online Library on [16/10/2026]. See the Terms and Conditions (https://onlinelibrary.wiley.com/terms-and-conditions) on Wiley Online Library for rules of use; OA articles are governed by the applicable Creative Commons License

proper sealing. After selecting an appropriate bonding method, qualitative burst tests or expensive mechanical multi-test stations are typically required.

Various bonding techniques have been explored for COC materials, each with its own advantages and considerations. Thermal bonding involves heating the substrates to near or above the T_g of the materials, causing interdiffusion of polymer chains and bond formation. This method is simple but can lead to channel deformation due to overheating. Solvent bonding takes advantage of COC's solubility in non-polar organic solvents, allowing the polymer chains to intermingle across the interface. Solvent bonding can produce strong bonds but also requires careful control to prevent clogging. Surface treatment techniques, such as plasma activation or silanization, can be used in conjunction with thermal or solvent bonding to enhance the interfacial compatibility and bond strength.

For example, Kratz et al. developed a cost-effective bonding test method for biochips using 3D-printed drive elements. These elements transform the compressive forces into shear and traction forces, which can be applied with manual or hydraulic presses. The system is adaptable to different biochip materials, reducing costs and preventing damage while maintaining the required biocompatibility and strength [193].

Silver et al. [194] presented a recent example of COCs for microfluidic applications, in which they demonstrated the advantages of using COCs as the substrate material for 3D-printed microfluidic-microwave devices (MMDs) compared to other polymers like PLA and PP (Figure 25). COC exhibited the lowest dielectric loss tangent of 0.002 at 2.7 GHz, making it a suitable material for high-frequency microwave devices. The low microwave losses of COC allowed the fabrication of high-quality factor (Q-factor) resonators, which is crucial for the sensitivity of MMDs in detecting changes in the dielectric properties of fluids flowing through the devices. In contrast, the higher microwave losses of PLA and PP substrates resulted in lower Q-factors and reduced performance for microwave sensing applications. The authors also evaluated the microwave sensing performance of 3D-printed COC MMDs on water-in-oil emulsions, and the obtained results were comparable to conventional metal-machined resonators. In addition, the authors highlighted the optical transparency, chemical resistance, and low permeability of COC, which make it suitable for various biomedical and microfluidic applications.

Another interesting application concerns COC microporous membranes, with typical pore diameters of 0.01–10 μm. They have been used for gas separation, in-vitro tissue-barrier modeling, moisture protection of electronic chips, and as proton-exchange membranes in fuel cells. Porous membranes are commonly fabricated via thermally induced phase separation (TIPS) and diffusion-induced phase separation (DIPS) or their variants. Sabzekar et al. produced porous COC membranes using non-solvent-induced phase separation, derived from DIPS: COC was dissolved in 1,2,4-trichlorobenzene, then the cast plate was immersed in an acetone coagulation bath. Solvent–nonsolvent exchange caused rapid COC precipitation, yielding membranes with a porous layer on one side and a dense layer on the other [195]. Gel et al. fabricated free-standing, micropore-patterned COC membranes using deep reactive ion etching (DRIE) and hot embossing: COC pellets were dissolved in toluene and spin-coated on a polyvinyl-alcohol-coated silicon wafer to obtain 1–2 μm thickness. The master was then hot-embossed at 165°C for 10 min under vacuum, and plasma treatment removed residual COC from the pores before integration with microfluidic chambers [196]. Nonetheless, the fabrication of porous COC membranes remains at an early stage.

7.3.2 | Lab-on-a-Chips (LoCs)

COCs have been selected in a number of laboratory applications for fabricating microfluidic devices, also called Lab-on-a-chips (LoCs), which serve for fluidic and cellular characterizations in forensics and biotechnology. For example, hybrid microfluidic dispositions based on COC and PDMS have been used for various applications such as screening of lipid mesophases [197], cell analysis [198, 199], and microfluidic mixing [200].

Lau et al. investigated the ability of a commercially available microfluidic perfusion system, based on a plasma-treated COC, to perform as a substrate for endothelial cells upon static and dynamic flow conditions. COC exhibited limited roughness and hydrophilicity. Dynamic flow conditions inhibited platelet adhesion while promoting endothelial cell proliferation, thus demonstrating the employability of COC as a substrate for thrombogenicity of drug essays for different applications, including cardiovascular implants [201].

In a different study, Rodrigues et al. utilized COCs to fabricate microfluidic structures, focusing on optimizing the molding, sealing, and liquid handling processes while thoroughly evaluating the material properties. In contrast to other earlier studies, the authors introduced a scalable procedure for fabricating microfluidic systems made of COC that eliminates the need for a heating ramp before the embossing of COC [202, 203]. The raised channel was sealed by thermal bonding, using another COC substrate as a cover. In thermal bonding, the substrates must be in contact to allow polymer molecules to diffuse between the two substrates, resulting in a strong bond [175]. The COC-based microfluidic devices outperformed PDMS-based devices, demonstrating higher pressure resistance, reduced bubble formation at elevated temperatures, and minimized molecular diffusion into the bulk. In biosensing tests, such as a DNA hybridization assay, COC devices produced results comparable to those made of PDMS, highlighting the potential of this material for use in biosensing and LoC applications [204].

Cesaria et al. focused on the study of the biofilm formed by the canonical wild-type strain BB120 of *Vibrio campbellii* on a COC LoC, comparing the physicochemical properties of COC with those of conventionally employed materials like hydroxyapatite (HA) and PDMS [205]. This study showed that COC, unlike other common polymers, can reduce biomass adhesion, thus enabling the regulation of biofilm formation. The developed biofilms showed markedly different morphologies with complex dendritic patterns present only in the specific case of COC. The different biofilm morphogenesis was related to the interaction of COC with the conditioning layer of the planktonic biological medium.

16163028, 2026, 47, Downloaded from https://advanced.onlinelibrary.wiley.com/doi/10.1002/adfm.75610 by Cochrane France, Wiley Online Library on [16/10/2026]. See the Terms and Conditions (https://onlinelibrary.wiley.com/terms-and-conditions) on Wiley Online Library for rules of use; OA articles are governed by the applicable Creative Commons License

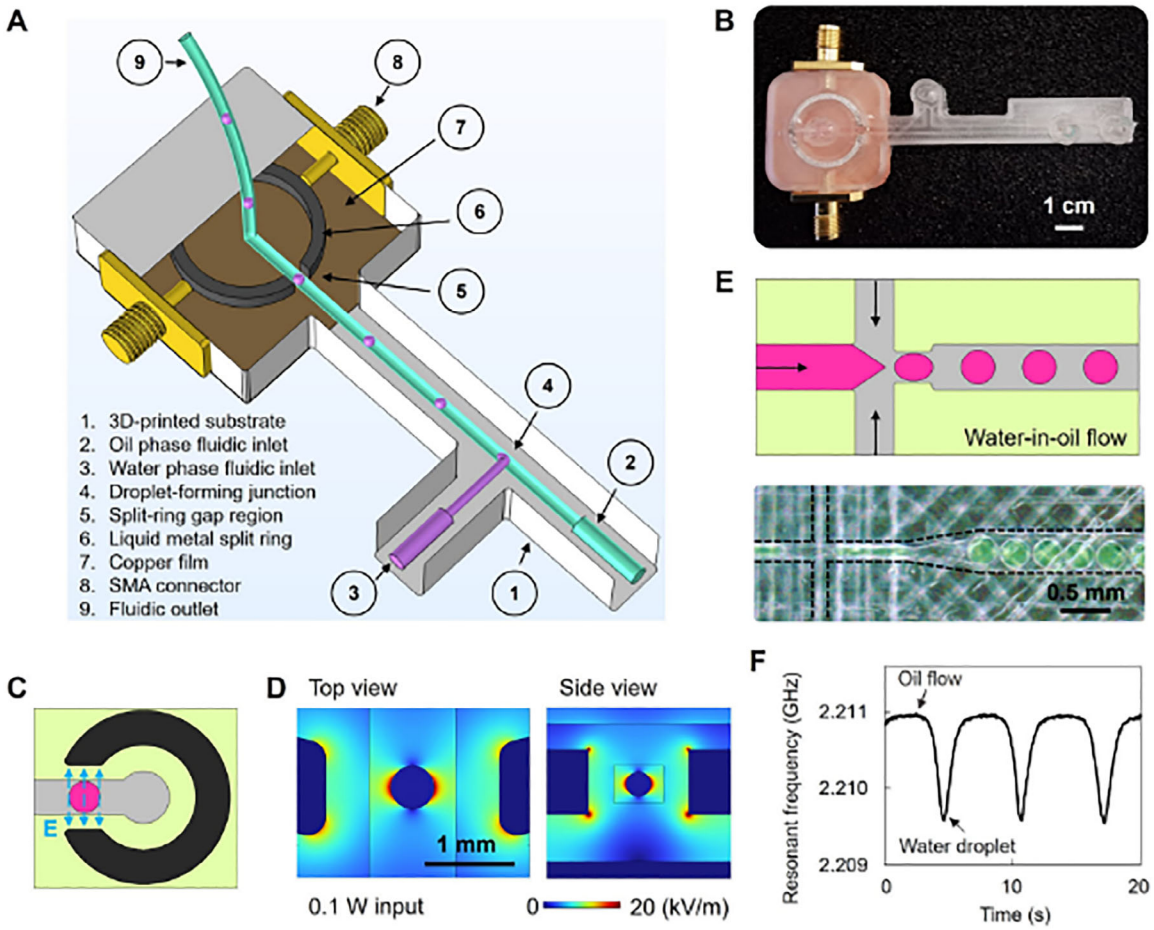


FIGURE 25 | Example of a microwave microfluidic device, with a 3D printed substrate made in COC. (a) Schematics of the device; (b) photograph of an assembled 3D printed device; (c,d) computational simulations of the electric field when a water droplet flows in the oil phase; (e) water droplet formation; (f) microwave signature of water droplet flow. Duplicated with permission from [194].

Finally, the use of the co-occurrence layer matrix analysis allowed to quantitatively evaluating the fractal development of biomass structure under different cover conditions.

Bruijns et al. demonstrated the versatility of COC as a material for 3D-printed LoC systems in forensic applications by making test devices, characterized for their chemical resistance to strong acids and optical transparency, to develop a presumptive on-chip color test able to indicate the presence of an illicit substance upon absorption spectroscopy. The compatibility of COC with a DNA amplification reaction was verified by performing the multiple displacement amplification reaction directly on the chip [206].

In another study, the same researchers developed an LOC able to perform fast and reliable DNA analyses on crime scenes, preventing any contamination. They compared the reactive properties of COCs for DNA profiling in contrast to other materials commonly employed in the field, including silicon, glass, and PDMS. The results showed that COC allowed correct identification and monitoring of DNA without any further coating on the walls of the microfluidic channels. This result has been considered a remarkable advancement in using disposable and inexpensive devices in forensics [207].

Jagannath et al. developed microfluidic chips made of COC to produce permanent three-dimensional superhydrophilic microwells [208]. Using the UV treatment, they oxidized the COC-based substrate. The COC-based substrate was coated with a polyvinyl alcohol (PVA) solution using an ultrasonic spray, thus providing a long-term uniform coating with high. To force selective filling into the wells, the coated COC surfaces were UV-cured before bonding with a pressure-sensitive hydrophobic adhesive. The surface hydrophilicity obtained using this method remained unchanged for up to 6 months. The COC-based and PVA-coated microfluidic chips were tested with kidney and breast cells, which remained viable for a 7-day test on the surface. The results showed that the coating did not influence the protein content, morphology, or quality of the cultured cells.

7.3.3 | Organ-on-a-Chips (OoCs)

COCs have been widely employed to fabricate Organ-on-a-Chip (OoC) devices to mimic specific functionalities of the targeted organs, in order to perform studies related to cell growth, viability, and metabolism, as well as investigate the activity of drugs on tissues. The employment of OoC is gaining interest

16163028, 2026, 47, Downloaded from https://advanced.onlinelibrary.wiley.com/doi/10.1002/adfm.75610 by Cochrane France, Wiley Online Library on [16/10/2026]. See the Terms and Conditions (https://onlinelibrary.wiley.com/terms-and-conditions) on Wiley Online Library for rules of use; OA articles are governed by the applicable Creative Commons License

from the scientific community as an effective in vitro tool to replace traditional approaches based on animal testing. However, its broader adoption in drug discovery and toxicity studies is often hampered by the limited production of sufficient material and incompatibility with standard laboratory equipment. In this scenario, the most widely used material for OoCs is PDMS, which, despite its popularity, presents several issues related to its high drug and water absorption that can lead to inaccurate results [209, 210]. However, the exclusive use of COC-based microfluidic devices could limit the efficiency of oxygen delivery to cell cultures within microchannels. In fact, although COC has good gas permeability, it does not reach the permeability levels of PDSM. For this reason, its use in cell culture applications that require high oxygen consumption is still limited [211]. In view of this, Bale et al. developed a dedicated COC microfluidic micro-physiological system with which they observed a decrease in oxygen concentration from 21% to 10% compared to other gas-permeable materials [212]. Other studies with thermoplastic microfluidic devices made of COC have shown a decrease in oxygen, resulting in hypoxia [213]. These studies demonstrate the low efficiency of using only COCs for this type of device in contact with cells. For example, the combination of two materials, such as COC and PDSM to make hybrid microfluidic devices exploits the advantages of both materials while minimizing the limitations of both materials. Aiming at studying drug absorption and liver physiology and metabolism in vitro, Kulsharova et al. developed a hybrid microfluidic platform combining COC and PDMS for culturing the Huh7 hepatoma cell line under dynamic conditions. These systems are important for drug development and assessment. The hepatic culture remained functional for 24 h, with biomarker levels comparable to other in vitro studies and 2D cell models. Computational Fluid dynamics simulations were also performed to analyze the formation of bubbles in the device and flow distribution, suggesting architectural modifications to optimize the experimental setting [214].

Several COC-based microfluidic devices have been developed for liver cell studies. Theobald et al. studied a simplified system based on cycloolefin polymers capable of metabolizing toxins and drugs by analyzing the toxicity of the resulting metabolites. The dual-camera liver kidney-on-chip model enables the detection of liver-mediated toxic effects. The system identified toxic effects undetectable in static cell cultures, highlighted flow direction-dependent toxic effects, and modulated toxicity with combined treatments [215, 216]. Mottet et al. developed a low-cost microfluidic chip based on COC with 3D microchambers for cell capture and analysis with reduced reagent consumption. The hot-embossed chip uses 3D microchannels to differentiate the flow speed, thus avoiding blocking in narrow areas and facilitating cell adhesion in larger 3D chambers. The chip was tested on cancer cell lines and pleural effusion samples with a positive response. The device can also be used with complex techniques effectively and with a significant reduction in costs [215, 216]. Rennet et al. created a human liver model using a COC-based system with a microfluidic flow able to assess how much sepsis can impact hepatocellular dysfunction [217]. Similarly, Wen et al. used a COC-based device to culture the HepaRG hepatoma cell line, effectively modeling the nonalcoholic fatty liver disease (Figure 26) [218]. A hybrid device for liver-on-a-chip applications based on COC and another oxygen-permeable material was used to culture primary human hepatocytes (PHH) under recirculating flow conditions [219].

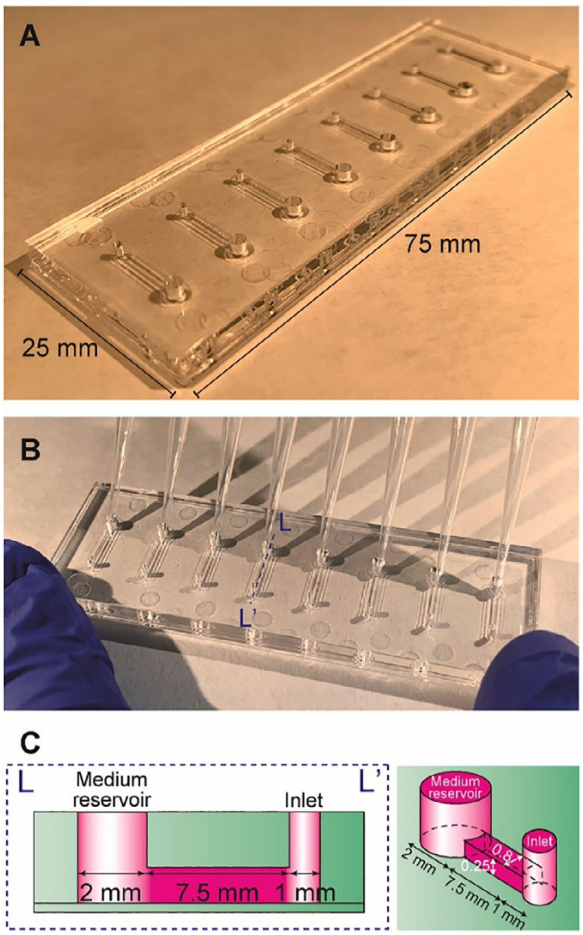


FIGURE 26 | Development of a microfluidic system for mimicking the liver. (A) Photograph of a micro-physiological system (MPS) made of cyclo-olefin polymer (COP), namely COP-MPS, for modeling nonalcoholic fatty liver disease (NAFLD). (B) Photograph of COP-MPS with eight tips and an octa-pipette to introduce cells and solutions into the microfluidic cell culture chambers simultaneously. (C) Schematic representation of a microfluidic cell culture chamber (L-L′) of the COP-MPS shown in (B). Reproduced with permission under the terms of Creative Commons license [218]. Copyright 2021, Elsevier.

Etxeberria et al. proposed, in contrast, a microfluidic COC-based device whose structure was shaped for mass production and to culture liver cell lines under dynamic conditions. The device was fabricated through injection molding and features luer-lock connectors, making it compatible with standard medical and laboratory instruments. The device was successfully used to culture HepG2/C3a cells, demonstrating its potential as a more effective and reliable alternative to PDMS for OoC applications [220].

A different use of COC and PDSM was also published to create the intermediate layer of an aorta-on-chip microfluidic system consisting of three channels, used for endothelial cell culture [214]. Table 3 summarizes all COC-based applications in microfluidics.

16163028, 2026, 47, Downloaded from https://advanced.onlinelibrary.wiley.com/doi/10.1002/adfm.75610 by Cochrane France, Wiley Online Library on [16/10/2026]. See the Terms and Conditions (https://onlinelibrary.wiley.com/terms-and-conditions) on Wiley Online Library for rules of use; OA articles are governed by the applicable Creative Commons License

TABLE 3 | Summary of the COCs for microfluidic devices.

Application	Processing	Main Properties	Main Results	Refs.
Forensic analysis	Micromilling	High chemical resistance. High optical transparency	Compatible with on-chip colorimetric tests. Compatible with DNA amplification. Reproducible absorbance spectra. Fast prototyping	[206]
Forensic analysis	Injection molding, micromilling, and hot embossing	Biocompatibility. Chemical resistance. Optical transparency. Suitability for microfluidic devices	Fast analysis times. Enhanced chain of custody. Direct DNA analysis in crime scenes. No need for channel wall coating	[207]
Biofilm studies	Mechanical shaping	Biocompatibility. Low biomass adhesion.	Reduced biofilm formation compared to HA and PDMS. Different biofilm morphologies on COC. Quantitative evaluation of biofilm structure using CGLM analysis	[205]
Drug discovery and toxicity studies	Injection molding	Compatibility with standard laboratory equipment	Successful culture of HepG2/C3a cells	[220]
Biochips	3D printing	Biocompatibility. Chemical resistance. Optical transparency. Suitable for bonding	Effective bonding with various materials. Cost-effective non-destructive testing	[193]
Microfluidic structures	Compression molding	High-pressure resistance. Reduced bubble formation. Minimal molecular diffusion in the bulk	Outperforms PDMS in several aspects. Scalable fabrication process. Microfluidic structure integrity maintained	[204]
Liver-on-a-chip	Injection molding	Biocompatibility. Chemical resistance. Optical transparency. Limited oxygen permeability	Used in various liver cell studies. Potential for modeling liver diseases. May require modifications for optimal oxygen transport	[218]
Liver-on-a-chip	Micromilling	Combination of COC and PDMS for enhanced properties	Successful culture of Huh7 hepatoma cells. Functional hepatic culture for 24 h. Comparable biomarker levels to other in vitro models. Optimized flow distribution through CFD simulation	[214]
Thrombogenicity testing	Plasma treatment	Poor roughness. Low hydrophilicity (before treatment)	Flow conditions inhibit platelet adhesion. Flow conditions promote endothelial cell proliferation. Potential uses as substrates for thrombogenicity testing	[201]

7.4 | Prefilled Biomedical Devices (PFDs)

The pharmaceutical market is seeing huge growth in prefilled biomedical devices (PFDs) due to their ability to store and dispense medication. Depending on the treatment and the specific pharmaceutical preparations, containers are in contact with chemical compounds for time spans that range from a few minutes to several weeks. Therefore, the development of materials physico-chemically inert throughout time with respect to the compounds with which they are in contact.

COC has been proposed as a potential candidate in this field as a substitute for commonly employed materials like brittle glasses. However, the lack of reactive sites for a chemical modification of COC may hinder its employability, leading to protein aggregation that limits drug stability and efficacy. A proper functionalization

16163028, 2026, 47, Downloaded from https://advanced.onlinelibrary.wiley.com/doi/10.1002/adfm.75610 by Cochrane France, Wiley Online Library on [16/10/2026]. See the Terms and Conditions (https://onlinelibrary.wiley.com/terms-and-conditions) on Wiley Online Library for rules of use; OA articles are governed by the applicable Creative Commons License

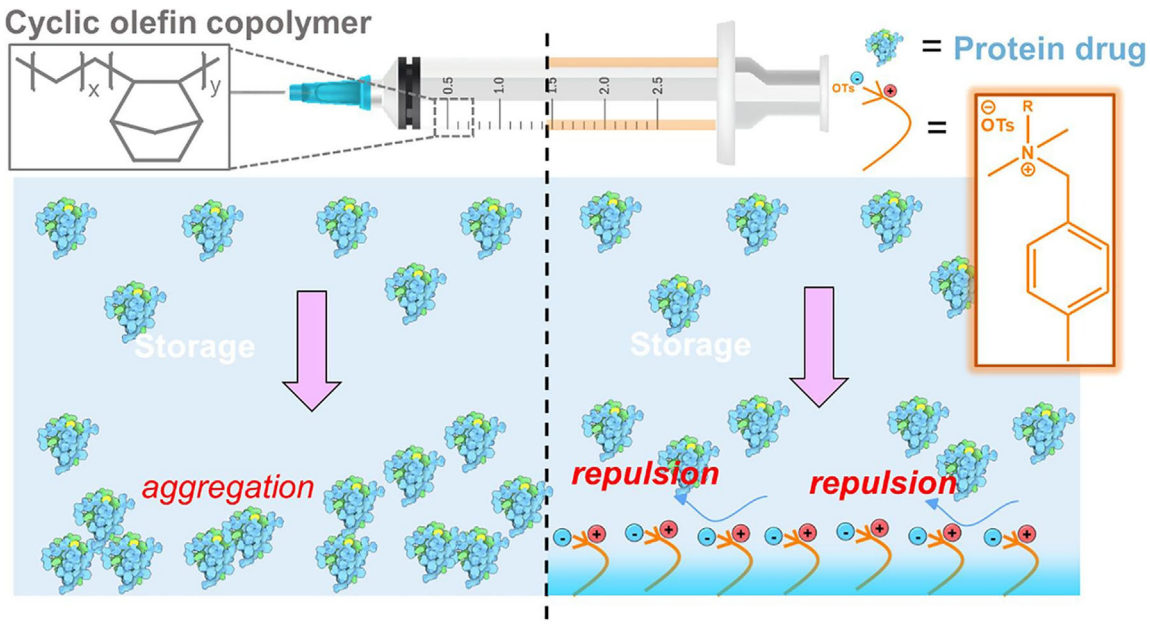


FIGURE 27 | Schematics of the interaction between insulin and COC or COC-C4, showing the effect of the hydration layer in preventing insulin aggregation. Reproduced with permission [229]. Copyright 2022, Elsevier.

of the COC material surface was studied as a possibility to overcome this issue [7]. Several methods have been proposed to tune the surface of COC, including plasma treatment [221], corona discharge [222], chemical oxidation, and UV irradiation [223]. These techniques, however, typically allow the grafting of only a limited range of functional groups, such as carboxyl, amine, epoxide, and aldehyde. Nikiforova et al. explored a novel method for covalently grafting various functional groups onto COCs by generating aryl radicals from aryldiazonium salts under acidic conditions [224]. The structural versatility of aryldiazonium compounds allowed this method to be applied in a number of applications, including biosensors [225, 226], anti-icing surfaces, medical implants, and antimicrobial devices [227, 228]. Despite its potential, none of these techniques, including the diazonium-based method, have been employed to enhance COC functionality for PFD, yet. Taking advantage of diazonium surface chemistry, surface functionalization of COC with portions of quaternary ammonium salts (QAS) was performed to improve the surface properties of COC for PFD applications. Raman spectroscopy and X-ray photoelectron spectroscopy (XPS) measurements confirmed the successful functionalization of COC using QAS diazonium salts with different alkyl chain lengths (C4, C8, C9, C10, C12). Nikiforova et al. demonstrated, through optical and fluorescence methodologies, that the ideal length of the alkyl chain COC-C4 enhances antibiofouling efficacy toward bovine serum albumin. According to dynamic light scattering and transmission electron microscope images, COC-C4 can preserve insulin for at least two weeks without any changes in protein structure, unlike glass, PP, or neat COC. Moreover, the high permeability resistance effect, transparency, and mechanical rigidity of diazonium are, in any case, retained upon functionalization. The stability of insulin was explained by the presence of an extra hydration layer that serves as a barrier to undesirable chemical interactions with biomolecules (Figure 27) [229].

In another study, Claves et al. evaluated the chemical reactivity of syringes made of either PP lubricated with silicone oil (SOL) or COC coated with crosslinked silicone (CLS), when in contact with three different drugs, i.e., paracetamol, diazepam, and insulin aspart [230]. COC-based syringes with cross-linked siliconized barrels are relatively new on the market. The barrel silicone, through crosslinking replaces silicone oil in the piston seal that can induce protein aggregation. COC-based syringes, in addition to being an inert polymer, have low leaching, and due to their hydrophobic surface, no interactions with proteins are known. In fact, COC/CLS-based syringes showed lower absorption of diazepam and insulin than that of the PP/SOL-based syringes, showing that the main cause of the higher drug absorption, in this case, depended on the plunger seal made of polyisoprene. Alkalinization of drugs was also observed only when in contact with PP/SOL. The authors concluded that, in the case of protein treatments or medications with a restricted therapeutic range that are lipophilic, COC/CLS syringes may be a reliable substitute for silicone oil-lubricated syringes currently in use.

Another application of PDF is related to the components for an implantable artificial pancreas. Type 1 diabetes is one of the most prevalent metabolic diseases globally, which causes reduced insulin production by the pancreas, leading to hyperglycemia; therefore, precise insulin delivery throughout the day is essential [231]. Mallegni et al. studied two types of COC (Topas 5013L-10 and Topas 8007S-04) for the fabrication of an insulin reservoir, selecting eventually the Topas 8007S-04 as the best candidate material to fabricate a 3D printed insulin reservoir due to its higher strength and lower T_g [162]. The fused deposition modeling technique was used to create a reservoir-like structure (Figure 28), later characterized to assess the ability of the material to prevent insulin aggregation. Although the surface of the material presented a localized roughness (in the order of 8 μm) due to

16163028, 2026, 47, Downloaded from https://advanced.onlinelibrary.wiley.com/doi/10.1002/adfm.75610 by Cochrane France, Wiley Online Library on [16/10/2026]. See the Terms and Conditions (https://onlinelibrary.wiley.com/terms-and-conditions) on Wiley Online Library for rules of use; OA articles are governed by the applicable Creative Commons License

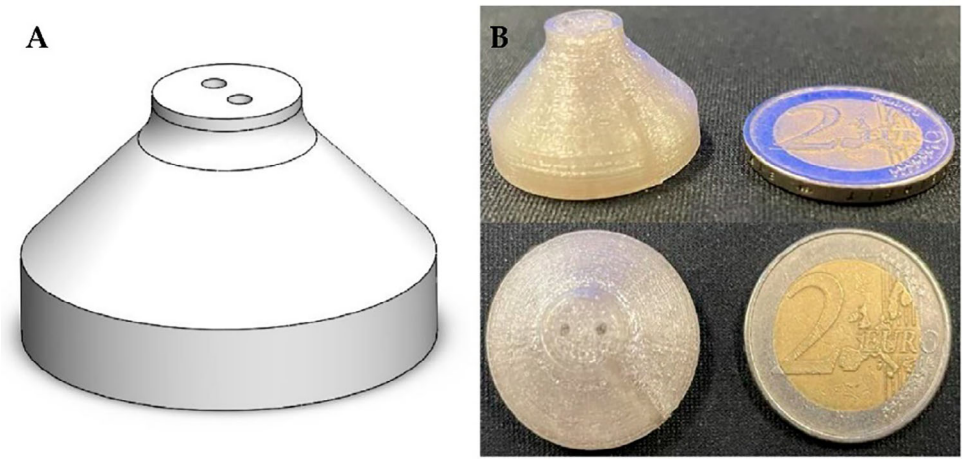


FIGURE 28 | COCs for fabricating containers for insulin for an implantable artificial pancreas. (A) Schematic design of the container. (B) Prototype fabricated via fused deposition modeling with a 2 EUR coin as a reference. Reproduced with permission under the terms of Creative Commons license [162]. Copyright 2023, MDPI.

TABLE 4 | Applications of COCs for pre-filled devices.

Application	Processing	Main Properties	Main Results	Refs.
Drug delivery (syringes)	—	Lower drug absorption (diazepam, insulin). Reduced alkalinization of drugs. Compatible with protein treatments and medications with limited therapeutic range	Outperforms PP-based syringes with silicone oil lubrication. Potential for improved drug delivery	[230]
Prefilled biomedical devices	Diazonium salt functionalization	Enhanced biocompatibility (reduced protein adsorption). Maintains transparency and mechanical rigidity	Preserves insulin structure for extended periods. Acts as a barrier to undesirable chemicals	[229]
Components for implantable artificial pancreas	3D printing	Biocompatible. Material's ability to prevent insulin aggregation	Effective insulin reservoir. Minimal insulin aggregation. Potential for long-term use	[162]
Cell culture (kidney, breast)	Injection molding	Enhanced hydrophilicity. Durable coating. Biocompatibility	High cell viability without affecting protein content	[208]

the step effect of the fabrication process, the analysis performed by UV spectroscopy did not detect significant aggregation of insulin in a time span of 14 days. Table 4 summarizes the applications of COCs for pre-filled devices.

7.5 | COCs as Self-Healing Materials

According to the definition of Lincoln et al., a multifunctional material is made of two or more materials that perform two or more functions in a manner that is constructive to the overall purpose of the structure [232]. Thus, to be classified as multifunctional, a material must possess an array of properties to sustain multiple simultaneous stimuli and be ready to perform in any designed scenario. Multifunctionality can be obtained by combining different properties, both structural and non-structural. In this sense, self-healing materials are multifunctional materials that can fully or partially restore a loss of functionality [233]. All organisms, ranging from the tiniest bacteria to the grandest animals and trees, possess diverse mechanisms of self-healing, i.e.,

16163028, 2026, 47, Downloaded from https://advanced.onlinelibrary.wiley.com/doi/10.1002/adfm.75610 by Cochrane France, Wiley Online Library on [16/10/2026]. See the Terms and Conditions (https://onlinelibrary.wiley.com/terms-and-conditions) on Wiley Online Library for rules of use; OA articles are governed by the applicable Creative Commons License

from the molecular repair of DNA via proteins to the regeneration of cells, thereby mending wounds and restoring the functionality of injured tissues. Scientists have dedicated substantial efforts to mimicking biological healing mechanisms using synthetic materials. By drawing inspiration from biological processes, researchers have identified the necessary chemical components and delivery systems to enable non-living synthetic materials to acquire self-healing properties [234]. Intrinsic potentialities of self-healing composites are numerous, such as the minimization of costs correlated to maintenance and repair operations, and the enhancement of the service life, thus improving their overall sustainability. In other words, self-healing materials could offer a strategy to overcome damage or failure, thus extending the service life. The ideal characteristics of self-healing materials for potential applications are an autonomous healing process, the possibility of multiple self-healing, low maintenance cost, and performance as good as traditional improved materials [235].

A common classification for self-healing materials is based on either being extrinsic or intrinsic [236, 237]. Extrinsic self-healing materials rely on an external healing agent, typically dispersed in the form of capsules or vascular systems. In these materials, the healing agent does not inherently interact with the polymer matrix. Being embedded within the matrix, the crack propagation can trigger its release, enabling the healing mechanism to occur. On the other hand, in intrinsic self-healing systems, the material itself heals molecular and macroscopic damage, such as cracks or defects, under external stimuli. These self-healing systems do not have an encapsulated healing agent but are characterized by a latent self-healing functionality, which is triggered by damage or by an external stimulus. Intrinsic self-healing materials rely on chain mobility and entanglement, reversible polymerizations, melting of thermoplastic phases, hydrogen bonding, or ionic interactions to initiate self-healing. The activation of the healing mechanism is strictly connected with the chemistry of the selected healing agent. One of the most important advantages in comparison to extrinsic self-healing systems is the fact that the healing process can be performed several times, theoretically, until the degradation of the healing agent after multiple healing processes is reached. This is possible due to the reversibility of the reactions and chain entanglement. The most important intrinsic self-healing systems are based on dynamic reversible bonds, ionomers, supramolecular polymers, molecular diffusion, and the addition of thermoplastic polymers. Figure 29 reports a schematization of the three main intrinsic self-healing mechanisms.

As reported in the paper of Hayes et al., it has been recently recognized that the incorporation of a meltable/softenable thermoplastic polymer within a matrix (either thermoplastic or thermosetting) could be an interesting technique for self-healing materials [238]. In this case, self-healing is facilitated by the melting and subsequent re-dispersion of the thermoplastic material into the crack plane, which fills the crack and mechanically interlocks with the surrounding matrix material. This healing mechanism is based on the interdiffusion across a polymer/polymer interface, and this process can be decomposed into five steps, namely surface approach, rearrangement, wetting, diffusion, and randomization. Diffusion is the most important step in healing, as it contributes significantly to strength development across the interface, and it depends on many factors, such as the chemical structures of the polymers, molecular weight, and polydispersity. If the polymer chain is shorter, the diffusion is higher. However, the long chains increase the entanglement of polymers, and thus the strength in the interface is higher. Thus, polymers with medium molecular weights are considered to provide the best bonding ability. The strength developed is a function of healing temperature, time, and pressure [239, 240].

Among the thermoplastic self-healing agents that could be considered, linear thermoplastic poly(bisphenol-A-co-epichlorohydrin) resin, poly(caprolactone) (PCL), poly(vinyl-acetate) (PVAc), poly(ethylene-co-methyl acrylate) (EMA), and poly(ethylene-co-methacrylic acid) (EMAA) have probably been the most widely investigated [241]. These matrices have been generally selected based on low viscosity in the molten state and their limited melting point, without taking into account their mechanical features. Interestingly, COCs have also been recently considered as thermoplastic healing additives for polymer matrices. COCs typically possess high chemical resistance, good low moisture absorption, moisture barrier properties, low density, but one of the peculiar aspects is that common commercial COC grades possess mechanical properties (elastic modulus = 2–3 GPa, tensile strength = 40–50 MPa, strain at break = 5%–10%) comparable to that of the matrices utilized for structural materials, i.e., epoxy resin. Moreover, the T_g of the COCs (and also their mechanical properties) can be modulated by varying the norbornene content, and the choice of the most suitable COC grade can thus be performed based on the required healing temperature.

In a recent work of Dorigato et al., a COC having a T_g of about 80°C was utilized as a thermoplastic healing agent in an epoxy resin typically utilized for structural composites [91, 241]. Blends were prepared by adding COC powder to the epoxy resin at different contents (from 10 to 40 wt.%), the resulting materials were then mechanically tested and thermally mended at various temperatures. Even if the immiscibility of the two phases in the blends led to a decrease in the mechanical properties under flexural and tensile loading modes, the fracture toughness of the virgin (i.e., unhealed) increased upon COC addition at elevated amounts. By the ratio of the fracture toughness (K_{IC}) value of the healed samples and the virgin ones, it was possible to determine the healing efficiency (η) of the repaired specimens. By applying a thermal repair of 145°C for 1 h on samples with 30 wt.% of COC, it was possible to obtain η values higher than 80%. In a subsequent paper of the same authors, this self-healing matrix was utilized to impregnate carbon fiber fabrics and to obtain novel composite laminates with repair capability [90]. The presence of COC particles in the interlaminar region and the increase in the viscosity of the resin led to a decrease in the relative concentration of carbon fibers and to a substantial porosity increase (up to 10–12 vol.%). Consequently, flexural modulus progressively decreased upon COC addition, and the interlaminar shear stress (ILSS) values were also considerably reduced. Fracture toughness and thermal mending behavior of the prepared laminates were evaluated through Mode I fracture toughness tests, and with a COC amount of 30 wt.% an overall efficiency as high as 180% was achieved. The observed increase in the interlaminar fracture toughness in the healed samples was due to the propagation of the crack within the

16163028, 2026, 47, Downloaded from https://advanced.onlinelibrary.wiley.com/doi/10.1002/adfm.75610 by Cochrane France, Wiley Online Library on [16/10/2026]. See the Terms and Conditions (https://onlinelibrary.wiley.com/terms-and-conditions) on Wiley Online Library for rules of use; OA articles are governed by the applicable Creative Commons License

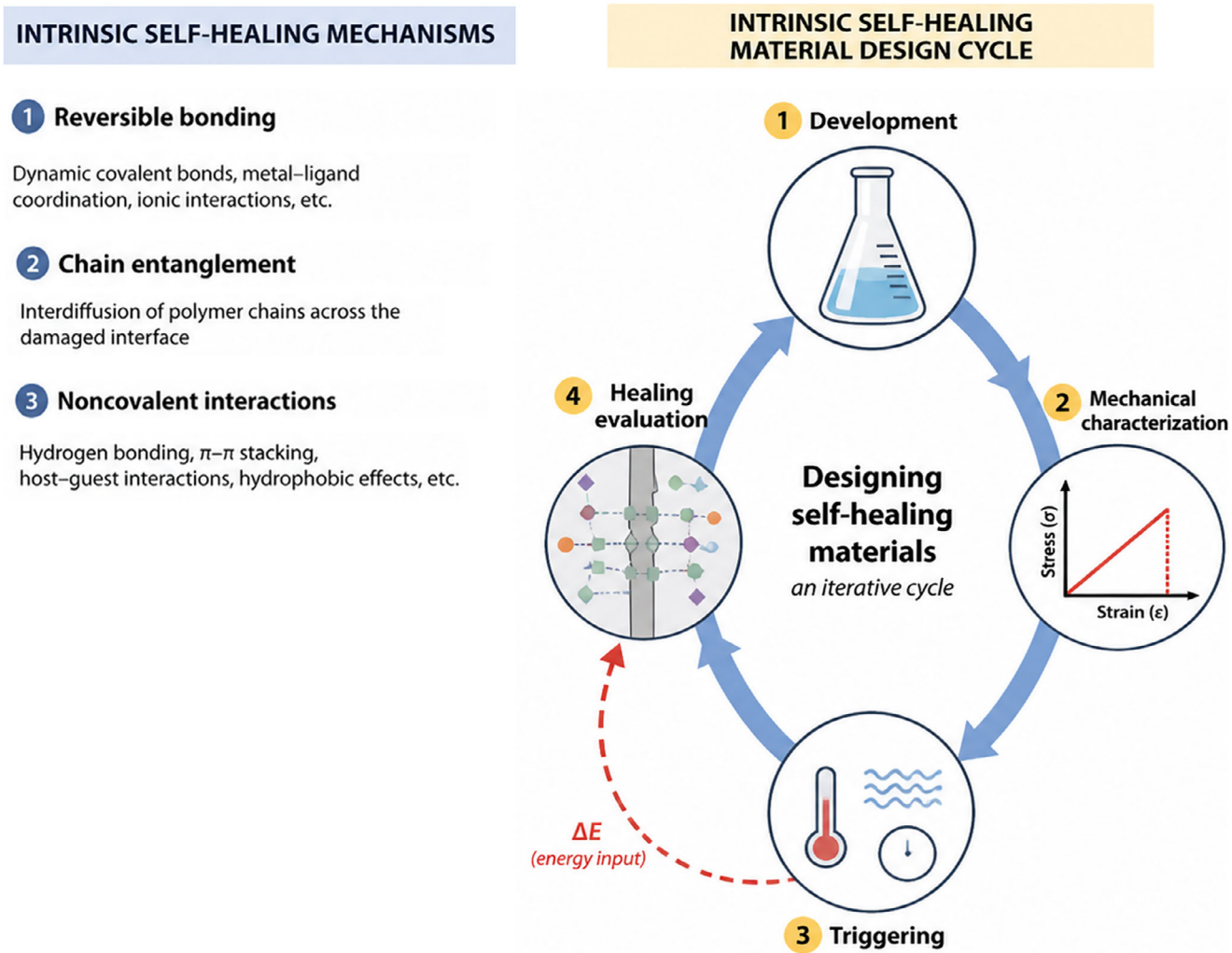


FIGURE 29 | Schematization of the three main intrinsic self-healing systems.

COC phase, with a progressive plasticization of the thermoplastic constituent.

In another work, thin COC foils were used as an intrinsic thermoplastic healing agent in carbon fiber (CF) reinforced epoxy laminates. COC films were produced by hot pressing and inserted in the interlaminar region between each epoxy/CF lamina during the hand layup fabrication [89]. It was observed that the fiber volume fraction decreased and the porosity increased with the introduction of COC layers, causing a drop in the mechanical properties of the laminates. Specimens subjected to the mode I interlaminar fracture toughness test were then thermally mended by resistive heating, through the Joule effect of conductive CFs, reaching a temperature of about 190°C. The healing efficiency was evaluated as the ratio of critical strain energy release rate (G_{IC}) of the healed and the virgin specimens, and healed materials exhibited η values up to 164%.

By following a different approach, Perin et al. examined the self-healing behavior of carbon fiber reinforced composites prepared by depositing jet-spun cyclic olefin copolymer (COC) meshes on dry CF plies, before lamination with epoxy resin [93]. Three different laminates were prepared, including a neat epoxy/CF sample and two composites with 4 wt.% and 8 wt.% of COC in the form of a jet-spun network as a healing agent. The laminates were thermally mended at 110°C by resistive heating generated by an electrical current flowing within the samples, and the laminates containing 8 wt.% COC reported a healing efficiency, evaluated as the ratio between the maximum load of virgin and healed samples in interlaminar fracture toughness tests, of about 34%. Fractography analysis evidenced that the limited healing capability of the prepared laminates could be ascribed to a poor adhesion between the COC mesh and the epoxy matrix, and to the presence of several COC microfibers trapped inside the epoxy phase without any possibility to diffuse inside the crack zone at the softened state.

Very recently, the rheological, morphological, and thermo-mechanical properties of compatibilized polyamide 6 (PA6)/COC blends were comprehensively investigated, with the aim of developing a novel self-healing matrix for thermoplastic structural composites [92, 94, 96]. After a preliminary selection of the best compatibilizer and COC amount, it was concluded that the addition of ethylene glycidyl methacrylate (E-GMA) decreased COC domain size and improved the interfacial interaction with PA6, which was at the basis of a higher tensile strength and strain at break compared to neat PA6/COC blends. E-GMA also significantly boosted the healing efficiency (η), measured via

16163028, 2026, 47, Downloaded from https://advanced.onlinelibrary.wiley.com/doi/10.1002/adfm.75610 by Cochrane France, Wiley Online Library on [16/10/2026]. See the Terms and Conditions (https://onlinelibrary.wiley.com/terms-and-conditions) on Wiley Online Library for rules of use; OA articles are governed by the applicable Creative Commons License

fracture toughness tests in quasi-static and impact conditions. Applying a healing temperature of 160°C (i.e., far below the melting point of PA6), the blend with an E-GMA content of 5 wt.% and a COC concentration of 30 wt.% showed η values of 38% in quasi-static mode and 82% in impact mode. The higher healing efficiency under impact conditions was attributed to the planar fracture surface, which facilitated the flow of the healing agent in the crack zone, as proven by fractography analysis.

This blend with optimized composition was then utilized to prepare via melt-compounding and injection molding thermoplastic composites with a discontinuous CF content of 20 wt.% [95]. The presence of COC domains within the matrix allowed the attainment of healing efficiencies of up to 80% in impact tests, whereas lower healing efficiency values are found in quasi-static fracture tests, due to PA6 plasticization hindering the COC flow in the fracture zone. Fatigue testing revealed the ability of PA6/COC/CF composites to repair microdamage during thermal mending, extending their own fatigue life by 77%, while PA6/CF samples were not able to heal. The same self-healing matrix was utilized by the same authors to prepare long carbon fiber self-healing thermoplastic composites [242]. The blend was prepared through melt compounding and then extruded into thin sheets having a thickness of 150 µm. The laminates were then prepared through film stacking followed by hot pressing. The void content in self-healing laminates was higher than in PA6/CF samples, due to the higher viscosity of the matrix that impaired its wetting ability. However, the mechanical properties of the self-healing laminates were comparable with those of PA6/CF, and also the evaluation of the interlaminar shear strength (ILSS) highlighted that there was no substantial difference between the two composites. Upon the thermal mending process, it was possible to demonstrate that self-healing laminates were capable of completely restoring the original ILSS values, with the microdamages induced in the matrix and at the interphase fully repaired. These results highlighted the potential of intrinsic self-healing thermoplastic composites to extend the service life of structural composites.

It is important to underline that the restoration of a lost functionality in self-healing materials does not only refer to the mechanical performance, but also to other physical properties, like surface wettability. In this sense, COC was recently considered by Zhou et al. as a self-healing matrix for the production of superhydrophobic coating with triboelectrification-induced liquid self-repellency [243]. In this work, COC, fluorinated alkyl silane (FAS) and polytetrafluoroethylene (PTFE) nanoparticles were mixed to prepare films with the dip coating technique (see Figure 30a). Thanks to the triboelectric negative features of COC and PTFE, this coating showed triboelectrification-induced repellence to water (and also to NaCl, strong acid, and alkali solutions) after rubbing with a polyamide fabric. Moreover, the coating demonstrated excellent endurance to severe mechanical, chemical, and environmental damages in a wide temperature range. It also showed self-healing capability from physical/chemical damage. After 5000 abrasion cycles, the fabric showed a lowering of the water contact angle (WCA) up to 122°, however, after 5 min heating at 130°C, the fabric had WCA of 156°, and the original coating superhydrophobicity was thus recovered (see Figure 30b). Moreover, after 96 h of UV-irradiation the fabric showed reduced water repellency (WCA of 116°) due to the formation of polar groups (-COOH, -OH) on the surface. However, after a short heating treatment, the WCA was restored to 158° (see Figure 30c). It is also interesting to notice that after a plasma treatment of 10 min the fabric became super-hydrophilic) (Figure 30).

7.6 | COC for Packaging Applications

COCs are biocompatible (ISO 10993 approved) and suitable for direct food contact. They can be combined with PE in monolayer blend films or used as layers in multilayer films for flexible packaging of foods, drugs, cosmetics, personal-care, and consumer products. In PE blends, they enhance stiffness and sealability. As the core layer in multilayer films, they provide a moisture barrier, clarity, and stiffness. COC coextruded with PE typically requires no tie layer due to high compatibility, while tie layers are generally needed in coextrusion with PP, PVC, PC, PAs, and polyesters (PET, Polybutylene Terephthalate – PBT, Polyethylene naphthalate – PEN), as well as Ethylene vinyl alcohol (EVOH) [12].

In addition to traditional multilayer structures, a strategy for obtaining more sustainable or partially bio-based packaging films with improved mechanical performance consists of blending poly(butylene succinate) (PBS) with COC. PBS/COC blends, prepared via solution casting, showed physical interactions between the phases and a significant increase in tensile strength, with an optimum at the 30PBS/70COC composition (≈91 MPa). The films also exhibited a compact morphology and antibacterial activity, highlighting the potential of these systems as partially bio-based materials for high-performance packaging applications [244].

COC-based multilayer barrier films for blister packaging can be processed similarly to PVC coated with polyvinylidene dichloride (PVDC): they thermoform at relatively low temperatures (110°C–130°C) on existing equipment and achieve 10%–20% shorter cycle times than PVC/PVDC films. Moreover, COC films form blisters with more uniform wall thickness, thus improving moisture-barrier performance, relative to competing materials. Monolayer COC blend films show good twist-wrap behavior and can be easily metallized, laminated, or extrusion-coated onto paperboard to provide an effective water-vapor barrier [12]. Furthermore, monoaxial orientation of neat and blended COC resins can produce shrink films with high shrink ratios and low shrink forces.

To overcome the intrinsic rigidity of COC in flexible packaging applications, blending strategies have been extensively explored. For example, Durmus et al. systematically studied cyclic olefin copolymer/poly ethylene-co-vinyl acetate (COC/EVA blends (90/10, 80/20, and 70/30) obtained by film extrusion, analyzing their morphology, rheological behavior, and mechanical properties. It was shown that morphology evolves from a matrix-drop structure to a co-continuous morphology as the EVA content increases, with a significant influence on the viscoelastic response and mechanical behavior. The addition of EVA increased melt strength and relaxation time, improving processability in film blowing and cast film, while reducing elastic modulus and yield stress, and increasing elongation at break and therefore the toughness of the film. The introduction of a compatibilizer,

16163028, 2026, 47, Downloaded from https://advanced.onlinelibrary.wiley.com/doi/10.1002/adfm.75610 by Cochrane France, Wiley Online Library on [16/10/2026]. See the Terms and Conditions (https://onlinelibrary.wiley.com/terms-and-conditions) on Wiley Online Library for rules of use; OA articles are governed by the applicable Creative Commons License

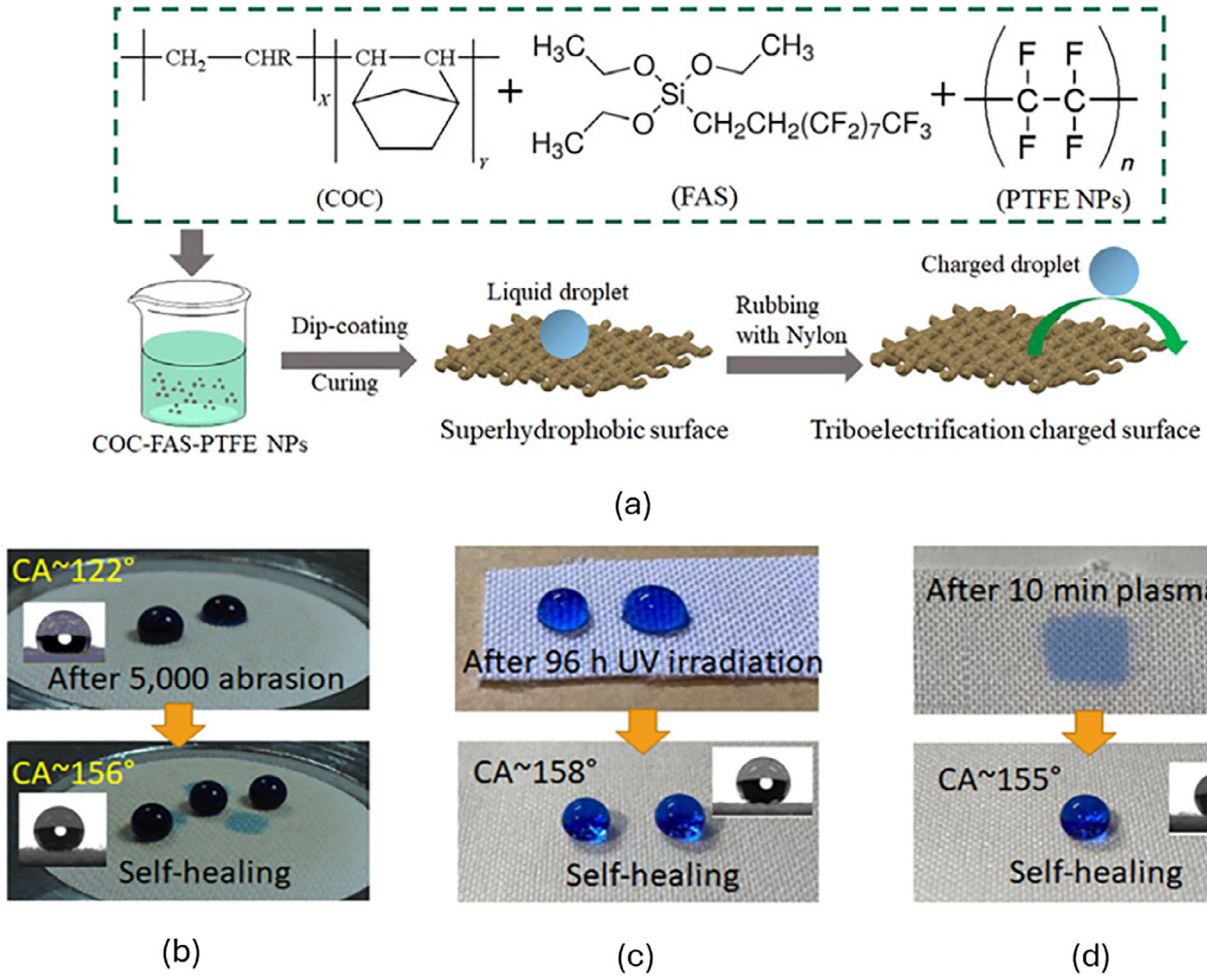


FIGURE 30 | (a) Chemical structures of the coating materials and procedure for coating treatment of the fabric substrates, (b) water droplets on the treated fabric after 5000 abrasion cycles and heat treatment, (c) water droplets on the treated fabric after 96 h UV irradiation and heat treatment, (d) Water droplet on the treated fabric after 10 min plasma treatment and heat treatment (adapted with permission from [243]).

such as the maleic anhydride grafted polyethylene (PE-g-MA), promotes finer phase dispersion and amplification of rheological effects. This study demonstrates how blending with EVA is an effective strategy for overcoming the intrinsic rigidity of COC, while maintaining its transparency and expanding its potential in flexible packaging applications [79]. A significant contribution in the field of flexible packaging concerns the study of linear low-density polyethylene/cyclic olefin copolymer (LLDPE/COC) blends for multilayer and heat-sealing applications. In parallel, blending COC with polyolefin matrices has also been investigated to optimize multilayer structures and heat- sealing performance. Lamnawar et al. studied LLDPE/COC blends containing 5–15 vol% COC, analyzing their rheological behavior, morphology, and peel strength. The rheological analysis showed partial compatibility between the phases, confirmed by microscopy observation of fine dispersion of COC in the LLDPE matrix. From an application point of view, the most innovative aspect concerns the heat sealing performance: LLDPE/COC blends show a significant improvement in peel strength, particularly on PET substrates, suggesting a potential industrial configuration in which a thin layer of LLDPE/COC blend is co-extruded onto PET to improve sealability to PE films. This study demonstrated that the controlled integration of COC into polyolefin matrices is an effective strategy for modulating rheological properties and interfacial adhesion, expanding the possibilities for using COC in multilayer packaging structures [74].

COC, in addition to being used as a barrier layer, can be melt-blended with polypropylene (PP) without the need for compatibilizers in order to effectively increase rigidity and dimensional stability. As the COC content increases, tensile strength and modulus rise, while elongation at break and impact resistance decrease, consistent with the inherently more rigid nature of COC. From a morphological standpoint, the COC/PP system evolved toward microfibrillar structures and, at compositions close to 50/50, shifts toward a co-continuous morphology that maximizes the reinforcing effect. Dynamic mechanical analysis confirmed the immiscibility of the phases, while rheology shows an increase in viscosity with shear-thinning behaviour. Overall, PP/COC blends emerged as a promising platform for rigid or semi-rigid packaging, with a clear trade-off in terms of impact performance [71].

When incorporated in the heat-seal layer of bags or stand-up pouches for beverages, cereals, candies, soups, and pet foods, COCs can improve hot-tack and ultimate seal strength with-

16163028, 2026, 47, Downloaded from https://advanced.onlinelibrary.wiley.com/doi/10.1002/adfm.75610 by Cochrane France, Wiley Online Library on [16/10/2026]. See the Terms and Conditions (https://onlinelibrary.wiley.com/terms-and-conditions) on Wiley Online Library for rules of use; OA articles are governed by the applicable Creative Commons License

out altering the PE film's seal-initiation temperature. Besides solution casting and doctor-blade casting, melt extrusion is the most widely used process for preparing dense membranes, as it avoids the lengthy drying times associated with solution methods [8].

Another approach to improving the barrier properties of COC involves the introduction of inorganic or carbonaceous nanofillers. Ou and Hsu reported one of the first systematic studies on COC/SiO_2 nanocomposites obtained by solution blending [98]. The addition of nanometric silica (1–15 wt.%) resulted in a significant increase in glass transition temperature (up to +20°C) and thermal stability, together with a reduction in oxygen permeability of approximately 30% already with 5 wt.% of SiO_2, while maintaining optical transparency above 85% up to 10 wt.% of filler. Subsequently, Roy et al. demonstrated that low amounts of fumed silica (1–5 wt.%), introduced by melt blending, further improved the mechanical and thermal properties of COC, increasing the tensile strength up to 55.6 MPa and the T_g up to approximately 194°C with 3 wt.% filler, while maintaining high transparency in the visible range [99].

Recently, the use of graphene nanofillers in extremely low concentrations has been studied to improve the barrier properties of COC without compromising its transparency. In particular, it has been shown that the addition of less than 0.1 wt.% of thermally reduced graphene allows significant reductions in water vapor permeability (up to 20%–65%) to be achieved, while maintaining high optical transmittance (>85%). This behavior cannot be explained solely by classical tortuosity models [245, 246], but is also attributed to the local stiffening of polymer chains at the COC–graphene interface and, in some cases, to the formation of nanocompound-induced semicrystalline domains. This approach makes it possible to obtain high-performance barrier films with 10–100× lower filler content than traditional polymer/clay or polymer/graphene systems, with clear advantages in terms of cost, processability, and maintenance of optical properties, making these materials particularly promising for advanced packaging applications [116].

In addition to traditional nanofillers (i.e., silica, graphene), recent studies have shown that functional metal oxides can also transform COC into a platform for active packaging. In particular, COC/TiO_2 nanocomposites (1–5 wt.%) obtained by solution casting showed a marked improvement in barrier properties (i.e., strong reduction in water vapor and oxygen permeability) and a significant increase in the mechanical behaviour, with an optimum around 3 wt.% where filler dispersion is most effective; at higher filler loads, agglomeration phenomena emerge with partial deterioration of properties. The presence of TiO_2 introduces antibacterial functionality (effective against bacteria like *Escherichia coli* or *Staphylococcus aureus*) while maintaining good biocompatibility, highlighting the potential use of COC not only as a barrier material but also as a multifunctional film for high-performance packaging applications when antimicrobial properties are also required [247].

A summary of the packaging applications for the COCs is reported in Table 5.

8 | Challenges and Future Perspectives

COCs are compelling as "platform" polymers, but their broad deployment will hinge on solving several open challenges and pursuing targeted research avenues: industrially, COCs often demand high processing temperatures within a narrow window and show poor melt strength – especially problematic for extrusion/blow molding, while intrinsic brittleness/rigidity, weak adhesion (for bonding, coating, printing), and limited compatibility with other polymers complicate device integration; economically, high raw-material cost and specialized equipment raise barriers; environmentally, acceptance in mainstream recycling streams remains limited and long-term degradability is low; and, in service, lower heat-deflection temperature (for some grades) and solvent-specific resistance can constrain operating envelopes. Looking forward, promising directions include (i) polymer design: catalyst/monomer and chain-architecture engineering (e.g., controlled long-chain branching, bimodal molecular weight distributions) to widen processing windows, lower melt temperatures, and boost melt strength without sacrificing optical/electrical performance; (ii) toughening without haze: index-matched elastomers, nanostructured core–shell rubbers, or block-copolymer tougheners that maintain transparency and low dielectric loss; (iii) interfaces that last: scalable, low-leach surface chemistries (plasma-activated grafting, corona, diazonium/photografts) with proven stability through sterilization and aging to fix adhesion and printing, plus primer/ink co-design for reliable graphics and metallization; (iv) compatibilized blends and composites: reactive compatibilizers and interphases that let COCs work with commodity polyolefins or elastomers for impact and flexibility, enabling coextrusion and multilayers without delamination; (v) recycling and circularity: mono-material device architectures, design-for-disassembly, solvent-based purification loops, and property-retention maps over multiple reprocess cycles, alongside pilot take-back schemes to address current sorting/stream limitations (and exploratory work on chemically recyclable/partially degradable COC-like chemistries); (vi) process intelligence: digital twins for thermal/bonding windows in microfluidics, print-parameter/process-property maps for RF/THz parts, and quantitative spec sheets for oxygen transport in hybrid OoC stacks (COC + targeted gas-permeable layers); and (vii) thermal/chemical robustness: higher-T_g grades or vitrimer-like crosslinkables to lift HDT and creep resistance, plus ultra-thin barrier/top-coat strategies to expand solvent compatibility. In parallel, pragmatic near-term mitigations, tight thermal control, and specialized hardware to stabilize melt behavior, judicious blending/additives for impact and flexibility, and routine surface treatments (plasma, corona) for adhesion, can reduce today's pain points, while dedicated recycling programs and cost-aware formulations make COCs more sustainable and accessible across optics, electronics, packaging, and bio-microfluidics.

Among the challenges outlined above, the most critical bottleneck for broader COC deployment is the limited interfacial compatibility, encompassing weak adhesion, poor blend compatibility, and insufficiently durable surface functionalization. These interfacial constraints directly restrict multilayer integration, printing, and metallization reliability, bonding in microfluidic systems, and hybrid material architectures, thereby limiting

16163028, 2026, 47, Downloaded from https://advanced.onlinelibrary.wiley.com/doi/10.1002/adfm.75610 by Cochrane France, Wiley Online Library on [16/10/2026]. See the Terms and Conditions (https://onlinelibrary.wiley.com/terms-and-conditions) on Wiley Online Library for rules of use; OA articles are governed by the applicable Creative Commons License

TABLE 5 | Packaging applications for the COCs.

Application	Processing	Main Properties	Main Results	Refs.
Flexible Packaging	Extrusion/coextrusion	Increased stiffness, improved sealability, moisture barrier, and high clarity	Improved film rigidity, enhanced heat-seal performance, effective moisture-barrier layer in multilayer structures, removal of tie layer when coextruded with PE	[4]
Flexible Packaging	Solution casting	Improved interfacial compatibility, enhanced mechanical strength	Significant increase in tensile strength, partially bio-based packaging films, antibacterial activity	[244]
Blister packaging	Thermoformor-ming (110-130°C)	moisture barrier	10–20% shorter cycle times vs PVC/PVDC, improved blister uniformity, enhanced moisture protection of packaged products	[4]
Flexible packaging	Extrusion	Increased elongation at break and toughness, reduced modulus and yield stress, processing stability	Improved processing stability, progressive reduction of rigidity, significant enhancement of film toughness, improved mechanical performance without significant transparency loss	[79]
Multilayer Flexible packaging	Extrusion	Partial phase miscibility/compatibility	Significant improvement in peel strength, especially on PET substrates, optimized adhesion at ~10 vol% COC, potential multilayer configuration: PET sheet coated with thin LLDPE/COC layer to enhance sealability to PE films	[74]
Rigid/semi-rigid packaging	Extrusion, injection molding	Increased shear viscosity, shear-thinning behavior	Increase in tensile and flexural strength and modulus with increasing COC content, reduction in elongation at break and impact strength, maximum reinforcing effect near co-continuous morphology (≈50/50 composition)	[71]
Oxygen barrier film	Solution blending	Improved thermal stability, good nanoparticle dispersion high optical transparency (>85% up to 10 wt.%)	31% reduction in oxygen permeability already at 5 wt.% SiO_2, further permeability decrease at 10 wt.%, maintained optical transparency suitable for optical applications	[98]
High-strength transparent films	Extrusion/compression molding	Increased tensile strength increased T_g, improved stiffness and scratch resistance	Optimal performance at 3 wt.% silica, ~24% increase in tensile strength vs neat COC, enhanced thermal stability and mechanical robustness while preserving optical transparency	[99]

(Continues)

16163028, 2026, 47, Downloaded from https://advanced.onlinelibrary.wiley.com/doi/10.1002/adfm.75610 by Cochrane France, Wiley Online Library on [16/10/2026]. See the Terms and Conditions (https://onlinelibrary.wiley.com/terms-and-conditions) on Wiley Online Library for rules of use; OA articles are governed by the applicable Creative Commons License

TABLE 5 | (Continued)

Application	Processing	Main Properties	Main Results	Refs.
Packaging application	Solution blending, film casting	Reduces the water vapor permeability, high optical transparency (>85%)	Reduced water vapor permeability (∼20%–65%) with <0.1 wt.% TRGO, barrier performance beyond Nielsen/Cussler predictions, similar improvements achieved with 10–100× lower filler content than conventional systems	[116]
Active antibacterial packaging	Casting solution	Improved barrier properties, enhanced mechanical strength, antibacterial activity	WVP and O_2 permeability reduced by ∼63–64%, tensile strength +113% at 3 wt.% TiO_2, antibacterial activity against E. coli and S. aureus, optimal performance at ∼3 wt.% before agglomeration	[247]

translation from material performance to device-level functionality. While processing temperature, melt strength, and brittleness remain important material concerns, they are increasingly addressable through formulation and equipment optimization. In contrast, interfacial reliability governs whether COCs can be seamlessly integrated into complex, application-relevant systems. Consequently, the most promising near- to mid-term direction lies in scalable and durable interface engineering strategies, including plasma-activated grafting, corona treatments, and photochemical surface modification approaches with demonstrated stability under sterilization and aging conditions. Such advances offer high leverage: they preserve the intrinsic optical and dielectric advantages of COCs while unlocking broader compatibility, functional integration, and manufacturing robustness.

Acknowledgements

Open access publishing facilitated by Universita degli Studi di Trento, as part of the Wiley - CRUI-CARE agreement.

Conflicts of Interest

The authors declare no conflicts of interest.

Data Availability Statement

The authors have nothing to report.

References

1. M. R. Buchmeiser, "Tandem Ring-Opening Metathesis—Vinyl Insertion Polymerization: Fundamentals and Application to Functional Polyolefins," *Macromolecular Rapid Communications* 38 (2017): 1600672.

2. J. Y. Shin, J. Y. Park, C. Liu, J. He, and S. C. Kim, "Chemical Structure and Physical Properties of Cyclic Olefin Copolymers (IUPAC Technical Report)," *Pure and Applied Chemistry* 77 (2005): 801–814.

3. W. Kaminsky, "The Discovery and Evolution of Metallocene-Based Olefin Polymerization Catalysts," *Rendiconti Lincei* 28 (2017): 87–95.

4. R. R. Lamonte and D. Mcnally, "Cyclic Olefin Copolymers," *AM&P Technical Articles* 159, no. 3 (2001): 33–36.

5. W. S. R. Lago, C. Aymes-Chodur, A. P. Ahoussou, and N. Yagoubi, "Physico-Chemical Ageing of Ethylene–Norbornene Copolymers: a Review," *Journal of Materials Science* 52 (2017): 6879–6904.

6. W. Zhao and K. Nomura, "Copolymerizations of Norbornene and Tetracyclododecene with α-Olefins by Half-Titanocene Catalysts: Efficient Synthesis of Highly Transparent, Thermal Resistance Polymers," *Macromolecules* 49 (2016): 59–70.

7. C. E. O'Neil, S. Taylor, K. Ratnayake, S. Pullagurla, V. Singh, and S. A. Soper, "Characterization of Activated Cyclic Olefin Copolymer: Effects of Ethylene/Norbornene Content on the Physiochemical Properties," *Analyst* 141 (2016): 6521.

8. A. Agha, W. Waheed, N. Alamoodi, et al., "A Review of Cyclic Olefin Copolymer Applications in Microfluidics and Microdevices," *Macromolecular Materials and Engineering* 307 (2022): 2200053.

9. C. Li, X. Lu, Y. Li, et al., "Research Progress and Prospects of Co_2 Flooding Sweep Characteristics and Sweep-Extend Technologies: a Review," *Huagong Jinzhan/Chemical Industry and Engineering Progress* 43 (2024): 4779.

10. L. S. Wu, J. Liu, T. T. Wang, Z. H. Luo, and Y. N. Zhou, "Synthesis of Cross-Linkable Norbornenyl Copolymers via ROMP for Fabricating Cyclic Olefin Vitrimers," *ACS Applied Polymer Materials* 6 (2024): 12598–12605.

11. G. Khanarian, "Optical Properties of Cyclic Olefin Copolymers," *Optical Engineering* 40 (2001): 1024.

12. R. R. Lamonte and D. Mcnally, "Cyclic Olefin Copolymers," *Advanced Materials and Processes* 159 (2001): 33–36.

13. M. Arndt and I. Beulich, "C_1-Symmetric Metallocenes for Olefin Polymerisation, 1. Catalytic Performance of $[Me_2C(3\text{-}^{tert}BuCp)(Flu)]ZrCl_2$ in Ethene/Norbornene Copolymerisation," *Macromolecular Chemistry and Physics* 199 (1998): 1221–1232.

14. M. Blochowiak, T. Pakula, H. J. Butt, M. Bruch, and G. Floudas, "Thermodynamics and Rheology of Cycloolefin Copolymers," *The Journal of Chemical Physics* 124 (2006): 134903.

15. Y. Chen, S. Mandal, and A. Sen, "Synthesis of (N−O)-Ligated Palladium(II) Complexes and Their Use in Ethene Homopolymerization and Norbornene Copolymerizations," *Organometallics* 29 (2010): 3160–3168.

16163028, 2026, 47, Downloaded from https://advanced.onlinelibrary.wiley.com/doi/10.1002/adfm.75610 by Cochrane France, Wiley Online Library on [16/10/2026]. See the Terms and Conditions (https://onlinelibrary.wiley.com/terms-and-conditions) on Wiley Online Library for rules of use; OA articles are governed by the applicable Creative Commons License

16. Y. Zou, D. Wang, K. Wurst, et al., "Group 4 Dimethylsilylenebisamido Complexes Bearing the 6-[2-(Diethylboryl)phenyl]Pyrid-2-Yl Motif: Synthesis and Use in Tandem Ring-Opening Metathesis/Vinyl-Insertion Copolymerization of Cyclic Olefins with Ethylene," *Chemistry—A European Journal* 17 (2011): 13832–13846.

17. I. Tritto, L. Boggioni, M. C. Sacchi, and P. Locatelli, "Cyclic Olefin Polymerization and Relationships Between Addition and Ring Opening Metathesis Polymerization," *Journal of Molecular Catalysis A: Chemical* 133 (1998): 139–150.

18. G. Zanchin, L. Vendier, I. Pierro, et al., "Homo- and Co-Polymerization of Ethylene with Cyclic Olefins Catalyzed by Phosphine Adducts of (Imido)Vanadium(IV) Complexes," *Organometallics* 37 (2018): 3181–3195.

19. L. Boggioni, D. Sidari, S. Losio, et al., "Ethylene–Co–Norbornene Copolymerization in the Presence of a Chain Transfer Agent," *European Polymer Journal* 107 (2018): 54–66.

20. S. Liu, Z. Yao, and K. Cao, "Comparison of Thermal Properties of Ethylene-Norbornene Copolymers Prepared by Batch and Semi-Batch Processes," *Journal of Applied Polymer Science* 112 (2009): 2493–2496.

21. T. Rische, A. J. Waddon, L. C. Dickinson, and W. J. MacKnight, "Microstructure and Morphology of Cycloolefin Copolymers," *Macromolecules* 31 (1998): 1871–1874.

22. T. Scrivani, R. Benavente, E. Perez, and J. M. Perena, "Stress-Strain Behaviour, Microhardness, and Dynamic Mechanical Properties of a Series of Ethylene-Norbornene Copolymers," *Macromolecular Chemistry and Physics* 202 (2001): 2547–2553.

23. K. Nomura, W. Wang, M. Fujiki, and J. Liu, "Notable Norbornene (NBE) Incorporation in Ethylene–NBE Copolymerization Catalysed by Nonbridged Half-Titanocenes: Better Correlation Between NBE Incorporation and Coordination Energy," *Chemical Communications* 25 (2006): 2659–2661.

24. H. Cheng and Z. Cai, "(Anilino)anthraquinone Nickel-Catalyzed Random Copolymerization of Norbornene and Ethylene," *Chemcatchem* 10 (2018): 497–500.

25. L. Cao, Z. Cai, and M. Li, "Phosphinobenzenamine Nickel Catalyzed Efficient Copolymerization of Methyl Acrylate with Ethylene and Norbornene," *Macromolecules* 55 (2022): 3513–3521.

26. L. Cao, M. Li, and Z. Cai, "Copolymerization of Norbornene and Methyl Acrylate by Nickel Catalyst Bearing 2-(Diarylphosphino)-N-phenylbenzenamine Ligands," *Catalysts* 13 (2023): 311.

27. M. Li, Z. Cai, and M. S. Eisen, "Rational Design of Aldimine Imidazolidin-2-imine/Guanidine Nickel Catalysts for Norbornene (Co)Polymerizations with Enhanced Catalytic Performance," *Journal of Catalysis* 420 (2023): 58–67.

28. X. He, Y. Guo, X. Chen, et al., "Synthesis of MWNTs/SiO_2 Supported Nickel and Palladium Complexes and Their Application as Catalysts for Cyclic Olefins Polymerization," *Journal of Organometallic Chemistry* 949 (2021): 121953.

29. K. L. Makovetsky, E. S. Finkelstein, V. I. Bykov, A. K. Bagdasaryan, B. L. Goodall, and L. F. Rhodes, *WO Patent* 9856837 (1998).

30. Y. Liu, R. Cong, Y. Pan, M. Chen, and M. Xu, "Efficient Copolymerization of Ethylene with Norbornene Mediated by Phosphine-Sulfonate Palladium Catalysts," *European Polymer Journal* 203 (2024): 112674.

31. Z. Zhang, Q. Wang, H. Jiang, A. Chen, and C. Zou, "Zeolitic Octahedral Metal Oxides for Catalysis," *European Journal of Inorganic Chemistry* 26 (2023): 202500105.

32. A. Bihun-Kisiel and W. Ochędzan-Siodłak, "Vanadium Catalysts for Ethylene-Norbornene Copolymerization," *Polimery/Polymers* 65 (2020): 757–770.

33. C. G. Chae, Y. Go, J. Choi, et al., "Palladium(II)-Catalyzed Synthesis of a Vinyl-Addition Ultrahigh-Molecular-Weight Polynorbornene Copolymer with an Entanglement Network for Enhanced Fracture Resistance," *Macromolecules* 57 (2024): 565–573.

34. F. Wang, D. Huang, H. Gao, F. Wang, L. Pan, and Y. Li, "Synthesis of Bimodal Distributed Cyclic Olefin Copolymers With Improved Tensile Properties," *Chinese Journal of Chemistry* 40 (2022): 1931–1938.

35. E. C. Kim, M. J. Kim, L. N. T. Ho, et al., "Synthesis of Vinyl-Addition Polynorbornene Copolymers Bearing Pendant n -Alkyl Chains and Systematic Investigation of Their Properties," *Macromolecules* 54 (2021): 6762–6771.

36. H. Yuan, T. Kida, R. Tanaka, et al., "Star Polymers with Norbornene/1-octene Gradient Copolymer Arms Synthesized by an Ansa-fluorenylamidodimethyltitanium-$[Ph_3C][B(C_6F_5)_4]$ catalyst System," *Polymer* 249 (2022): 124844.

37. D. Huang, X. Lu, K. Zhang, et al., "Ultra-High-Molecular Weight Cyclic Olefin Copolymers with Excellent All-Round Performance Prepared via Highly Effective Quasi-Living Copolymerization," *Chemical Engineering Journal* 494 (2024): 153256.

38. D. Huang, J. Li, X. Lu, et al., "Well-Controlled Block-Type Cyclic Olefin Copolymers with High Heat Resistance, Outstanding Strength and Low-Temperature Toughness," *Chinese Journal of Chemistry* 43 (2025): 983–994.

39. I. Tritto, L. Boggioni, and D. R. Ferro, "Metallocene Catalyzed Ethene- and Propene Co-Norbornene Polymerization: Mechanisms from a Detailed Microstructural Analysis," *Coordination Chemistry Reviews* 250 (2006): 212–241.

40. L. Boggioni and I. Tritto, "State of the Art of Cyclic Olefin Polymers," *MRS Bulletin* 38 (2013): 245–251.

41. T. Shiono, M. Sugimoto, T. Hasan, Z. Cai, and T. Ikeda, "Random Copolymerization of Norbornene with Higher 1-Alkene with Ansa -Fluorenylamidodimethyltitanium Catalyst," *Macromolecules* 41 (2008): 8292–8294.

42. H. Y. Jung, S. D. Hong, M. W. Jung, H. Lee, and Y. W. Park, "Norbornene Copolymerization with α-olefins Using Methylene-bridged Ansa-Zirconocene," *Polyhedron* 24 (2005): 1269–1273.

43. T. Hasan, T. Ikeda, and T. Shiono, "Random Copolymerization of Propene and Norbornene with Ansa -Fluorenylamidodimethyltitanium-Based Catalysts," *Macromolecules* 38 (2005): 1071–1074.

44. W. Zhao and K. Nomura, "Design of Efficient Molecular Catalysts for Synthesis of Cyclic Olefin Copolymers (COC) by Copolymerization of Ethylene and α-Olefins with Norbornene or Tetracyclododecene," *Catalysts* 6 (2016): 175.

45. K. Nomura, M. Tsubota, and M. Fujiki, "Efficient Ethylene/Norbornene Copolymerization by (Aryloxo)(indenyl)Titanium(IV) Complexes−MAO Catalyst System," *Macromolecules* 36 (2003): 3797–3799.

46. W. Apisuk, H. Ito, and K. Nomura, "Efficient Synthesis of Cyclic Olefin Copolymers with High Glass Transition Temperatures by Ethylene Copolymerization with Tetracyclododecene Using (tert -BuC_5H_4)$TiCl_2$(N=CtBu_2)—MAO Catalyst," *Journal of Polymer Science Part A: Polymer Chemistry* 54 (2016): 2662–2667.

47. Y. Zhang, Y. Ding, Z. Jiang, et al., "Synthesis and Properties of Highly Transparent Cyclic Olefin Copolymers from Dual-Selective Catalysts," *Acta Polymerica Sinica* 56 (2025): 431–441.

48. N. Naga, G. Tsuchiya, and A. Toyota, "Synthesis and Properties of Polyethylene and Polypropylene Containing Hydroxylated Cyclic Units in the Main Chain," *Polymer* 47 (2006): 520–526.

49. R. Tanaka, A. Sasaki, T. Takenaka, Y. Nakayama, and T. Shiono, "Selective Synthesis of Highly Soluble Cyclic Olefin Copolymers with Pendant Vinyl Groups Using 1,5-hexadiene as a Comonomer," *Polymer* 136 (2018): 109–113.

50. X. Song, L. Yu, T. Shiono, T. Hasan, and Z. Cai, "Synthesis of Hydroxy-Functionalized Cyclic Olefin Copolymer and Its Block Copoly-

16163028, 2026, 47, Downloaded from https://advanced.onlinelibrary.wiley.com/doi/10.1002/adfm.75610 by Cochrane France, Wiley Online Library on [16/10/2026]. See the Terms and Conditions (https://onlinelibrary.wiley.com/terms-and-conditions) on Wiley Online Library for rules of use; OA articles are governed by the applicable Creative Commons License

mers with Semicrystalline Polyolefin Segments," *Macromolecular Rapid Communications* 38 (2017): 1600815.

51. S. Dong, X. Duan, T. Nan, C. Lin, B. Liu, and D. Cui, "Substituent Effect of Styryl Monomers on Composition and Property Enhancement of Dicyclopentadiene-Based Cycloolefin Copolymers," *Macromolecules* 56 (2023): 8912–8919.

52. H. Gao, S. Chen, B. Du, et al., "Cyclic Olefin Copolymers Containing both Linear Polyethylene and Poly(ethylene- co -norbornene) Segments Prepared from Chain Shuttling Copolymerization of Ethylene and Norbornene," *Polymer Chemistry* 13 (2022): 245–257.

53. J. Liu, H. Gao, F. Wang, D. Huang, L. Pan, and Y. Li, "Chain Shuttling Copolymerization for Synthesis of Multi-block Cyclic Olefin Copolymers," *Acta Polymerica Sinica* 54 (2023): 1708.

54. M. Yasir and A. F. M. Kilbinger, "Cascade Ring-Opening/Ring-Closing Metathesis Polymerization of a Monomer Containing a Norbornene and a Cyclohexene Ring," *ACS Macro Letters* 10 (2021): 210–214.

55. S. Kiyohara, N. Miyasako, Y. Ota, S. Matsuoka, and M. Suzuki, "Synthesis and Properties of Cyclic Olefin Polymers by Ring-Opening Metathesis (co)Polymerization of α-methyl-substituted Norbornene Lactones," *Polymer Chemistry* 13 (2022): 5882–5888.

56. S. Ishii, Y. Ota, S. Matsuoka, and M. Suzuki, "Spiro-Fluorene-Containing Cyclic Olefin Polymers," *ACS Applied Polymer Materials* 5 (2023): 7614–7620.

57. M. Hong, L. Cui, S. Liu, and Y. Li, "Synthesis of Novel Cyclic Olefin Copolymer (COC) with High Performance via Effective Copolymerization of Ethylene with Bulky Cyclic Olefin," *Macromolecules* 45 (2012): 5397–5402.

58. E. Funahashi, Y. Iwata, and S. I. Matsuoka, "Hexacyclotetradecenes as Polycyclic Fused Exo -Norbornene Monomers: Synthesis of Cyclic Olefin Copolymers via Ti-Catalyzed Controlled Polymerization," *Polymer Chemistry* 15 (2024): 3003–3009.

59. K. Nomura, "Development of Half-Titanocene Catalysts for Synthesis of Cyclic Olefin Copolymers," *Polyolefins Journal* 10 (2023): 59–70.

60. M. Okabe and K. Nomura, "Propylene/Cyclic Olefin Copolymers with Cyclopentene, Cyclohexene, Cyclooctene, Tricyclo[6.2.1.0(2,7)]Undeca-4-ene, and Tetracyclododecene: The Synthesis and Effect of Cyclic Structure on Thermal Properties," *Macromolecules* 56 (2023): 81–91.

61. X.-H. Zhang, X.-H. Mao, H. Gao, et al., "Preparation and Hydrogenation of Dicyclopentadiene-Based Cyclic Olefin Copolymers," *Chinese Journal of Polymer Science* 43 (2025): 1527–1536.

62. J. Kolařík, A. Pegoretti, L. Fambri, and A. Penati, "Non-Linear Long-Term Tensile Creep of Poly (propylene)/Cycloolefin Copolymer Blends with Fibrous Structure," *Macromolecular Materials and Engineering* 288 (2003): 629–641.

63. A. Pegoretti, J. Kolarik, L. Fambri, and A. Penati, "Polypropylene/Cycloolefin Copolymer Blends: Effects of Fibrous Phase Structure on Tensile Mechanical Properties," *Polymer* 44 (2003): 3381–3387.

64. S. Pimbert, "Evaluation of the Fractionated Crystallization of Isotactic Polypropylene and High Density Polyethylenes in Their Blends with Cycloolefin Copolymers," *Macromolecular Symposia* 203 (2003): 277–284.

65. M. Šlouf, J. Kolařík, and L. Fambri, "Phase Morphology of PP/COC Blends," *Journal of Applied Polymer Science* 91 (2003): 253–259.

66. S. Pimbert, "Fractionated Crystallization and Morphology in Binary Blends of Isotactic PP and HDPE with Cycloolefin Copolymers," *International Polymer Processing* 19 (2004): 27–34.

67. L. Fambri, J. Kolarik, A. Pegoretti, and A. Penati, "Thermal, Thermo-Mechanical, and Dynamic Mechanical Properties of Polypropylene/Cycloolefin Copolymer Blends," *Journal of Applied Polymer Science* 122 (2011): 3406–3414.

68. R. Jester, "Cyclic Olefin Copolymer Enhances Polyolefin Blends for Film Packaging," *Plastics Technology* 57 (2011): 30.

69. T. A. Vacková, M. Šlouf, M. Nevoralová, and L. Kaprálková, "Processing-Improved Properties and Morphology of PP/COC Blends," *Journal of Applied Polymer Science* 122 (2011): 1168–1175.

70. A. Gopanna, R. N. Mandapati, S. P. Thomas, K. Rajan, and M. Chavali, "Fourier Transform Infrared Spectroscopy (FTIR), Raman Spectroscopy and Wide-Angle X-Ray Scattering (WAXS) of Polypropylene (PP)/Cyclic Olefin Copolymer (COC) Blends for Qualitative and Quantitative Analysis," *Polymer Bulletin* 76 (2019): 4259–4274.

71. A. Gopanna, S. P. Thomas, K. P. Rajan, et al., "Investigation of Mechanical, Dynamic Mechanical, Rheological and Morphological Properties of Blends Based on Polypropylene (PP) and Cyclic Olefin Copolymer (COC)," *European Polymer Journal* 108 (2018): 439–451.

72. J. Kolařík, Z. Kruliš, M. Šlouf, and L. Fambri, "High-Density Polyethylene/Cycloolefin Copolymer Blends. Part 1: Phase Structure, Dynamic Mechanical, Tensile, and Impact Properties," *Polymer Engineering and Science* 45 (2005): 817–826.

73. J. Kolařík, A. Pegoretti, L. Fambri, and A. Penati, "High-Density Polyethylene/Cycloolefin Copolymer Blends, Part 2: Nonlinear Tensile Creep," *Polymer Engineering and Science* 46 (2006): 1363–1373.

74. K. Lamnawar, F. Vion-Loisel, and A. Maazouz, "Rheological, Morphological, and Heat Seal Properties of Linear Low Density Polyethylene and Cyclo Olefine Copolymer (LLDPE/COC) Blends," *Journal of Applied Polymer Science* 116 (2010): 2015–2022.

75. A. Dorigato, A. Pegoretti, L. Fambri, C. Lonardi, M. Šlouf, and J. Kolařik, "Linear Low Density Polyethylene/Cycloolefin Copolymer Blends," *Express Polymer Letters* 5 (2011): 23–37.

76. T. Vacková, M. Slouf, M. Nevoralová, and L. Kaprálková, "HDPE/COC Blends with Fibrous Morphology and Their Properties," *European Polymer Journal* 48 (2012): 2031–2039.

77. Y. Zhang, C. Jiang, H. Li, et al., "Melt-Reprocessable Linear Low-Density Polyethylene/Cyclic Olefin Copolymer Blends with Low Dielectric Constant and Low Thermal Expansion," *Journal of Applied Polymer Science* 141 (2024): 55142.

78. S. H. Jafari, M. N. Hesabi, H. A. Khonakdar, and M. Asl-Rahimi, "Correlation of Rheology and Morphology and Estimation of Interfacial Tension of Immiscible COC/EVA Blends," *Journal of Polymer Research* 18 (2011): 821–831.

79. A. Durmus, M. B. Alanalp, and I. Aydin, "Investigation of Morphological, Rheological, and Mechanical Properties of Cyclic Olefin Copolymer/Poly(ethylene- co -vinyl acetate) Blend Films," *Journal of Plastic Film & Sheeting* 34 (2018): 140–159.

80. G. Khanarian, "Rubber Toughened and Optically Transparent Blends of Cyclic Olefin Copolymers," *Polymer Engineering & Science* 40 (2000): 2590–2601.

81. K. Chai, S. Du, W. Wang, and X. He, "Viscoelasticity, Tensile Properties, and Microstructure of Cyclic Olefin Copolymer/SBS/SEBS Elastomer Blends," *Macromolecular Chemistry and Physics* 224 (2023): 2300127.

82. P. Doshev, D. Tomova, A. Wutzler, and H. J. Radusch, "Morphology and Mechanical Properties of Reactive and Non-Reactive COC/EOC Blends," *Journal of Polymer Engineering* 25 (2005): 375.

83. X. Pei, Y. Li, S. Zhao, and X. He, "Viscoelasticity, Tensile Properties, and Microstructure Development in Cyclic Olefin Copolymer/Polyolefin Elastomer Blends," *Macromolecular Chemistry and Physics* 223 (2022): 2200018.

84. H. A. Khonakdar, S. H. Jafari, and M. N. Hesabi, "Miscibility Analysis, Viscoelastic Properties and Morphology of Cyclic Olefin Copolymer/Polyolefin Elastomer (COC/POE) Blends," *Composites Part B: Engineering* 69 (2015): 111–119.

85. F. Shamsoddini-Zarch, Y. Jahani, M. Karrabi, and M. Ohshima, "Influence of Different Molecular Weights of Polyhexene-1 on the Morphology and Rheology of Cyclic Olefin Copolymer Blends," *Polymer Engineering & Science* 61 (2021): 1485–1501.

16163028, 2026, 47, Downloaded from https://advanced.onlinelibrary.wiley.com/doi/10.1002/adfm.75610 by Cochrane France, Wiley Online Library on [16/10/2026]. See the Terms and Conditions (https://onlinelibrary.wiley.com/terms-and-conditions) on Wiley Online Library for rules of use; OA articles are governed by the applicable Creative Commons License

86. F. Shamsoddini-Zarch, M. Karrabi, and Y. Jahani, "Effects of Different Molecular Architectures in Terms of Comonomer Content and Composition Distribution on the Miscibility of Cyclic Olefin Copolymer/Polyolefin (COC/POE and COC/LLDPEB) Blends," *Iranian Polymer Journal* 30 (2021): 593–612.

87. Y. Y. Cheng, H. M. Hsiao, Z. X. Li, M. J. Ho, M. F. Hsu, and S. J. Hsiang, "Synthesis and Characterization of Polyimide/Modified mCOC Composites," *Journal of Applied Polymer Science* 133 (2016): 44144.

88. F. Nazir, M. Iqbal, A. N. Khan, M. Mazhar, and Z. Hussain, "Fabrication of Robust Poly L-lactic Acid/Cyclic Olefinic Copolymer (PLLA/COC) Blends: Study of Physical Properties, Structure, and Cytocompatibility for Bone Tissue Engineering," *Journal of Materials Research and Technology* 13 (2021): 1732–1751.

89. R. C. Zovi, H. Mahmood, A. Dorigato, G. Fredi, and A. Pegoretti, "Cyclic Olefin Copolymer Interleaves for Thermally Mendable Carbon/Epoxy Laminates," *Molecules* 25 (2020): 5347.

90. H. Mahmood, A. Dorigato, and A. Pegoretti, "Healable Carbon Fiber-Reinforced Epoxy/Cyclic Olefin Copolymer Composites," *Materials* 13 (2020): 2165.

91. A. Dorigato, H. Mahmood, and A. Pegoretti, "Optimization of the Thermal Mending Process in Epoxy/Cyclic Olefin Copolymer Blends," *Journal of Applied Polymer Science* 138 (2021): 49937.

92. D. Perin, A. Dorigato, and A. Pegoretti, "Thermoplastic Self-Healing Polymer Blends for Structural Composites: Development of Polyamide 6 and Cyclic Olefinic Copolymer Blends," *Journal of Applied Polymer Science* 140 (2023): 53751.

93. D. Perin, H. Mahmood, D. Rigotti, A. Dorigato, and A. Pegoretti, "Novel Epoxy/Cyclic Olefin Copolymer/Carbon Structural Composites with Electro-Activated Self-Healing Properties," *Polymer Composites* 44 (2023): 5173–5187.

94. D. Perin, A. Dorigato, and A. Pegoretti, "Compatibilization of Polyamide 6/Cyclic Olefinic Copolymer Blends for the Development of Multifunctional Thermoplastic Composites with Self-Healing Capability," *Materials* 17 (2024): 1880.

95. M. Coser, D. Perin, G. Fredi, et al., "Self-healing of Polyamide 6/Cyclic Olefin Copolymer/Carbon fiber Composites under Quasi-static, Impact, and Fatigue Conditions," *Composites Science and Technology* 268 (2025): 111213.

96. D. Perin, L. Botta, D. Rigotti, A. Dorigato, G. Fredi, and A. Pegoretti, "Tuning the Compatibilizer Content and Healing Temperature in Thermally Mendable Polyamide 6/Cyclic Olefin Copolymer Blends," *Polymers* 17 (2025): 280.

97. S. T. Gobena and A. D. Woldeyonnes, "A Review of Synthesis Methods, and Characterization Techniques of Polymer Nanocomposites for Diverse Applications," *Discover Materials* 4 (2024): 52.

98. C. F. Ou and M. C. Hsu, "Preparation and Characterization of Cyclo Olefin Copolymer (COC)/Silica Nanoparticle Composites by Solution Blending," *Journal of Polymer Research* 14 (2007): 373–378.

99. S. Roy, T. Das, C. Y. Yue, and X. Hu, "Transparent Cyclic Olefin Copolymer/Silica Nanocomposites," *Polymer International* 63 (2014): 327–332.

100. A. Dorigato, A. Pegoretti, L. Fambri, M. Slouf, and J. Kolarik, "Cycloolefin Copolymer/Fumed Silica Nanocomposites," *Journal of Applied Polymer Science* 119 (2011): 3393–3402.

101. A. Pegoretti, A. Dorigato, A. Biani, and M. Slouf, "Cyclic Olefin Copolymer–Silica Nanocomposites Foams," *Journal of Materials Science* 51 (2016): 3907–3916.

102. A. Dorigato, A. Pegoretti, and C. Migliaresi, "Physical Properties of Polyhedral Oligomeric Silsesquioxanes–Cycloolefin Copolymer Nanocomposites," *Journal of Applied Polymer Science* 114 (2009): 2270–2279.

103. A. Petrella, M. Striccoli, M. L. Curri, and A. Agostiano, "Optical Properties of Nanocomposites Based on (CdSe)ZnS Core Shell Nanocrystals in Cyclic Olefin Copolymer," *Synthetic Metals* 245 (2018): 121–126.

104. Q. Wang, H. Wang, C. Zhang, Q. Zhang, and H. Yang, "Core-Shell Sr_2CeO_4@SiO_2 Filled COC-Based Composites with Low Dielectric Loss for High-Frequency Substrates," *Polymers* 13 (2021): 4006.

105. E. I. Ionete, A. Visse, R. D. Andrei, M. I. Petreanu, S. I. Spiridon, and R. E. Ionete, "Electrical and Dielectrical Properties of Composites Based on Alumina and Cyclic Olefin Copolymers," *Materials* 17 (2024): 5349.

106. T. C. K. Yang, S. S. Y. Lin, and T. H. Chuang, "Kinetic Analysis of the Thermal Oxidation of Metallocene Cyclic Olefin Copolymer (mCOC)/TiO_2 Composites by FTIR Microscopy and Thermogravimetry (TG)," *Polymer Degradation and Stability* 78 (2002): 525–532.

107. F. Nazir and M. Iqbal, "Comparative Study of Crystallization, Mechanical Properties, and In Vitro Cytotoxicity of Nanocomposites at Low Filler Loadings of Hydroxyapatite for Bone-Tissue Engineering Based on Poly(l-lactic acid)/Cyclo Olefin Copolymer," *Polymers (Basel)* 13 (2021): 3865.

108. Q. U. Ain, A. N. Khan, M. Nabavinia, and M. Mujahid, "Enhanced Mechanical Properties and Biocompatibility of Novel Hydroxyapatite/TOPAS Hybrid Composite for Bone Tissue Engineering Applications," *Materials Science and Engineering: C* 75 (2017): 807–815.

109. Z. H. Chen, C. Zeng, C. Zhang, B. Wang, K. Cao, and Z. Yao, "Preparation and Properties of Cyclic Olefin Copolymers Multiwalled Carbon Nanotube Nanocomposites," *Journal of Applied Polymer Science* 126 (2012): 1121–1128.

110. M. Saadatmand-Navaran, H. Azizi, and S. Ahmadjo, "Polyolefin Elastomer/Cyclic Olefin Copolymer/Multi-Walled Carbon Nanotubes Nanocomposites: Rheological, Morphological, Electrical and Mechanical Study," *Polymer Composites* 45 (2024): 14008–14021.

111. P. Pal, M. K. Kundu, A. Malas, and C. K. Das, "Thermo Mechanical Properties of Organically Modified Halloysite Nanotubes/Cyclic Olefin Copolymer Composite," *Polymer Composites* 36 (2015): 955–960.

112. T. M. Wu and C. W. Wu, "Surface Characterization and Properties of Plasma-Modified Cyclic Olefin Copolymer/Layered Silicate Nanocomposites," *Journal of Polymer Science Part B: Polymer Physics* 43 (2005): 2745–2753.

113. A. Kasgoz, D. Akin, and A. Durmus, "Rheological and Electrical Properties of Carbon Black and Carbon Fiber Filled Cyclic Olefin Copolymer Composites," *Composites Part B: Engineering* 62 (2014): 113–120.

114. A. Kasgoz, D. Akin, A. I. Ayten, and A. Durmus, "Effect of Different Types of Carbon Fillers on Mechanical and Rheological Properties of Cyclic Olefin Copolymer (COC) Composites," *Composites Part B: Engineering* 66 (2014): 126–135.

115. D. Akin, A. Kasgoz, and A. Durmus, "Quantifying Microstructure, Electrical and Mechanical Properties of Carbon fiber and Expanded Graphite Filled Cyclic Olefin Copolymer Composites," *Composites Part A: Applied Science and Manufacturing* 60 (2014): 44–51.

116. C. L. Lai, Y. J. Fu, J. T. Chen, et al., "Composite of Cyclic Olefin Copolymer with Low Graphene Content for Transparent Water-Vapor-Barrier Films," *Carbon* 90 (2015): 85–93.

117. A. Biani, A. Dorigato, W. Bonani, M. Slouf, and A. Pegoretti, "Mechanical Behaviour of Cyclic Olefin Copolymer/Exfoliated Graphite Nanoplatelets Nanocomposites Foamed through Supercritical Carbon Dioxide," *Express Polymer Letters* 10 (2016): 977–989.

118. A. Dorigato, A. Biani, W. Bonani, and A. Pegoretti, "Thermo-Electrical Behaviour of Cyclic Olefin Copolymer/Exfoliated Graphite Nanoplatelets Nanocomposites Foamed Through Supercritical Carbon Dioxide," *Journal of Cellular Plastics* 55 (2019): 263–282.

119. J.-W. Lee, S. Jantasee, B. Jongsomsjit, R. Tanaka, Y. Nakayama, and T. Shiono, "Copolymerization of Norbornene with ω-Alkenylaluminum as a

16163028, 2026, 47, Downloaded from https://advanced.onlinelibrary.wiley.com/doi/10.1002/adfm.75610 by Cochrane France, Wiley Online Library on [16/10/2026]. See the Terms and Conditions (https://onlinelibrary.wiley.com/terms-and-conditions) on Wiley Online Library for rules of use; OA articles are governed by the applicable Creative Commons License

Precursor Comonomer for Introduction of Carbonyl Moieties," *Journal of Polymer Science Part A: Polymer Chemistry* 51 (2013): 5085–5090.

120. B. Palucci, G. Zanchin, G. Ricci, L. Vendier, C. Lorber, and G. Leone, "Vanadium-Catalyzed Terpolymerization of α,ω-Dienes with Ethylene and Cyclic Olefins: Ready Access to Polar-Functionalized Polyolefins," *Macromolecules* 54 (2021): 10700–10711.

121. G. Leone, B. Palucci, G. Zanchin, A. Vignali, G. Ricci, and F. Bertini, "Dynamically Cross-Linked Polyolefins via Hydrogen Bonds: Tough yet Soft Thermoplastic Elastomers with High Elastic Recovery," *ACS Applied Polymer Materials* 4 (2022): 3770–3778.

122. X. Song, L. Cao, R. Tanaka, T. Shiono, and Z. Cai, "Optically Transparent Functional Polyolefin Elastomer with Excellent Mechanical and Thermal Properties," *ACS Macro Letters* 8 (2019): 299–303.

123. S. I. Chowdhury, R. Tanaka, Y. Nakayama, and T. Shiono, "Copolymerization of Norbornene and Styrene with Anilinonaphthoquinone-Ligated Nickel Complexes," *Polymers* 11 (2019): 1100.

124. Y. Iwata, T. Shiono, and S. Matsuoka, "Functionalized Cyclic Olefin Copolymers: Chemoselective Polymerization of a Cyclopropane-containing Norbornadiene Dimer Using a Titanium Catalyst and Post-Polymerization Modification," *Polymer Chemistry* 16 (2025): 1096–1101.

125. P. Sharma, R. T. Ako, Q. Wang, S. Atakaramians, S. Walia, and S. Sriram, "Ultra-thin Freestanding Terahertz Frequency Selective Surface on Flexible Cyclic Olefin Copolymer," *Journal of Physics D: Applied Physics* 57 (2024): 215304.

126. R. R. Carvalho, S. P. Pujari, E. X. Vrouwe, and H. Zuilhof, "Mild and Selective C–H Activation of COC Microfluidic Channels Allowing Covalent Multifunctional Coatings," *ACS Applied Materials & Interfaces* 9 (2017): 16644–16650.

127. S. Bourg, S. Griveau, F. d'Orlyé, et al., "Surface Functionalization of Cyclic Olefin Copolymer by Plasma-enhanced Chemical Vapor Deposition Using Atmospheric Pressure Plasma Jet for Microfluidic Applications," *Plasma Processes and Polymers* 16 (2019): 1800195.

128. S. Roy, C. Y. Yue, and Y. C. Lam, "Influence of Plasma Surface Treatment on Thermal Bonding and Flow Behavior in Cyclic Olefin Copolymer (COC) Based Microfluidic Devices," *Vacuum* 85 (2011): 1102–1104.

129. S. Roy and C. Y. Yue, "Surface Modification of COC Microfluidic Devices: a Comparative Study of Nitrogen Plasma Treatment and Its Advantages Over Argon and Oxygen Plasma Treatments," *Plasma Processes and Polymers* 8 (2011): 432–443.

130. K. S. Ma, F. Reza, I. Saaem, and J. Tian, "Versatile Surface Functionalization of Cyclic Olefin Copolymer (COC) with Sputtered SiO_2 Thin Film for Potential BioMEMS Applications," *Journal of Materials Chemistry* 19 (2009): 7914.

131. L. El Fissi, D. Vandormael, L. Houssiau, and L. A. Francis, "Surface Functionalization of Cyclic Olefin Copolymer (COC) with Evaporated TiO_2 Thin Film," *Applied Surface Science* 363 (2016): 670–675.

132. R. K. Jena, C. Y. Yue, and L. Anand, "Improvement of Thermal Bond Strength and Surface Properties of Cyclic Olefin Copolymer (COC) Based Microfluidic Device Using the Photo-Grafting Technique," *Sensors and Actuators B: Chemical* 157 (2011): 518–526.

133. R. K. Jena and C. Y. Yue, "Cyclic Olefin Copolymer Based Microfluidic Devices for Biochip Applications: Ultraviolet Surface Grafting Using 2-methacryloyloxyethyl Phosphorylcholine," *Biomicrofluidics* 6 (2012): 12822.

134. F. Dawaymeh, Y. Abbas, M. Khaleel, A. Alazzam, and N. Alamoodi, "Tuning the Surface Wettability of Cyclic Olefin Copolymer by Plasma Treatment and Graphene Oxide Deposition and Reduction," *Polymers (Basel)* 13 (2021): 2305.

135. F. M. Michael, M. Khalid, R. Walvekar, H. Siddiqui, and A. B. Balaji, *Biodegradable and Biocompatible Polymer Composites: Processing, Properties and Applications* (Woodhead Publishing Duxford, 2017).

136. M. K. Kim, I. S. Park, H. D. Park, et al., "Effect of Poly(Ethylene Glycol) Graft Polymerization of Poly(methyl methacrylate) on Cell Adhesion," *Journal of Cataract and Refractive Surgery* 27 (2001): 766–774.

137. Z. Yang, H. Peng, W. Wang, and T. Liu, "Crystallization Behavior of Poly(ε-caprolactone)/Layered Double Hydroxide Nanocomposites," *Journal of Applied Polymer Science* 116 (2010): 2658–2667.

138. D. J. Eyckens, J. D. Randall, F. Stojcevski, et al., "Examining Interfacial Interactions in a Range of Polymers Using Poly(ethylene oxide) Functionalized Carbon Fibers," *Composites Part A: Applied Science and Manufacturing* 138 (2020): 106053.

139. S. S. M. Sastry, S. Panjikar, and R. S. Raman, "Graphene and Graphene Oxide as a Support for Biomolecules in the Development of Biosensors" *Nanotechnology, Science and Applications* 14 (2021): 197–205.

140. S. Zheng, H. Chen, H. Chen, W. Zhang, Q. Xue, and W. Che, "Cyclic Olefin Copolymer-Based Copper Clad Laminate and the Application for Low Loss Broadband Baluns," *International Journal of RF and Microwave Computer-Aided Engineering* 32 (2022): 22956.

141. N. A. Zulkifli, M. A. Johar, O. M. F. Marwah, and M. H. I. Ibrahim, "Review on Advances of Functional Material for Additive Manufacturing," In *IOP Conference Series: Materials Science and Engineering* 226, (IOP Publishing, 2017): 12177.

142. N. Valentine, M. H. Azarian, and M. Pecht, "Metallized Film Capacitors Used for EMI Filtering: A Reliability Review," *Microelectronics Reliability* 92 (2019): 123–135.

143. M. D. Z. Islam, Y. Fu, H. Deb, M. D. K. Hasan, Y. Dong, and S. Shi, "Polymer-based Low Dielectric Constant and Loss Materials for High-Speed Communication Network: Dielectric Constants and Challenges," *European Polymer Journal* 200 (2023): 112543.

144. L. Cai, Z. H. Jiang, J.-B. Wu, H. Chen, and W. Hong, "Low-loss and Flexible Terahertz Bandpass Frequency Selective Surface Based on Cyclic Olefin Copolymer Substrate via Solvent-Free Synthesis," *Optics Express* 31 (2023): 21706.

145. F. Pavanello, G. Ducournau, E. Peytavit, S. Lepilliet, and J.-F. Lampin, "High-Gain Yagi–Uda Antenna on Cyclic Olefin Copolymer Substrate for 300-GHz Applications," *IEEE Antennas and Wireless Propagation Letters* 13 (2014): 939–942.

146. M. Xiao, M. Zhang, B. Du, and K. Fan, "Improving the Dielectric Properties of Polypropylene for Metallised Film Capacitors Based on Cyclic Olefin Copolymer Blending," *IET Nanodielectrics* 7 (2024): 140–149.

147. H. J. Kang, N. Yang, and Y. S. Song, "Enhanced Thermal, Mechanical, and Optical Properties of Cellulose Nanocrystal Embedded Cyclic Olefin Copolymer Composite Film," *Korea-Australia Rheology Journal* 36 (2024): 223–230.

148. Y. Zhao, L. Cui, Y. Zhang, and Z. Jian, "All-Hydrocarbon High-Refractive-Index Cyclic Olefin Copolymer Optical Materials," *Macromolecules* 57 (2024): 8869.

149. H. T. Ban, H. Hagihara, K. Nishii, Y. Tsunogae, S. Nojima, and T. Shiono, "A New Approach for Controlling Birefringent Property of Cyclic Olefin Copolymers," *Journal of Polymer Science Part A: Polymer Chemistry* 46 (2008): 7395–7400.

150. S. Kefer, T. Limbach, N. Pape, K. Klamt, B. Schmauss, and R. Hellmann, "Birefringence in Injection-Molded Cyclic Olefin Copolymer Substrates and Its Impact on Integrated Photonic Structures," *Polymers* 16 (2024): 168.

151. I. P. Johnson, W. Yuan, A. Stefani, et al., "Optical Fibre Bragg Grating Recorded in TOPAS Cyclic Olefin Copolymer," *Electronics Letters* 47 (2011): 271–272.

152. W. Pongruengkiat, T. Jungpanich, K. Ittipornnuson, S. Pechprasarn, and N. Albutt, "Development of Low-Cost Abbe Refractometer," *Applied Mechanics and Materials* 879 (2018): 227–233.

153. H. Asfour, J. Otridge, R. Thomasian, C. Larson, and N. Sarvazyan, "Autofluorescence Properties of Balloon Polymers Used

16163028, 2026, 47, Downloaded from https://advanced.onlinelibrary.wiley.com/doi/10.1002/adfm.75610 by Cochrane France, Wiley Online Library on [16/10/2026]. See the Terms and Conditions (https://onlinelibrary.wiley.com/terms-and-conditions) on Wiley Online Library for rules of use; OA articles are governed by the applicable Creative Commons License

in Medical Applications," *Journal of Biomedical Optics* 25 (2020): 106004.

154. M. Cutroneo, L. Silipigni, A. Mackova, et al., "Mask-Assisted Deposition of Ti on Cyclic Olefin Copolymer Foil by Pulsed Laser Deposition," *Micromachines* 14 (2023): 1298.

155. M. Cutroneo, L. Torrisi, L. Silipigni, et al., "Laminated Cyclic Olefin Copolymer Foil by Pulsed Laser Deposition," *Coatings* 13 (2023): 596.

156. Y. Li, Y. Liu, R. Li, et al., "Collagen-based Biomaterials for Bone Tissue Engineering," *Materials & Design* 210 (2021): 110049.

157. C. Liu, J. Yu, X. Sun, J. Zhang, and J. He, "Thermal Degradation Studies of Cyclic Olefin Copolymers," *Polymer Degradation and Stability* 81 (2003): 197–205.

158. M. O. Liu, H.-F. Lin, M.-C. Yang, et al., "Thermal Oxidation and Molding Feasibility of Cycloolefin Copolymers (COCs) with High Glass Transition Temperature," *Polymer Degradation and Stability* 91 (2006): 1443–1447.

159. M. Gutiérrez-Villarreal, H. B. León-Molina, and R. Acosta, "Kinetic Study on the Thermal Degradation of Ethylene–Norbornene Copolymers Under the Effect of Fe and Mn Stearates," *Reaction Kinetics, Mechanisms and Catalysis* 122 (2017): 995–1010.

160. M. H. Gutiérrez-Villarreal and S. A. Zavala-Betancourt, "Thermo-Oxidative Stability of Cyclic Olefin Copolymers in the Presence of Fe, Co and Mn Stearates as Pro-Degradant Additives," *Polymer-Plastics Technology and Engineering* 53 (2014): 1804–1810.

161. M. Pęśko, M. Janczarek, Ł. Klapiszewski, and A. Masek, "Characterization of Polymers Based on Ethylene–norbornene Copolymer (Topas E-140) with Natural Additives Using Thermal Analysis Techniques," *Journal of Thermal Analysis and Calorimetry* 150 (2025): 19861–19875.

162. N. Mallegni, M. Milazzo, C. Cristallini, et al., "Characterization of Cyclic Olefin Copolymers for Insulin Reservoir in an Artificial Pancreas," *Journal of Functional Biomaterials* 14 (2023): 145.

163. S. Y. Choi, O. Habimana, P. Flood, et al., "Material- and Feature-Dependent Effects on Cell Adhesion to Micro Injection Moulded Medical Polymers," *Colloids and Surfaces B: Biointerfaces* 145 (2016): 46–54.

164. C. W. Tsao, L. Hromada, J. Liu, P. Kumar, and D. L. DeVoe, "Low Temperature Bonding of PMMA and COC Microfluidic Substrates Using UV/Ozone Surface Treatment," *Lab on a Chip* 7 (2007): 499.

165. A. V. Kazakov, E. M. Oks, and N. A. Panchenko, "Influence of Electron Emission on Operation of a Constricted Arc Discharge in a Pulsed Forevacuum Plasma-Cathode Electron Source," *Journal of Physics: Conference Series* 2064 (2021): 012124.

166. K. Bischoff, D. Mücke, G. L. Roth, C. Esen, and R. Hellmann, "UV-Femtosecond-Laser Structuring of Cyclic Olefin Copolymer," *Polymers* 14 (2022): 2962.

167. T. Guan, S. Yuket, H. Cong, D. W. Carton, and N. Zhang, "Permanent Hydrophobic Surface Treatment Combined with Solvent Vapor-assisted Thermal Bonding for Mass Production of Cyclic Olefin Copolymer Microfluidic Chips," *ACS Omega* 7 (2022): 20104.

168. P. Aubrecht, P. Malinský, J. Novák, J. Smejkal, A. Jagerová, J. Matoušek, and M. Štofik, "Patterning of COC Polymers by Middle-Energy Ion Beams for Selective Cell Adhesion in Microfluidic Devices," *Advanced Materials Interfaces* 11 (2024): 2301077.

169. S. Y. Chou, P. R. Krauss, and P. J. Renstrom, "Imprint of Sub-25 Nm Vias and Trenches in Polymers," *Applied Physics Letters* 67 (1995): 3114–3116.

170. K. Mönkkönen, T. T. Pakkanen, J. Hietala, et al., "Replication of Sub-Micron Features Using Amorphous Thermoplastics," *Polymer Engineering and Science* 42 (2002): 1600–1608.

171. C. Li, Y. Yang, H. G. Craighead, and K. H. Lee, "Isoelectric Focusing in Cyclic Olefin Copolymer Microfluidic Channels Coated by Polyacrylamide Using a UV Photografting Method," *Electrophoresis* 26 (2005): 1800–1806.

172. M. L. Hupert, W. J. Guy, S. D. Llopis, et al., "Evaluation of Micromilled Metal Mold Masters for the Replication of Microchip Electrophoresis Devices," *Microfluid Nanofluidics* 1 (2007): 1–11.

173. J. Saez, L. Basabe-Desmonts, and F. Benito-Lopez, "Low-cost Origami Fabrication of 3D Self-aligned Hybrid Microfluidic Structures," *Microfluidics and Nanofluidics* 20 (2016): 116.

174. S. Damodara, S. Shahriari, W. I. Wu, P. Rezai, H. H. Hsu, and R. Selvaganapathy, *Microfluidic Devices for Biomedical Applications* (Elsevier, 2021), 1–78.

175. J. Cai, J. Jiang, F. Gao, et al., "Rapid Prototyping of Cyclic Olefin Copolymer Based Microfluidic System with CO_2 Laser Ablation," *Microsystem Technologies* 23 (2017): 5063–5069.

176. N. Bhattacharjee, A. Urrios, S. Kang, and A. Folch, "The Upcoming 3D-Printing Revolution in Microfluidics," *Lab on a Chip* 16 (2016): 1720–1742.

177. M. Kaluza, M. Walczakowski, and A. Siemion, "Exploring the Impact of 3D Printing Parameters on the THz Optical Characteristics of COC Material," *Materials* 17 (2024): 5104.

178. R. Gunasekaran, G. V. Kaliyannan, M. R. A. Refaai, and U. Gandhi, "Sustainable Manufacturing of 3D-Printed Cyclic Olefin Copolymer Coversheets with Gahnite for Enhanced Silicon Photovoltaic Efficiency," *Ceramics International* 51 (2025): 2002–2013.

179. M. R. A. Refaai, "Industry 4.0-Enabled 3D Printing for Sustainable Antireflection Coversheets: Enhancing Photovoltaic Performance with Silicon Nitride-Modified Copolymers," *Ceramics International* 51 (2025): 39970–39982.

180. A. Domingues, A. Martínez-Carboneres, and S. Carlson, "Evaluation of 3D-printed Plastics for Ultra-High Vacuum Applications: Outgassing, and Residual Gas Analysis," *Vacuum* 233 (2025): 113970.

181. L. Zhang, J. Wen, N. Wang, H. Wu, and X. Ma, "The Challenges and Focuses on Plastic Welding by Picosecond Laser in the Field of Camera Module Assembly," *Optics & Laser Technology* 181 (2025): 111751.

182. S. Singaravelu, J. M. Klopf, K. E. Schriver, H. Park, M. J. Kelley, and R. F. Haglund, "Resonant Infrared Pulsed Laser Deposition of Cyclic Olefin Copolymer Films," *Applied Physics A* 114 (2014): 1285–1293.

183. V. K. Shinoj, V. M. Murukeshan, S. B. Tor, N. H. Loh, and S. W. Lye, "Design, Fabrication, and Characterization of Thermoplastic Microlenses for Fiber-Optic Probe Imaging," *Applied Optics* 53 (2014): 1083.

184. S. Appasamy, W. Li, S. H. Lee, J. T. Boyd, and C. H. Ahn, "High-Throughput Plastic Microlenses Fabricated Using Microinjection Molding Techniques," *Optical Engineering* 44 (2006): 123401.

185. J. Yeo, J. Ryu, B. K. Lee, E. Byeon, T. H. Kwon, and D. S. Kim, "Theoretical and Experimental Characterization of Wettability of Various Nanolens Arrayed Polymer Surfaces Replicated with Nanodimpled Aluminum Mold Insert," *Microsystem Technologies* 16 (2010): 1425–1430.

186. C. Baek, J. Yi, and J. Seo, "Low-cost, Thermoplastic Micro-Lens Array with a Carbon Black Light Screen for Bio-Mimetic Vision," *Optics Express* 29 (2021): 35172.

187. C. S. A. Musgrave and F. Fang, "Contact Lens Materials: A Materials Science Perspective," *Materials* 12 (2019): 261.

188. C. Baek and J. M. Seo, "Encapsulation Material for Retinal Prosthesis with Photodetectors or Photovoltaics," *IEEE Sensors Journal* 22 (2022): 1767–1774.

189. C. Musgrave, L. O'Toole, T. Mao, Q. Li, M. Lai, and F. Fang, "Manufacturing of Soft Contact Lenses Using Reusable and Reliable Cyclic Olefin Copolymer Moulds," *Polymers* 14 (2022): 4681.

16163028, 2026, 47, Downloaded from https://advanced.onlinelibrary.wiley.com/doi/10.1002/adfm.75610 by Cochrane France, Wiley Online Library on [16/10/2026]. See the Terms and Conditions (https://onlinelibrary.wiley.com/terms-and-conditions) on Wiley Online Library for rules of use; OA articles are governed by the applicable Creative Commons License

190. C. Baek, J. Kim, Y. Lee, and J. M. Seo, "Fabrication and Evaluation of Cyclic Olefin Copolymer Based Implantable Neural Electrode," *IEEE Transactions on Biomedical Engineering* 67 (2020): 2542–2551.

191. W. Waheed, S. Anwer, M. U. Khan, M. Sajjad, and A. Alazzam, "2D $Ti_3C_2T_x$-MXene Nanosheets and Graphene Oxide Based Highly Sensitive Humidity Sensor for Wearable and Flexible Electronics," *Chemical Engineering Journal* 480 (2024): 147981.

192. F. Dawaymeh, A. Agha, A. Alazzam, and M. Abd-Ellah, "Exploring Cyclic Olefin Copolymer (COC) for Flexible Silver Nanowire Electrode," *Scientific Reports* 14 (2024): 16989.

193. S. R. A. Kratz, B. Bachmann, S. Spitz, et al., "A Compression Transmission Device for the Evaluation of Bonding Strength of Biocompatible Microfluidic and Biochip Materials and Systems," *Scientific Reports* 10 (2020): 1400.

194. K. Silver, J. Li, A. Porch, et al., "3D-printed Microfluidic–microwave Device for Droplet Network Formation and Characterisation," *Lab on a Chip* 24 (2024): 5101–5112.

195. M. Sabzekar, M. P. Chenar, Z. Maghsoud, O. Mostaghisi, M. C. García-Payo, and M. Khayet, "Cyclic Olefin Polymer as a Novel Membrane Material for Membrane Distillation Applications," *Journal of Membrane Science* 621 (2021): 118845.

196. M. Gel, S. Kandasamy, K. Cartledge, and D. Haylock, "Fabrication of Free Standing Microporous COC Membranes Optimized for in Vitro Barrier Tissue Models," *Sensors and Actuators A: Physical* 215 (2014): 51–55.

197. A. Galmozzi, E. Dominguez, B. F. Cravatt, and E. Saez, "Application of Activity-Based Protein Profiling to Study Enzyme Function in Adipocytes," *Methods in Enzymology* 538 (2014): 151–169.

198. B. Zhang, H. Xu, Y. Huang, et al., "Presence of HPV DNA in Extracellular Vesicles from HeLa Cells and Cervical Samples," *Enfermedades Infecciosas y Microbiología Clínica* 144 (2020): 7185.

199. F. Paquin, J. Rivnay, A. Salleo, N. Stingelin, and C. Silva, "Multi-Phase Microstructures Drive Exciton Dissociation in Neat Semicrystalline Polymeric Semiconductors," *Journal of Materials Chemistry C* 3 (2015): 10715–10722.

200. H. Jang, A. S. Pawate, R. Bhargava, and P. J. A. Kenis, "Polymeric Microfluidic Continuous Flow Mixer Combined with Hyperspectral FT-IR Imaging for Studying Rapid Biomolecular Events," *Lab on a Chip* 19 (2019): 2598–2609.

201. S. Lau, Y. Liu, A. Maier, et al., "Establishment of an in Vitro Thrombogenicity Test System with Cyclic Olefin Copolymer Substrate for Endothelial Layer Formation," *MRS Communications* 11 (2021): 559–567.

202. S. A. Aghvami, A. Opathalage, Z. K. Zhang, et al., "Rapid Prototyping of Cyclic Olefin Copolymer (COC) Microfluidic Devices," *Sensors and Actuators B: Chemical* 247 (2017): 940–949.

203. J. Steigert, S. Haeberle, T. Brenner, et al., "Rapid Prototyping of Microfluidic Chips in COC," *Journal of Micromechanics and Microengineering* 17 (2007): 333–341.

204. R. G. Rodrigues, P. G. M. Condelipes, R. R. Rosa, V. Chu, and J. P. Conde, "Scalable Processing of Cyclic Olefin Copolymer (COC) Microfluidic Biochips," *Micromachines* 14 (2023): 1837.

205. M. Cesaria, M. Calcagnile, V. Arima, M. Bianco, P. Alifano, and R. Cataldo, "Cyclic Olefin Copolymer (COC) as a Promising Biomaterial for Affecting Bacterial Colonization: Investigation on Vibrio Campbellii," *International Journal of Biological Macromolecules* 271 (2024): 132550.

206. B. Bruijns, A. Veciana, R. Tiggelaar, and H. Gardeniers, "Cyclic Olefin Copolymer Microfluidic Devices for Forensic Applications," *Biosensors* 9 (2019): 85.

207. B. Bruijns, R. Tiggelaar, and H. Gardeniers, "A Microfluidic Approach for Biosensing DNA within Forensics," *Applied Sciences* 10 (2020): 7067.

208. A. Jagannath, M. Yu, J. Li, N. Zhang, and M. D. Gilchrist, "Improving Assay Feasibility and Biocompatibility of 3D Cyclic Olefin Copolymer Microwells by Superhydrophilic Modification via Ultrasonic Spray Deposition of Polyvinyl Alcohol," *Biomaterials Advances* 163 (2024): 213934.

209. Y. H. Tennico, M. T. Koesdjojo, S. Kondo, D. T. Mandrell, and V. T. Remcho, "Surface Modification-Assisted Bonding of Polymer-Based Microfluidic Devices," *Sensors and Actuators B: Chemical* 143 (2010): 799–804.

210. H. Becker and L. E. Locascio, "Polymer Microfluidic Devices," *Talanta* 56 (2002): 267–287.

211. R. Jellali, P. Paullier, M. J. Fleury, and E. Leclerc, "Liver and Kidney Cells Cultures in a New Perfluoropolyether Biochip," *Sensors and Actuators B: Chemical* 229 (2016): 396–407.

212. S. S. Bale, A. Manoppo, R. Thompson, et al., "A Thermoplastic Microfluidic Microphysiological System to Recapitulate Hepatic Function and Multicellular Interactions," *Biotechnology and Bioengineering* 116 (2019): 3409–3420.

213. W. Wang and K. Park, *Biomimetic Polymers for In Vivo Drug Delivery* (Bone, 2014).

214. G. Kulsharova, A. Kurmangaliyeva, E. Darbayeva, L. Rojas-Solórzano, and G. Toxeitova, "Development of a Hybrid Polymer-Based Microfluidic Platform for Culturing Hepatocytes towards Liver-on-a-Chip Applications," *Polymers* 13 (2021): 3215.

215. J. Theobald, A. Ghanem, P. Wallisch, et al., "Liver-Kidney-on-Chip To Study Toxicity of Drug Metabolites," *ACS Biomaterials Science & Engineering* 4 (2018): 78–89.

216. G. Mottet, K. Perez-Toralla, E. Tulukcuoglu, et al., "A Three Dimensional Thermoplastic Microfluidic Chip for Robust Cell Capture and High Resolution Imaging," *Biomicrofluidics* 8 (2014): 024109.

217. K. Rennert, S. Steinborn, M. Gröger, et al., "A Microfluidically Perfused Three Dimensional Human Liver Model," *Biomaterials* 71 (2015): 119–131.

218. X. Wen, K. Yoshimoto, M. Yamanaka, S. Terada, and K. Kamei, "In Vitro Nonalcoholic Fatty Liver Disease Model with Cyclo-Olefin-Polymer-Based Microphysiological Systems," *Organs-on-a-Chip* 3 (2021): 100010.

219. K. Tan, P. Keegan, M. Rogers, et al., "A High-throughput Microfluidic Microphysiological System (PREDICT-96) to Recapitulate Hepatocyte Function in Dynamic, Re-circulating Flow Conditions," *Lab on a Chip* 19 (2019): 1556–1566.

220. L. Etxeberria, T. Messelmani, J. H. Badiola, et al., "Validation of HepG2/C3A Cell Cultures in Cyclic Olefin Copolymer Based Microfluidic Bioreactors," *Polymers* 14 (2022): 4478.

221. J. Raj, G. Herzog, M. Manning, et al., "Surface Immobilisation of Antibody on Cyclic Olefin Copolymer for Sandwich Immunoassay," *Biosensors and Bioelectronics* 24 (2009): 2654–2658.

222. A. ul Haq, A. Boyd, J. Acheson, J. McLaughlin, and B. J. Meenan, "Corona Discharge-Induced Functional Surfaces of Polycarbonate and Cyclic Olefins Substrates," *Surface and Coatings Technology* 362 (2019): 185–190.

223. A. Rifai, N. Tran, P. Reineck, et al., "Engineering the Interface: Nanodiamond Coating on 3D-Printed Titanium Promotes Mammalian Cell Growth and Inhibits Staphylococcus aureus Colonization," *ACS Applied Materials & Interfaces* 11 (2019): 24588–24597.

224. F. Brisset, J. Vieillard, B. Berton, S. Morin-Grognet, C. Duclairoir-Poc, and F. L. Derf, "Surface Functionalization of Cyclic Olefin Copolymer with Aryldiazonium Salts: a Covalent Grafting Method," *Applied Surface Science* 329 (2015): 337–346.

225. O. Guselnikova, P. Postnikov, A. Trelin, V. Švorčík, and O. Lyutakov, "Dual Mode Chip Enantioselective Express Discrimination of Chiral

16163028, 2026, 47, Downloaded from https://advanced.onlinelibrary.wiley.com/doi/10.1002/adfm.75610 by Cochrane France, Wiley Online Library on [16/10/2026]. See the Terms and Conditions (https://onlinelibrary.wiley.com/terms-and-conditions) on Wiley Online Library for rules of use; OA articles are governed by the applicable Creative Commons License

Amines via Wettability-Based Mobile Application and Portable Surface-Enhanced Raman," *ACS Sensors* 4 (2019): 1032.

226. O. Guselnikova, B. Dvorankova, K. Kakisheva, et al., "Rapid SERS-based Recognition of Cell Secretome on the Folic Acid-Functionalized Gold Gratings," *Analytical and Bioanalytical Chemistry* 411 (2019): 3309–3319.

227. Y. Kalachyova, A. Olshtrem, O. A. Guselnikova, et al., "Synthesis, Characterization, and Antimicrobial Activity of Near-IR Photoactive Functionalized Gold Multibranched Nanoparticles," *ChemistryOpen* 6 (2017): 254–260.

228. E. Sviridova, A. Barras, A. Addad, et al., "Surface Modification of Carbon Dots with Tetraalkylammonium Moieties for Fine Tuning Their Antibacterial Activity," *Biomaterials Advances* 134 (2022): 112697.

229. K. Nikiforova, A. Gorbunova, E. Plotnikov, P. Postnikov, and O. Guselnikova, "Antifouling Surface for Biomedical Devices: Modification of COC Surface by Quaternary Ammonium Moieties via Diazonium Chemistry," *Applied Surface Science* 603 (2022): 154415.

230. J. Claves, P. Chennell, Y. Le Basle, N. Krautwurst, and V. Sautou, "Comparative Study of Sorption Phenomena between Three Medications and Syringes Made of Cyclic Olefin Copolymer or Polypropylene," *Pharmaceutical Research* 41 (2024): 51–62.

231. Z. Almubaid, Z. Alhaj, O. Almosa, M. Marikh, and W. Khan, "The Impact of Social Support on Health Outcomes of Diabetic Patients: A Systematic Review," *Cureus* 16 (2024): 67842.

232. R. L. Lincoln, F. Scarpa, V. P. Ting, and R. S. Trask, "Multifunctional Composites: A Metamaterial Perspective," *Multifunctional Materials* 2 (2019): 043001.

233. D. G. Bekas, K. Tsirka, D. Baltzis, and A. S. Paipetis, "Self-Healing Materials: A Review of Advances in Materials, Evaluation, Characterization and Monitoring Techniques," *Composites Part B: Engineering* 87 (2016): 92–119.

234. O. Speck and T. Speck, "An Overview of Bioinspired and Biomimetic Self-Repairing Materials," *Biomimetics* 4 (2019): 26.

235. N. J. Kanu, E. Gupta, U. K. Vates, and G. K. Singh, "Self-Healing Composites: A state-of-the-Art Review," *Composites Part A: Applied Science and Manufacturing* 121 (2019): 474–486.

236. B. J. Blaiszik, S. L. B. Kramer, S. C. Olugebefola, J. S. Moore, N. R. Sottos, and S. R. White, "Self-Healing Polymers and Composites," *Annual Review of Materials Research* 40 (2010): 179–211.

237. S. Utrera-Barrios, R. Verdejo, M. A. López-Manchado, and M. H. Santana, "Evolution of Self-Healing Elastomers, from Extrinsic to Combined Intrinsic Mechanisms: A Review," *Materials Horizons* 7 (2020): 2882–2902.

238. S. A. Hayes, W. Zhang, M. Branthwaite, and F. R. Jones, "Self-Healing of Damage in Fibre-Reinforced Polymer-Matrix Composites," *Journal of The Royal Society Interface* 4 (2007): 381–387.

239. Z. Y. Wang, C. Y. Yue, and S. Roy, "Strength Development and Diffusion in Symmetric and Asymmetric Pairs of Amorphous COCs in the Vicinity of Tg: A New Modified Temperature–Pressure Dependent Model," *Polymer* 53 (2012): 1932–1938.

240. A. Cohades and V. Michaud, "Thermal Mending in E-Glass Reinforced Poly(ε-caprolactone)/Epoxy Blends," *Composites Part A: Applied Science and Manufacturing* 99 (2017): 129–138.

241. H. Mahmood, A. Dorigato, and A. Pegoretti, "Thermal Mending in Novel Epoxy/Cyclic Olefin Copolymer Blends," *Express Polymer Letters* 14 (2020): 368–383.

242. D. Perin, G. Fredi, P. Russo, A. Pegoretti, and A. Dorigato, "Intrinsic self-healing of polyamide 6/carbon fiber thermoplastic laminates," *Composites Part A: Applied Science and Manufacturing* (2026): 109393.

243. H. Zhou, H. Wang, H. Shao, T. Lin, H. Xu, and H. Niu, "Super-Robust Self-Healing Superhydrophobic Coating with Triboelectrification Induced Liquid Self-Repellency," *Materials & Design* 211 (2021): 110145.

244. S. Janjua, Z. Hussain, Z. Khan, M. A. Liaqat, and M. A. Umer, "Biopolymer Blended Films of Poly(butylene succinate)/Cyclic Olefin Copolymer with Enhanced Mechanical Strength for Packaging Applications," *Journal of Applied Polymer Science* 138 (2021): 50081.

245. L. E. Nielsen, "Models for the Permeability of Filled Polymer Systems," *Journal of Macromolecular Science: Part A—Chemistry* 1 (1967): 929–942.

246. E. L. Cussler, S. E. Hughes, W. J. Ward, and R. Aris, "Barrier Membranes," *Journal of Membrane Science* 38 (1988): 161–174.

247. Z. Riaz, M. Ali, A. D. Abbasi, K. A. Khan, and O. Aydin, "Multifunctional Cyclic Olefin Copolymer-Titanium Dioxide-Based Nanocomposites for Enhanced Antibacterial and Biocompatible Properties," *ACS Omega* 10 (2025): 15052.

16163028, 2026, 47, Downloaded from https://advanced.onlinelibrary.wiley.com/doi/10.1002/adfm.75610 by Cochrane France, Wiley Online Library on [16/10/2026]. See the Terms and Conditions (https://onlinelibrary.wiley.com/terms-and-conditions) on Wiley Online Library for rules of use; OA articles are governed by the applicable Creative Commons License